U.PORTO

FEUP FACULDADE DE ENGENHARIA
UNIVERSIDADE DO PORTO

Mechanics of hybrid polymer composites

Rodrigo Paiva Tavares

Supervisor:
Prof. Dr. Pedro P. Camanho

A Thesis submitted for the degree of
Master of Science in Mechanical Engineering
to the Faculty of Engineering, University of Porto

Porto, June 2015

Abstract

Composite materials, more specifically fibre-reinforced composites, play a huge role in structural applications, however their use is sill hampered partly due to the low toughness they exhibit. Fibre hybridisation is a strategy that can lead to improved composite properties and performance, as it not only changes the material properties but also changes the damage propagation mechanisms leading to failure. The failure of hybrid composites is, usually, less catastrophic than that of to non-hybrid composites.

Predicting the tensile failure of unidirectional composites is a demanding task as there are multiple interacting failure mechanisms. The tensile behaviour of hybrid composites represents even more challenges as there are two types of fibres whose properties, including failure strain, differ.

This thesis aims to increase the understanding of the tensile failure of unidirectional hybrid and non-hybrid composite when subjected to tensile loadings. To achieve this goal several models with increasing complexity have been developed and implemented and the effects of hybridization have been studied.

A model for the tensile failure of dry tows of fibres, no matrix, based on the statistics of fibre strength has been developed and implement for hybrid and non-hybrid tows. This simple model considers the fibres to act independently of each other and cannot be used to predict the behaviour of composite materials. Nonetheless, it is useful to understand the effects of the fibre strength distributions, as well as the effects of hybridizing tows with different fibres using real distributions for the strength of the fibres parameters, in the tensile behaviour at the tow level. With careful selection of the hybridizing fibres it was possible to achieve a tow with increased ductility, whose failure was not catastrophic but was a progressive one.

To account for the presence of the matrix in a composite material a model, based on the fibre fragmentation process, was extended for composite materials. This simplified model helps understanding the effects of hybridization in the tensile failure of composites. The concept of pseudo-ductile strain is introduced and a parametric study is done with the objective of maximizing this parameter and understanding

the main factors controlling the increase of ductility in composite materials.

In order to accurately predict the tensile behaviour of unidirectional composite materials with a correct representation of the damage mechanisms direct numerical simulation is necessary.

A material damage model that is able to account for the fibre strength variability was developed and implemented in a commercial finite element software. Alongside a material model for the matrix material a micromechanical model, with random fibre distributions, was developed to study the tensile failure of composite materials. The interfaces between these two constituents of the composite are modelled by considering a cohesive behaviour.

Representative volume elements with random fibre distributions were created to study the sequence mechanisms leading to failure in composite materials and to validate the implemented models. Similar volume elements, with random fibre distributions, were developed for hybrid composites and the effects of the hybrid volume fraction on the tensile response of the materials was studied. The changes in the failure mechanisms due to the introduction of two types of fibres in a single unidirectional composite were also studied. These models allow to accurately represent the damage mechanisms in composites, including dynamic effects.

Resumo

Os materiais compósitos, mais especificamente os polímeros reforçados com fibras, têm um papel fundamental em aplicações estruturais, no entanto o seu uso ainda tem algumas limitações principalmente devido à baixa tenacidade que apresentam. A hibridização, principalmente através do uso de vários tipos de fibras, é uma estratégia que pode melhorar as propriedades e desempenho dos materiais, pois altera não só as propriedades do material mas também os mecanismos de propagação de dano que levam à rutura do compósito. A fratura dos compósitos híbridos é, usualmente, menos catastrófica do que a fratura dos compósitos não-híbridos.

A previsão da fratura longitudinal de compósitos unidirecionais é uma tarefa difícil devido à interação entre múltiplos mecanismos de dano. Para compósitos híbridos esta previsão é ainda dificultada pela existência de dois tipos de fibras com propriedades diferentes, incluindo a deformação de rutura.

O objetivo deste trabalho é aumentar o conhecimento sobre o comportamento de compósitos unidirecionais, híbridos e não híbridos, quando sujeitos a cargas longitudinais. Para alcançar este objetivo forem desenvolvidos e implementados modelos com crescentes níveis de complexidade, que permitiram não só estudar o comportamento dos compósitos não-híbridos mas também analisar os efeitos da hibridização.

Um modelo de previsão da falha de tows de fibras, sem presença de matriz, baseado em distribuições estatísticas para a tensão de rutura das fibras foi desenvolvido e implementado para tows híbridos e não-híbridos. Este modelo simplificado considera que não existe interção entre as fibras e, como tal, não pode ser usado para a previsão do comportamento de materiais compósitos, onde está presente a matriz. Não obstante, o modelo é útil para perceber os efeitos dos parâmetros estatísticos da tensão de rutura das fibras, bem como o efeito da hibridização, usando distribuições reais, no comportamento dos tows. Através da cuidada seleção das fibras a hibridizar foi possível obter um tow com maior ductilidade, cuja falha é mais progressiva.

De maneira a ter em conta a presença da matriz nos materiais compósitos foi desenvolvido um modelo baseado no processo de fragmentação das fibras. Este

modelo, apesar de simplificado, permite perceber os efeitos da hibridização no comportamento à tração dos materiais compósitos. É também introduzido o conceito de pseudo-ductilidade e é feito um estudo paramétrico com a finalidade de maximizar este parâmetro e perceber os parâmetros que controlam a ductilidade nos materiais compósitos.

Apesar destes modelos serem úteis, para ser possível prever o comportamento de compósitos unidirecionais à tração longitudinal, com uma representação correta dos mecanismos de dano, é necessário recorrer a simulação numérica.

Um modelo material capaz de ter em conta a variação estocástica da tensão de rutura das fibras foi desenvolvido e implementado num software comercial de elementos finitos. Em conjunto com um modelo material para a matriz, um modelo micromecânico, com uma distribuição aleatória de fibras, foi desenvolvido para estudar a fratura longitudinal de materiais compósitos. Foi também considerado o comportamento da interface entre as fibras e matriz através do uso de modelos coesivos.

Foram criados diversos elementos de volume representativos, com o objetivo de estudar a sequência de mecanismos de dano que levam à rutura dos materiais compósitos e validar os modelos materiais implementados. Foram também criados elementos de volume representativos para compósitos híbridos e o efeito da fração volúmica de cada tipo de fibras no comportamento à tração deste material foi estudado. Foram ainda estudas as alterações nos mecanismos de falha devido à introdução de dois tipos de fibras no compósito. Os modelos implementados são capazes de representar corretamente os mecanismos de dano nos materiais compósitos, incluindo os efeitos dinâmicos.

Acknowledgements

Firstly, I wish to express my gratitude to Prof. Dr. Pedro P. Camanho, supervisor of this thesis, for all the support, patience and availability during the development of this thesis, even at the most occupied times. I also would like to thank for the opportunity to work in such an interesting field and for all the encouragement.

To Miguel Bessa, PhD candidate, for his help and cooperation during this work. Even though separated by an ocean he always managed to have time to help me in the problems I've encountered, even when time was hard to find.

To Dr. António Melro for providing the tools that were the base of work and for helping me in the very early stages of this work and for giving me guidance when I didn't even know what I was doing.

To my workgroup, Giuseppe Catalanotti, Albertino Arteiro, Ricardo Pinto, Hélder Mata and Claudia Cardoso, I thank for the support and for all the valuables discussions, usually over a cup of coffee.

I would also like to thank everyone that I met during this stage at FEUP. A special thanks for Rodrigo Carvalho and Luis Máximo for the friendship and support. To Carolina Furtado, for many deserved breaks and for all the shared knowledge and motivation.

To my girlfriend, Rita Frade that, although being far during the development of this thesis, was always there to support me and push me forward. I would also like to thank Guilherme Pereira and all my friends whose friendship I can always count on.

Lastly, a very special thanks to all my family. To my brother, Rafael, for always helping me move forward. To my parents, Magda and José, for everything, especially for always expecting the best of me.

Contents

Abstract i

Resumo iii

Acknowledgements v

Contents vi

List of symbols xi

List of figures xv

List of tables xx

1 Introduction 1

2 Mechanisms of longitudinal fracture 7

2.1 Distributions for fibre strength 8

2.1.1 Weibull distribution 8

2.1.2 Modified Weibull distributions 8

2.1.3 The normal distribution 9

2.2 Size effects in composites 10

2.3 Stress redistribution after fibre failure 11

2.4 Critical cluster size 12

2.5 Effects of the matrix and fibre-matrix interface 14

2.6 Modelling the tensile failure of unidirectional composites 15

2.6.1 Deterministic rule of mixtures 15

2.6.2 Analytical fibre bundle models 16

2.6.3 Micromechanical models based on Monte-Carlo simulations . 21

2.6.4 Continuum damage mechanic based models 25

2.6.5 Hierarchical scaling law for the strength of composite fibre bundles 26

2.7 Conclusion 28

3 Hybridization- State-of-the-art **31**
3.1 Hybrid composites . . . 31
3.1.1 Hybrid effect . . . 33
3.2 Mechanical properties of hybrid composites . . . 37
3.2.1 Tensile properties . . . 37
3.2.2 Flexural properties . . . 39
3.2.3 Impact resistance . . . 40
3.2.4 Fatigue resistance . . . 41
3.2.5 Pseudo-ductile behaviour . . . 42
3.3 Failure development and stress redistribution in UD hybrid composites 44
3.4 Modelling the tensile failure of UD hybrid composites . . . 48
3.5 Influencing parameters in the strength of hybrid composites . . . 53
3.5.1 Failure strain ratio . . . 53
3.5.2 Hybrid volume fraction . . . 54
3.5.3 Elastic properties of the fibres . . . 54
3.5.4 Fibre strength distribution . . . 55
3.5.5 Fibre dispersion . . . 55
3.5.6 Matrix properties . . . 56
3.6 Conclusion . . . 56

4 Model for the tensile failure of dry tows **59**
4.1 Model development . . . 59
4.2 Non-hybrid tow behaviour . . . 61
4.3 Hybrid tow behaviour . . . 68
4.3.1 Carbon-Carbon hybridization . . . 70
4.3.2 Glass-Glass hybridization . . . 75
4.3.3 Kevlar-Kevlar hybridization . . . 78
4.3.4 Carbon-Glass hybridization . . . 80
4.3.5 Carbon-Kevlar hybridization . . . 83
4.4 Conclusion . . . 87

5 Progressive damage model for hybrid composites **89**
5.1 Model development . . . 89
5.1.1 Fibre break density . . . 89
5.1.2 Fibre stress . . . 90
5.2 Composite damage model . . . 92
5.3 Non-hybrid composite behaviour . . . 94
5.3.1 Matrix properties . . . 94
5.3.2 Weibull scale parameter . . . 96
5.3.3 Weibull shape parameter . . . 96
5.3.4 Fibre strength dispersion . . . 98
5.3.5 Conclusions . . . 100

5.4 Hybrid composite behaviour 101
5.4.1 Carbon-carbon hybridization 102
5.4.2 Glass-glass hybridization 107
5.4.3 Kevlar-kevlar hybridization 110
5.4.4 Carbon-glass hybridization 113
5.4.5 Carbon-kevlar hybridization 115
5.5 Conclusion 119

6 Micromechanical models 121
6.1 RVE generation 121
6.2 Damage models 125
6.2.1 Damage model for the fibres 125
6.3 Analysis of results 132
6.3.1 AS4 carbon composite material 132
6.3.2 M50S carbon composite 137
6.3.3 M30S carbon composite 139
6.3.4 Hybrid AS4-M50S carbon composite 141
6.4 Conclusion 145

7 Conclusions and future work 147
7.1 Conclusions 147
7.2 Future work 151

Bibliography 147

List of symbols

Chapter 2

$\boldsymbol{B}^N$	Deformation matrix of the constituent N;
E_N	Young's modulus of the constituent N;
$\boldsymbol{f}$	Vector of applied forces;
$f(\varepsilon)$	Gaussian probability density function;
G_m	Matrix shear modulus;
K	Stress concentration factor;
$\boldsymbol{K}^N$	Stiffness matrix of the constituent N;
L	Gauge length;
L_0	Characteristic length for the Weibull parameters m and σ_0;
m	Weibull shape parameter;
$P(\sigma)$	Failure probability at the applied stress σ;
S	Standard deviation of the Gaussian distribution;
u	Displacement vector;
V	Volume associated with the gauge length L;
V_0	Volume associated with the characteristic length L_0;
V_N	Volume fraction of the constituent N;
X_N^t	Tensile strength of the constituent N;
α	Length dependency parameter;
δ	Ineffective length;
ε	Strain;
ε^∞	Remote strain;
μ	Mean of the Gaussian distribution;
σ	Stress;
σ_0	Weibull scale parameter;
σ^∞	Remote stress;
ϕ_f	Fibre diameter;

Chapter 3

d_m	Fibre spacing;
E_N	Young's modulus of the constituent N;
R_{hyb}	Hybrid effect;
S_N	Cross section area of the constituent N;
t_m	Matrix thickness;
V_N	Volume fraction of the constituent N;
ρ	Ratio of normalized stiffness of the hybridized fibres;

Chapter 4

E_N	Young's modulus of the constituent N;
E_0	Initial Young's modulus of the hybrid tow;
F	Loading force at the applied strain ε;
L	Gauge length;
L_0	Characteristic length for the Weibull parameters m and σ_0;
m	Weibull shape parameter;
N_f	Number of broken fibres;
N_t	Number of fibres in the bundle;
$P(\sigma)$	Failure probability at the applied stress σ;
R_f	Fibre radius;
S_N	Sectional area of the constituent N;
V_N	Volume fraction of the constituent N;
$\langle\varepsilon\rangle$	Average failure strain of the fibres;
ε_d	Pseudo-ductile strain;
$\Gamma()$	Gamma function;
$\langle\sigma\rangle$	Average failure stress of the fibres;
$\bar{\sigma}$	Averaged stress in the fibre bundle;
σ_0	Weibull scale parameter;

Chapter 5

C^N_{ijkl}	Constitutive tensor of the material N;
d_N	Damage variable of the constituent N;
E_N	Young's modulus of the constituent N;
L	Gauge length;
L_0	Characteristic length for the Weibull parameters m and σ_0;
l_{ex}	length of the recovery region;
m	Weibull shape parameter;
$\langle N\rangle$	Average number of breaks in a fibre;
$P(\sigma)$	Failure probability at the applied stress σ;
R_f	Fibre radius;

T^N_{ijkl}	Influence tensor of the constituent N;
V_N	Volume fraction of the constituent N;
ε_{ij}	Strain tensor;
ε_c	Critical strain;
ε_d	Pseudo-ductile strain;
Λ	Number of breaks in a fibre per unit length;
$\langle\sigma\rangle$	Average failure stress of the fibres;
$\Sigma(x)$	Average stress in a fragment with length x;
σ_0	Weibull scale parameter;
σ_c	Critical strength;
σ_m	Average stress in a broken fibre;
τ	Interfacial shear strength;
Ξ	Rate of dissipation;
ψ_N	Free energy of the material N;
ψ^0_N	Free energy of the undamaged material N;

Chapter 6

A_f	Internal parameter for the fibre model;
$\boldsymbol{C_f}$	Stiffness tensor of the fibre material;
$\boldsymbol{C_f^0}$	Undamaged stiffness tensor of the fibre material;
d_f	Damage variable of the fibre material;
E_i	Elastic modulus in the i-direction;
F_f^d	Damage activation function for the fibre model;
G_{ff}	Fracture energy release rate of the fibre material in mode I;
G_i	Shear modulus in the i-direction;
$\mathscr{G}_f$	Complementary free energy of the fibre material;
G_m	Fracture energy release rate of the matrix material;
$\boldsymbol{H_f}$	Compliance tensor of the fibre material;
$\boldsymbol{H_f^0}$	Compliance tensor for the undamaged fibre material;
L	Gauge length;
L_0	Characteristic length for the Weibull parameters m and σ_0;
l^e	Characteristic element length;
m	Weibull shape parameter;
$P(\sigma)$	Failure probability at the applied stress σ;
r_f	internal damage variable for the fibre model;
V_N	Volume fraction of the constituent N;
X	Random number between 0 and 1;
X_f^t	Fibre tensile strength;
Y_f	Associated thermodynamic force in the fibre model;
α_L	Longitudinal thermal expansion coefficient;

α_T	Transverse thermal expansion coefficient;
α_C^m, α_T^m, α_S^m	Rate dependence parameter for the matrix model;
δ_τ	Maximum displacement for the fibre-matrix interface;
$\boldsymbol{\varepsilon}$	Strain tensor;
μ_τ	Friction at the fibre-matrix interface;
ν_i	Poisson coefficient in the i-direction;
$\boldsymbol{\sigma}$	Stress tensor
$\tilde{\boldsymbol{\sigma}}$	Effective stress tensor;
σ_0	Weibull scale parameter;
τ_i	Matrix-fibre interfacial shear strength in the i-direction;
ϕ_f^d	Loading function for the fibre model;
Ψ_f	Energy dissipated per volume unit for the fibre model;

List of Figures

2.1 Size effects in glass/epoxy composites [1]. 10
2.2 Schematic illustration of fibre packings: (a) 1D regular packing, (b) 2D regular packing (c) 1D random packing and 2D random packing [2]. 12
2.3 Cluster of 14 fibres observed by Scott et al. [3] using synchrotron computed tomography. 13
2.4 Effect of matrix cracks in the ineffective length (left) and the stress concentration factors (right) [2]. 15
2.5 Diagram of a fibre bundle model [4]. 18
2.6 Representation of the node lattice of a single-step spring-based model. 22
2.7 Schematics of the enhanced super-position stress redistribution: (a) stress concentration around a single break, (b) linear superposition results and (c) enhanced super-position [2]. 24
2.8 Flow chart of the model developed by Swolfs [2]. 24
2.9 Stress profile in a fibre with multiple fractures, according to shear-lag model[5]. 26
2.10 Hierarchical fibre bundles [6]. 27
2.11 Definition of control region [6]. 27

3.1 Hybrid configurations: (a) interlayer, (b) intralayer and (c) intrayarn configurations [7]. 32
3.2 Diagrams for the definition of the hybrid effect: (a) first definition proposed by Hayashi and (b) general definition based on the rule-of-mixtures [7]. 33
3.3 Dispersion in hybrid composites: the degree of dispersion increases from (a) to (d) [7]. 34
3.4 Hybrid effect for tensile failure strain. Information in Black was gathered by Kretsis and information in colour by Swolfs. The information inside the red line should be interpreted with care, due to errors [7]. 38
3.5 Bilinear rule-of-mixtures for tensile strength. Experimental data for carbon/glass hybrids [7]. 39
3.6 Effects in the flexural modulus of hybridizing carbon fibre composites with glass fibres in the compressive layers [8]. 39

3.7 Effects in the flexural strength of hybridizing carbon fibre composites with glass fibres in the compressive layers [8]. 40
3.8 Fatigue response of several fibre reinforced composites [9]. 42
3.9 Schematic stress-strain diagrams for: (a) non hybrid composites, (b) typical hybrid composites and (c) pseudo-ductile hybrid composites [2]. 43
3.10 Failure modes as a function of absolute and relative layer thickness in carbon/glass hybrid composites [10]. 44
3.11 Stress redistribution in hybrid composites with 50% carbon and glass fibres: (a) SCFs in both fibre types, considering the same and different radii; (b) ineffective length of the broken carbon fibre considering fibres with the same and different radii [11]. 45
3.12 Stress concentration factors in glass fibres as a function of the distance from the broken fibre [11]. 46
3.13 Stress concentration factors in carbon fibres as a function of the distance from the broken fibre [11]. 46
3.14 The ineffective length of carbon–glass hybrids for different hybrid volume fractions. The error bars indicates the 95% confidence interval based on five realisations[11]. 47
3.15 The ineffective length in carbon and HE fibres as a function of HE stiffness[2]. 47
3.16 Representation of the fibre packings used in Zweben's model : (a) non-hybrid LE composite and (b) hybrid composite with alternating LE and HE fibres [2]. 48
3.17 Hybrid unit-cells with different hybridization ratios (N^B) and hybridization degrees [12]. 52
3.18 Stress concentration factors, according to very local load sharing, around (a) a broken carbon fibre and (b) a broken glass fibre [2]. . . 52
3.19 Influence of failure strain ratio in the hybrid effect, for a hybrid composite with 50% of each fibre type [2]. 53
3.20 Illustration of the (a) bundle-by-bundle and (b) layer-by-layer dispersion considered by Swolfs et al. (Adapted from[13]). 56

4.1 Flowchart of the model for dry bundle failure. 61
4.2 Effect of the scale parameter (σ) in the strength of the fibres. 62
4.3 Force-Strain diagrams for tows of fibres with different scale parameters (σ). 63
4.4 Effect of the shape parameter (m) in the strength of the fibres. . . . 64
4.5 Force-Strain diagrams for tows of fibres with different shape parameters (m). 64
4.6 Effect of dispersion in the strength of the fibres, maintaining the same average strength. 66

4.7 Force-Strain diagrams for fibres with different dispersions, but same average strength. 66
4.8 Effect the gauge length (L) in the strength of the fibres. 67
4.9 Force-Strain diagrams for tows of fibres with lengths (L). 67
4.10 Diagram of pseudo-ductile strain. 69
4.11 Failure strain distributions for different carbon fibres. 71
4.12 Stress-strain diagrams at various hybrid volume fractions for AS4/T300 hybridization. 71
4.13 Stress-strain diagrams at various hybrid volume fractions for AS4/M40S hybridization. 72
4.14 Stress-strain diagrams at various hybrid volume fractions for AS4/M50S hybridization. 74
4.15 Failure strain distributions for the carbon fibres used for hybridization. 75
4.16 Failure strain distributions for several glass fibres. 76
4.17 Stress-strain diagrams at various hybrid volume fractions for HD/HP AR glass hybridization. 77
4.18 Failure strain distributions for several kevlar fibres. 78
4.19 Stress-strain diagrams at various hybrid volume fractions for kevlar 49/119 hybridization. 79
4.20 Stress-strain diagrams at various hybrid volume fractions for kevlar 119/129 hybridization. 80
4.21 Stress-strain diagrams at various hybrid volume fractions for T300 carbon and AR-HP glass hybridization. 81
4.22 Stress-strain diagrams at various hybrid volume fractions for 1000°C carbon and AR-HP glass hybridization. 82
4.23 Stress-strain diagrams at various hybrid volume fractions for AS4 carbon and kevlar 49 hybridization. 84
4.24 Stress-strain diagrams at various hybrid volume fractions for M40S carbon and kevlar 49 hybridization. 85
4.25 Stress-strain diagrams at various hybrid volume fractions for M43S carbon and kevlar 119 hybridization. 86

5.1 Stress profile in a fibre with multiple fractures, according to shear-lag model [5]. 91
5.2 Stress-Strain diagrams for composites with different interfacial shear strength (τ). 95
5.3 Stress-Strain diagrams for composites with fibres with different scale parameters (σ). 96
5.4 Stress-Strain diagrams for composites with fibres with different shape parameters (m), with $\tau = 40$ MPa. 97

5.5 Stress-Strain diagrams for composites with fibres with different shape parameters (m), with $\tau = 10$ MPa. 98
5.6 Stress-Strain diagrams for composites with fibres with different with different dispersion and the same average failure strength. 99
5.7 Stress-Strain diagrams for composites with fibres with different Weibull shape parameter (m) and same critical strength (σ_c). 100
5.8 Failure strain distributions for different carbon fibres. 103
5.9 Stress-strain diagrams at various hybrid volume fractions for AS4/T300 hybridization. 103
5.10 Stress-strain diagrams at various hybrid volume fractions for AS4/M40S hybridization. 105
5.11 Stress-strain diagrams at various hybrid volume fractions for AS4/M50S hybridization. 106
5.12 Failure strain distributions for several glass fibres. 108
5.13 Stress-strain diagrams at various hybrid volume fractions for HD/HP glass hybridization. 108
5.14 Stress-strain diagrams at various hybrid volume fractions for HD/E-glass hybridization. 109
5.15 Failure strain distributions for several kevlar fibres. 111
5.16 Stress-strain diagrams at various hybrid volume fractions for kevlar 49/kevlar 119 hybridization. 111
5.17 Stress-strain diagrams at various hybrid volume fractions for kevlar 119/kevlar 129 hybridization. 112
5.18 Stress-strain diagrams at various hybrid volume fractions for T300 carbon and AR-HP glass hybridization. 114
5.19 Stress-strain diagrams at various hybrid volume fractions for M50S carbon and AR-HP glass hybridization. 114
5.20 Stress-strain diagrams at various hybrid volume fractions for AS4 carbon and kevlar 49 hybridization. 116
5.21 Stress-strain diagrams at various hybrid volume fractions for AS4 carbon and kevlar 129 hybridization. 117
5.22 Stress-strain diagrams at various hybrid volume fractions for AS4 carbon and kevlar 119 hybridization. 118

6.1 Flowchart of RAND_uSTRU_GEN algorithm [14]. 122
6.2 Flowchart of the hard-core model for the generation of the microstructure. 124
6.3 Stress-strain diagrams for the fibre damage model for various element lengths. 129
6.4 Flowchart of the constitutive model for the fibres. 131
6.5 Distributions of tensile strength of all the elements present in the model, for two different random generators. 133

6.6 Stress-strain curves for the AS4 carbon and epoxy matrix for a RVE of dimensions $15 \times 15 \times 15$ fibre radius. 134
6.7 Stress-strain curves for the AS4 carbon and epoxy matrix: solid line - RVE $20 \times 20 \times 20$; dashed line - RVE $15 \times 15 \times 15$ 135
6.8 Damage in the interface of a broken fibre. 135
6.9 Damage progression in the RVE: (a) damage prior to fibre failure; (b) damage after first fibre failure; and (c) damage after failure of the composite material. 136
6.10 Broken fibre: (a) Location of the fibre break; (b) Stress field at fibre failure and (c) Stress field after dynamic effect. 137
6.11 Distributions of tensile strength of all the elements present in the model for the M50S fibres using both random generators. 138
6.13 Matrix crack developed after a fibre breaks (a) and stress concentrations in the neighbouring fibres of a broken one (b). 138
6.12 Stress-strain curves for the M50S carbon and epoxy matrix. 139
6.14 Distributions of tensile strength of all the elements present in the model for the M30S fibres using both random generators. 139
6.15 Stress-strain curves for the M30S carbon and epoxy matrix. 140
6.16 Crack development in the matrix: (a) Fibre failure and (b) development of a crack in the matrix surrounding the broken fibre. 140
6.17 Stress-strain curves for the hybridization between the AS4 and M50S carbon fibres. 142
6.18 Stress-strain curves for the hybrid composite with a volume fraction equal to 0.75 of AS4 carbon fibres and 0.25 of M50S (LE) carbon fibres. 142
6.19 Multiple fractures of the M50S (LE) carbon fibres for a composite with a $V_{\mathrm{LE}} = 0.5$. 143
6.20 Stress-strain curves for the hybrid composite with a volume fraction equal to 0.5 of AS4 carbon fibres and 0.5 of M50S carbon fibres. . . 143
6.21 Stress-strain curves for the hybrid composite with a volume fraction equal to 0.25 of AS4 carbon fibres and 0.75 of M50S (LE) carbon fibres. 144
6.22 Fracture process of an high elongation fibre (AS4 carbon) for a hybrid composite. 145

List of Tables

4.1 Effect of the shape parameter (m) in some reference properties. . . . 63
4.2 Effect of the shape parameter (m) in some reference properties. . . . 65
4.3 Effect of dispersion in some reference properties (distributions with the same average strength). 65
4.4 Effect of the gauge length (L) in some reference properties. 68
4.5 Mechanical properties for carbon fibres. 70
4.6 Stress-strain reference properties for AS4/T300 hybridization. 72
4.7 Stress-strain reference properties for AS4/M40S hybridization. . . . 73
4.8 Stress-strain reference properties for AS4/M50S hybridization. . . . 74
4.9 Mechanical properties for glass fibres. 76
4.10 Stress-strain reference properties for HD/HP AR glass hybridization. 77
4.11 Mechanical properties for kevlar fibres. 78
4.12 Stress-strain reference properties for kevlar 49/119 hybridization. . . 79
4.13 Stress-strain reference properties for kevlar 119/129 hybridization. . 80
4.14 Stress-strain reference properties for T300 carbon and AR-HP glass hybridization. 82
4.15 Stress-strain reference properties for 1000°C carbon and AR-HP glass hybridization. 83
4.16 Stress-strain reference properties for AS4 carbon and kevlar 49 hybridization. 84
4.17 Stress-strain reference properties for M40S carbon and kevlar 49 hybridization. 85
4.18 Stress-strain reference properties for M30S carbon and kevlar 119 hybridization. 86

5.1 Effect of interface shear strength (τ in some reference properties. . . 95
5.2 Effect of the scale parameter (σ) in some reference properties. 96
5.3 Effect of the shape parameter (m) in some reference properties, with $\tau = 40$ MPa. 97
5.4 Effect of the shape parameter (m) in some reference properties, with $\tau = 10$ MPa. 98
5.5 Effect of the fibre strength dispersion in some reference properties. . 99

5.6 Effect of the Weibull shape parameter (m) for composites with same critical strength (σ_c). 100
5.7 Mechanical properties for carbon fibres. 102
5.8 Stress-strain reference properties for AS4/T300 hybridization. 104
5.9 Stress-strain reference properties for AS4/M40S hybridization. . . . 105
5.10 Stress-strain reference properties for AS4/M50S hybridization. . . . 106
5.11 Mechanical properties for Glass fibres. 107
5.12 Stress-strain reference properties for HD/HP glass hybridization. . . 109
5.13 Stress-strain reference properties for HD/E-glass hybridization. . . . 110
5.14 Mechanical properties for kevlar fibres. 110
5.15 Stress-strain reference properties for kevlar 49/kevlar 119 hybridization.112
5.16 Stress-strain reference properties for kevlar 119/kevlar 129 hybridization. 113
5.17 Stress-strain reference properties for M50S carbon and AR-HP glass hybridization. 115
5.18 Stress-strain reference properties for AS4 carbon and kevlar 49 hybridization. 116
5.19 Stress-strain reference properties for AS4 carbon and kevlar 129 hybridization. 117
5.20 Stress-strain reference properties for AS4 carbon and kevlar 119 hybridization. 119

6.1 Fibre properties required for the material models. 132
6.2 Matrix properties required for the material models. 132
6.3 Properties for the cohesive surfaces in the fibre-matrix interfaces. . . 133

Chapter 1

Introduction

Composite materials are considered the materials of the future, manly in industries that have very high standards in terms of weight such as the aeronautical and aerospace industry. These materials can provide high level of performance with reduced weighs due to their excellent specific properties, namely strength and stiffness.

A composite is a material that results of the combination of two or more macroscopic components, resulting in a new material with superior properties than the constituents by themselves. At the time composite materials are considered materials with a high stiffness and resistance reinforcing component - long fibres, short fibres or particles- involved in a matrix with weaker properties that acts as connector and protects the reinforcing material.

Although composite materials are considered to be the materials of the future, they are widely available in the nature and have been used by humans since the beginning of civilization. The muscles in the human body are an example of a fibrous material. The arrangement of muscular fibres with different orientations allows the creation of a very adaptable material with outstanding properties in a preferential direction. Another example of a composite material is wood, whose arrangement of cellulose fibres provide the necessary strength while the matrix (lignin) provides the necessary connection between the fibres and gives the material its compressive resistance.

Man-made composites have existed for a long time. The first evidences of a man-made composite appeared in the Egyptian era, where straw and mud were mixed and burnt together by Israelites in order to obtain tougher bricks for construction. Another example of composite materials from the Egyptian era is papyrus, where layers of stems of the papyrus plant were stacked in perpendicular directions in order to manufacture paper with enough resistance to be written on and handled without

falling apart, thus creating the first man-made laminate. Throughout the ages other examples of composite material usage can be found. In the 19^{th} century the steel reinforced concrete appeared and revolutionized the industry of construction. This composite material, constituted by steel bars that reinforce the concrete, allowed construction to evolve not only in the hight but also in longevity.

The advanced composite materials, as they are known, only appeared in the 20^{th} century, with the emergence of the glass fibres. This material rapidly gained market in the aeronautical industry, during the II world war, and in the aerospace industry, with the beginning of the space era. During the second half of the 20^{th} century other types of fibres appeared, namely the widely used carbon fibre and others such as baron and aramid fibres.

Nowadays composite materials are widely available and the advances reached in the aerospace industry have been transferred to other industries. The applicability of composite materials is wide, from non-structural, secondary applications to structural and highly demanding applications. The widespread use of composite materials is manly due to the wide range of material properties that can be achieved with a correct design of these materials. This design is not only done in terms of shape and form, but also in selecting the composite's constituents and its manufacturing process. The advanced composite materials, used in structural applications, are known for their high specific properties (strength and stiffness), as good fatigue, ballistic, thermal, corrosion, and electro- magnetic properties.

The growth in usage of composite materials is also related to the recent advances in the computational techniques. The ability to simulate the behaviour of a material or component without having the need to fabricate and test helped reducing the cost and time of the design process, allowing the development of new and better materials, designed for specific applications.

Computational simulations can be performed at different scales. Macromechanical simulations are the ones that required less computational effort. These simulations allow the designer to simulate the behaviour of a full component and study the stresses and deformations in the component, however the material is considered to be homogeneous, which is a simplification from the complex geometry of a composite material.

At a more detailed scale it is possible to perform mesomechanical simulations where the composite material is considered to be composed by several plies (laminas), considered homogeneous, that are stacked together with different orientations. Although the laminas are still considered homogeneous, this type of simulations allows a more detailed analysis and the study of several mechanisms of failure such as delaminations, therefore providing better insight insight on the behaviour of com-

posite materials.

As the composite materials are constituted by more than one macroscopic material, it is non-homogeneous. In order to simulate their microstructure it is necessary to resort to micromechanical simulations. These simulations consider that the different constituents have different behaviours and allow to accurately simulate the interfaces between them. Despite of being more computationally demanding, these simulations allow a deep understanding of the influence of the properties of the constituents in the composite behaviour, as well as the mechanisms that lead to the failure of composite materials.

Thesis motivation

Fibre-reinforced composites play a fundamental role in aircraft structural applications, however their optimal use is still hampered partly due to the relatively low toughness they exhibit. The tensile failure of UD composites is a drastic process due to the propagation of a cluster of broken fibres and hybridization may change this behaviour by changing the failure mechanisms in composite materials, leading to more ductile composites.

Although the hybridization of composite materials was a large field of study since the invention of carbon fibre until the late 80s, the interest has since then faded away, mainly due to the price reduction of carbon fibres and development of accurate models to predict the failure of non-hybrid composites. In the last years, hybridization has become a field of interest mainly due to the possibility of delaying and achieving a more gradual failure of composite materials by controlling the damage mechanisms.

Despite the fact that composite materials are generally composed by layers with different orientations, the failure of composites is usually associated with the failure of the 0° layer. This makes understanding the failure mechanisms in the tensile failure of unidirectional composites and the effects of hybridization in the failure mechanisms essential.

Thesis objectives

This thesis aims to develop the knowledge on the mechanical behaviour of unidirectional composites under tensile loadings. Especially the mechanisms that lead to the failure of these materials and the effects that including fibres of different types, with different properties, has in these mechanisms.

The theme of hybridization of composite materials has recently become a field of focus due to the potential of these materials. There can be different objectives in hybridizing composite materials. The main focus of hybridization in this work is the increase of ductility in composite materials and understanding the fibre and matrix properties required to achieve this goal. The ultimate goal is to be able to design a composite material with a pseudo-ductile behaviour without damaging the main composite properties such as stiffness and resistance.

The understanding of the effects of hybridization on the tensile failure of UD composites can be done at different levels. The first is the tow level, where tows of dry fibres - without the presence of a matrix- are hybridized allowing to understand the effects of the fibre strength distributions in the tensile behaviour of these fibre bundles. The following level requires the introduction of a matrix. This can be done through simplified semi-analytical models or by direct numerical simulation. Both these forms of modelling are present in this thesis in order to characterize the failure of hybrid and non-hybrid composite materials under tensile loadings.

Thesis layout

This thesis is organized by chapters that address different topics that are connected to the main goal of understanding the tensile failure of UD hybrid and non-hybrid composites.

Chapter 2 presents the state of the art in tensile failure of UD composites. Different topics are addressed, including the size effects in composite materials, critical cluster size and the effects of the matrix in the tensile failure. The different statistical distributions to characterize the tensile strength of the fibres, which is important in the formation of the cluster of broken fibres before failure, are also presented. This chapter also addresses the topic of the modelling of the tensile failure of UD composites, where different models with different backgrounds are presented and analysed in order to better understand the controlling factors in the tensile failure of UD composites.

Chapter 3 presents the state of the art in hybridization of composite materials, focusing in fibre hybrid composites. A brief analysis on the effects of hybridization on the different materials properties is done. The concept of pseudo-ductility and ductile composites are introduced and several experimental studies that demonstrated the pseudo-ductile behaviour are presented. The models for the tensile failure of hybrid composite are also presented.

Chapter 4 presents the development, implementation and results of a semi-analytical model for the tensile failure of dry tows of fibres, based on the statistical

distributions for the strength of the fibres. A parametric study is done to understand the effects of the fibre statistical parameters in the tensile failure of non-hybrid tows and a extensive study of hybridization of tows of fibres is done using real fibres. This study is done for carbon, glass and kevlar fibres, whose fibre statistical parameters were gathered from the available literature.

A analytical model for the tensile failure of UD composites based on fibre fragmentation is presented in Chapter 5. A similar study to the one in Chapter 4 is presented where it is analysed the effects of fibre properties in the tensile failure of non-hybrid UD composites and a parametric study on hybridization is done using real fibre distributions.

Chapter 6 presents the micromechanical modelling and simulation of the tensile failure of UD composites. The development of a damage model for the fibre constitutive behaviour that is able to account for fibre strength variability is presented. It is also presented the micromechanical simulation results for the tensile failure of hybrid and non-hybrid composites and the sequence of mechanisms that lead to the failure of these materials is analysed.

Lastly, in Chapter 7, the main conclusions regarding the work carried out during this thesis and some follow-up work in the mechanics of hybrid polymer composites is proposed.

Chapter 2

Mechanisms of longitudinal fracture

Modelling of composite materials is a difficult task due to the complexity of its internal structure and interactions between constituents (fibre and matrix). However, having models that are able to predict the behaviour of this materials is essential in order to optimize their design.

The mechanisms of longitudinal failure of unidirectional (UD) composites under longitudinal loadings are well understood, and are based in two essential aspects: (1) fibres do not possess a deterministic value for tensile strength [15] and (2), after a fibre fractures, the stress is redistributed among the intact fibres in a complex way [16]. The failure sequence is as follows: the increase of the applied strain leads to the failure of the weakest fibre, which means that, locally, it is no longer able to carry stress. As the matrix is loaded, it transfer the load back to the broken fibre, making it able to carry stress away from the point of fracture. The stress is redistributed to the remaining intact fibres by the matrix, which leads to stress concentrations in the intact fibres, increasing their probability of failure. At low applied stresses the fibres break appear in random locations and there is nearly no interaction between breaks. Afterwards, the stress concentration in the intact fibres will cause the creation of a cluster of broken fibres. These clusters will grow, when other fibres fail and, when a cluster reaches a certain critical size, it will propagate unstably leading to the failure of the composite. The tensile failure of a UD composite is, therefore, of statistical nature and function of the mechanics of load redistribution around broken fibres.

In this chapter we will describe the different models to predict the tensile behaviour of UD composites, starting with the different statistical distributions used to characterize fibre strength.

2.1 Distributions for fibre strength

The tensile strength of a technical fibre cannot be represented by a single average value. Due to their brittle behaviour the fibre tensile strength is governed by surface or volume flaws [15] and exhibits weak-link characteristics. There are several statistical distributions that can be used to characterize the strength of fibres, being the most used the Weibull distribution, proposed by Weibull in 1951 [17].

2.1.1 Weibull distribution

The standard Weibull probability distribution can be written as:

$$P(\sigma) = 1 - \exp\left(1 - \left(\frac{L}{L_0}\right)\left(\frac{\sigma}{\sigma_0}\right)^m\right) , \tag{2.1}$$

where P is the failure probability at the applied stress σ, L is the characteristic gauge length, L_0 is the reference gauge length (these can also be characterised as volumes [18]), σ_0 the scale parameter and m the shape parameter or Weibull modulus [17].

This distribution leads to the underestimation of the fibre strength at short gauge lengths [2] and is very sensitive to the statistical parameters [19]. The discrepancy between the Weibull distribution and the experimental results for short gauge lengths can be attributed to variations in fibre diameter, variations of the Weibull distribution from fibre to fibre and presence of different flaw populations [2]. According Curtin [20] this distribution is not the most accurate to describe the strength of fibres, however is still the most used to characterize tensile strength of technical fibres.

2.1.2 Modified Weibull distributions

Several authors found that the fibre strength is governed by more than one flaw population [21, 22] and therefore a bimodal Weibull distribution should be used:

$$P(\sigma) = 1 - \exp\left(-\left(\frac{L}{L_0}\right)\left(\frac{\sigma}{\sigma_{01}}\right)^{m_1} - \left(\frac{L}{L_0}\right)\left(\frac{\sigma}{\sigma_{02}}\right)^{m_2}\right) , \tag{2.2}$$

where σ_{01} and σ_{02} are the scale parameters and m_1 and m_2 the Weibull moduli for both populations of flaws. The use a traditional Weibull distribution indicates that there is no threshold stress below which the failure probability is zero, which is

common in brittle materials like fibres, however if such threshold exists the bimodal distribution is able to capture that limit [2].

As mentioned before, the traditional Weibull distribution fails to characterise the fibre strength at short gauge lengths, therefore was proposed a modified Weibull distribution that adds an exponent α to capture this dependency [23]:

$$P\left(\sigma_f\right) = 1 - \exp\left(1 - \left(\frac{L}{L_0}\right)^{\alpha}\left(\frac{\sigma}{\sigma_0}\right)^{m}\right) . \tag{2.3}$$

This equation leads to the traditional Weibull distribution when α equals 1. Curtin [20] proposed a model, entitled "Weibull of Weilbulls" that considers that the strength along a fibre follows a traditional Weibull distribution (eq. 2.1), therefore it is possible to calculated the characteristic strength for the gauge length L. Curtin also states that the characteristic strength of each fibre are different and follow another Weibull distribution, leading to the "Weibull of Weibulls" distribution of fibre strength. There is still no consensus whether traditional Weibull or the modified Weibull distributions better represent the fibre strength.

2.1.3 The normal distribution

M. R'Mili et al. [19] studied the normal distribution to characterize the distribution of flaw strengths. They compared both normal and Weibull distributions to the results of tensile testing with large sample sizes of 500-100 data per test. The tensile tests were done in tows and the fractures were determined by acoustic emission monitoring. In order to eliminate the variability associated with the fibre radius the probability functions were determined as a function of strain (ε), which leads to the following equation for the Gaussian probability density function:

$$f\left(\varepsilon\right) = \frac{1}{S\sqrt{2\pi}}\exp\left[-\frac{\left(\varepsilon-\mu\right)^2}{2S^2}\right] , \tag{2.4}$$

where μ is the mean and S is the standard deviation, which can be fitted to the experimental failure data. The Weibull distribution can also be written in terms of strain (ε) resulting in:

$$P_W = 1 - \exp\left[-\left(\frac{V}{V_0}\right)\left(\frac{\varepsilon}{\varepsilon_0}\right)^{m}\right] , \tag{2.5}$$

whith $\varepsilon_0 = \sigma_0/E$. M. R'Mili et al. [19] concluded that the normal distribution is appropriate to describe the flaw strengths in brittle fibres, but also concluded that the Weibull distribution is a good approximation to this distribution and leads to simpler equations of failure probability.

As discussed there are several distribution to characterize the failure probability of fibres being the most used the traditional Weibull distribution (Equation 2.1). The determination of the parameters necessary for these distributions is not a simple one, meaning that large samples need to be tested in order to obtain representative parameters. The problems in obtaining the statistical parameters for fibre strength makes it hard to get a single distribution to characterise this property and, therefore, many statistical parameters can be found in the literature for the same type of fibre.

2.2 Size effects in composites

Size effects affect, not only the strength of individual fibres, but also influencing the failure process and longitudinal strength of composite structures [1]. There are several factors that lead to this size effects, being that most authors agree that the statistics of fibre strength are essential for this. Several authors have experimentally proven this size scaling behaviour (see Figure 2.1).

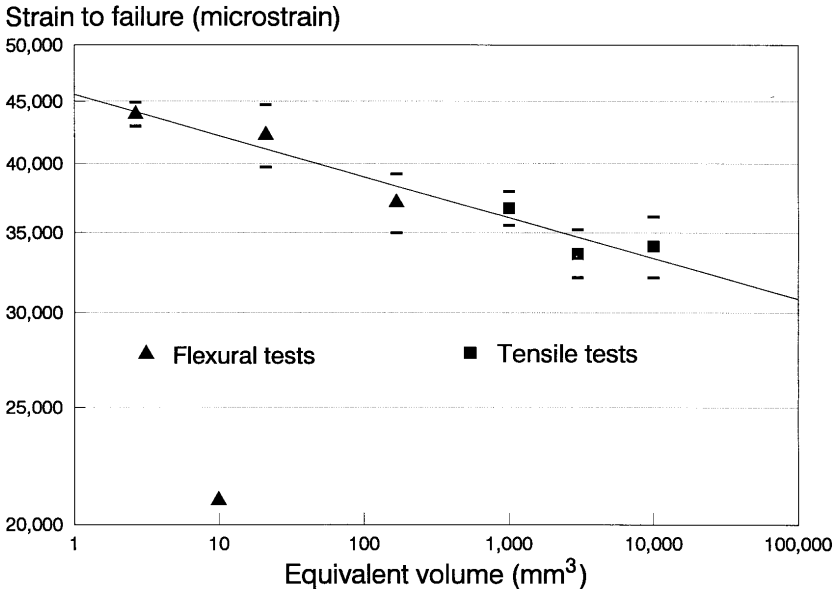

Figure 2.1: Size effects in glass/epoxy composites [1].

The size effect is not only affected by statistical aspects, but is also by deterministic factors, that include the effects of the damage process zone and the change of the failure modes [24]. There are other influencing factors, namely the influence of manufacturing and testing. This means that in order to achieve a good design of large composite structures based on coupon testing, one has to take into account that the coupons should be representative of the manufacturing process of the large scale component and that larger structures have lower strength due to being more

probable the existence of a critical defect [1]. One of the factors that leads to size effect due to manufacturing is the fact have larger fibre waviness and overall defects present in larger components than in small coupons.

2.3 Stress redistribution after fibre failure

The statistical distributions presented allow the determination of the strain at which a fibre will fracture. If a global load sharing rule is considered, then the stress that the fractured fibre carried is transferred equally to all the remaining intact fibres. This type of load sharing rule is able to predict the failure of lubricated tows, where the fibre interaction is low [18], but it's not accurate for composite materials where the fibres are bonded by a matrix, where their is high interaction between fibres.

The interaction between the fibres and between the fibres and the matrix results in a non uniform stress redistribution to the intact fibres, which is highly dependent on the composite geometry [25]. The models that consider a non uniform stress redistribution are said to consider a local load sharing rule. For composite systems the redistribution of stresses is a complex process that depends on several parameters, including the strength and sliding resistance of the fibre/matrix interface, the fibre to matrix moduli ratio, the matrix cracking or yield stress and the regularity of the fibre spacing [26]. This complex stress redistribution is often characterised by the stress concentration factor (SCF) and the ineffective length [2]. The SCF is the an adimensional parameter that is defined as the ratio between the longitudinal stress in an intact fibre after the failure of a neighbour fibre and the longitudinal stress in the absence of breaks. The stress in the absence of breaks is usually considered the stress in the intact fibre far from the plane of break, which simplifies the determination of this parameter. After a fibre breaks it locally looses the ability to carry stress, even so, away from the failure plane it is still able to carry loads, which means that a fibre doesn't fully loose the ability to carry stress after it breaks. The ineffective length is a measure of the stress recovery length of the fibre and can be defined as twice the length at which the broken fibre can carry 90% of the applied stress [27]. These parameters are crucial in the modelling of composite materials as they will affect the stress redistribution and, therefore, the damage accumulation and the formation of clusters of broken fibres.

The redistribution of stress is closely related with the fibre packing. There are several types of fibre packings that one can consider when modelling the microstructure of a composite material, some are represented in Figure 2.2.

A 1D packing consists in a single row of fibres that can be equally spaced or

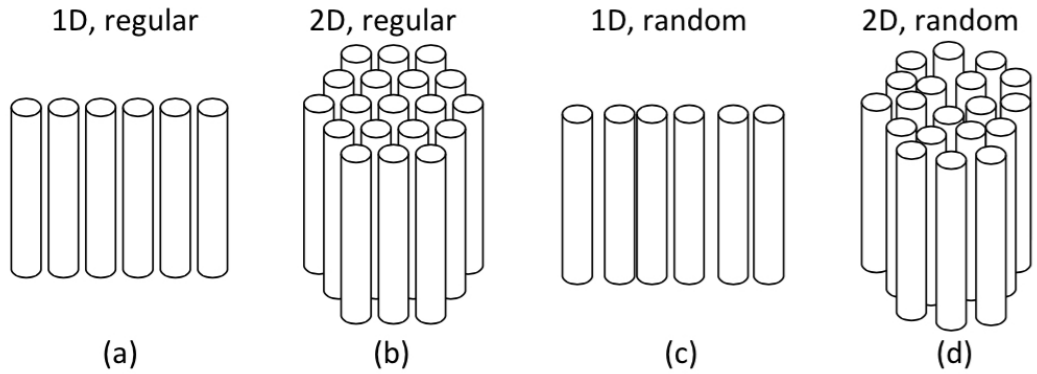

Figure 2.2: Schematic illustration of fibre packings: (a) 1D regular packing, (b) 2D regular packing (c) 1D random packing and 2D random packing [2].

randomly spaced. This type of packing is more common than 2D packings as it is easier to obtain, however it fails to give a accurate representation of the composite behaviour and leads to an overestimation of the stress concentration factors, making 2D packings more accurate to describe the micro-structure of composite materials. Being so, a 2D packing with random distribution of fibres is the model that most accurately represents the microstructure of a composite material, as it better relates with the real distribution of fibres in these materials [28]. The random distribution of fibres instead of a regular packing, leads to a varying fibre spacing and, therefore, changes the stress distribution. Obtaining this random distributions is more difficult and computationally expensive than regular ones, however the random fibre generator developed by Melro et al. [14] is able to do so in a reduced time. Another problem of using random fibre packings in FE analysis is that the variations of fibre spacing lead to some problems with the meshing. Nonetheless, if it is possible to use a random distribution, one should do so, as it translates better into the real microstructures and behaviour of fibrous composites.

2.4 Critical cluster size

As already mentioned, the failure of a UD composite under tensile loads is due to the unstable propagation of a cluster of broken fibres. The clusters are formed due to stress concentrations in the intact fibres that neighbour a broken one. This increase in SCF causes the stress in the intact fibres to increase, thus increasing their probability of failure, making it more probable that fibres will fail in clusters. When a cluster of broken fibres is large enough, it propagates in an unstable manner, leading to the composite failure. Critical cluster size is, therefore, an important topic in understanding the failure of UD composites.

Ibnabdeljalil and Curtin [29] studied this problem and derived an equation for

the critical cluster size (n^{crit}):

$$n^{\text{crit}} = 403m^{-1.28} , \tag{2.6}$$

where m is the Weibull modulus. This equation was derived from numerical simulations using Green's function for stress redistribution, whose parameter Ω characterises the level of localization of the stress redistribution. The result presented in Equation 2.6 is for $\Omega = 0.001$, that represents a very local load sharing model ($\Omega \to \infty$ corresponds to global load sharing).

As the Weibull modulus presents some degree of dispersion, even for the same type of fibre, one can expect that, in a composite material, there are stronger and weaker regions [29], which will translate in variations of the critical cluster size and composite strength.

Although with some difficulties, the critical cluster size was also tackled in an experimental way. Using synchrotron computed tomography, Scott et al. [3] found a cluster size of 14 fibres (14-plet) prior to failure (Figure 2.3). This cluster was found at 94% of the failure strain, which means that the critical cluster size should be superior to 14.

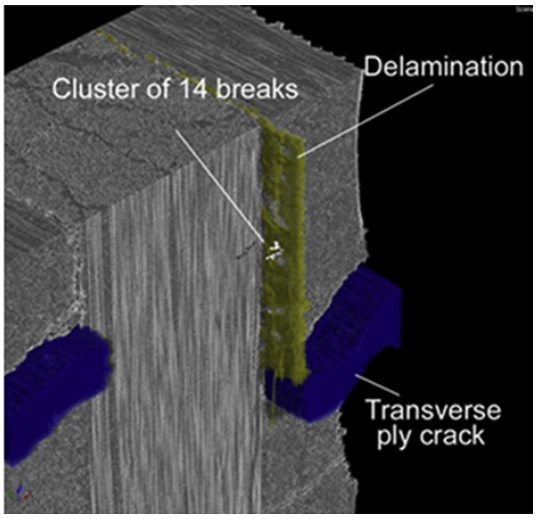

Figure 2.3: Cluster of 14 fibres observed by Scott et al. [3] using synchrotron computed tomography.

Other authors have done similar studies. For example Aroush et al. [30] found a critical cluster size in the range 9-33 for quartz fibre reinforced epoxy resin.

2.5 Effects of the matrix and fibre-matrix interface

The tensile failure of composite materials is a fibre dominated phenomena, however the matrix also plays an important role. The matrix allows the stress recovery of a broken fibre due to shear stress transfer [2] and its properties affect the stress concentration factors and failure mechanisms.

Several models consider the fibres and matrix to be perfectly bonded, which leads to a infinite stress concentration factor in the matrix around a fibre break. The matrix and the interface is unable to support such a high stress three scenarios can occur: (1) the matrix yields, (2) the interface debonds and (3) the matrix cracks in the break plane. [2] There can also be a combination of these. Zeng et al. [31] studied the influence of interfacial damage in the stress redistribution in UD composites and concluded that the stress concentrations increased with increasing the strength of the interface. He also concluded that matrix shear yielding resulted in lower stress concentration factors in intact fibres. The matrix yield strength also affects the ineffective length significantly. The lower the shear yield stress, the larger the ineffective length [32]. Interfacial debonding tends to occur in composites with weak interfacial bonds, and has a similar effect as matrix yielding. Both matrix yielding and interfacial debonding have been extensively studied in the literature, however the matrix cracking hasn't been objective of focus.

Recently, Swolfs et al. [33] studied the influence of matrix cracks in both the SCF and the ineffective length in a composite with a random distribution of fibres. The authors concluded that the matrix cracking increases the ineffective length, drastically changing the stress recovery profile. As one can see in Figure 2.4, the stress in the broken fibre rapidly increases to 35% when there isn't a crack in the matrix, however, in the model with a crack, the stress slowly increases from zero, due to the presence of a crack in the matrix. Swolfs et al.[33] also showed that matrix cracks not only increases the ineffective length but, also the stress concentration factor, leading to an overall higher failure probability of the intact fibres.

According to Hobbiebrunken et al. [34] the matrix strength is size dependent. In fibrous composites the matrix usually has a small thickness in the order of a few microns, thus having a strength higher than that of large test specimens. As the matrix strength affects the tensile behaviour of composites, not accounting for this size effect may lead less accurate results.

Morais [35] studied the effect of the matrix shear modulus in the range $1.2 - 1.6$ GPa and he concluded that the tensile strength of the composite material is practically insensitive to this parameter. However, he concluded the matrix shear strength is an important factor in the composite tensile strength. His results showed that increasing the shear strength from 40 to 100 MPa increased the composite

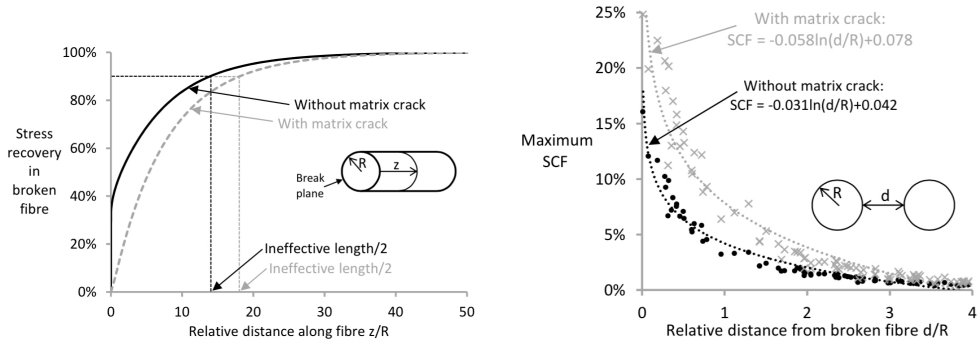

Figure 2.4: Effect of matrix cracks in the ineffective length (left) and the stress concentration factors (right) [2].

strength from 1300 to 1600 MPa for T300 carbon fibre and from 2400 to 3100 MPa for T800 carbon fibre. This changes are due to modifications in the stress recovery profiles of the fibres. Pimenta and Pinho [6] reached similar conclusions using a different model.

2.6 Modelling the tensile failure of unidirectional composites

There are several models to predict the tensile failure strength of UD composites in the literature. Mishnaevsky and Brøndsted [36] consider four categories of models: analytical models, fibre bundle models, fracture mechanics models and continuum damage mechanics models. The latter models usually lead to complex simulations, being therefore limited in the size of the models.

In the next sections several models to predict the tensile failure of composites will be presented. The models are presented in five subsections. The first is about the deterministic rule of mixtures, the second presents the analytical fibre bundle models, the third presents the micromechanical models based on Monte-Carlo simulations, continuum damage mechanics based models and the last one presents a recent model based on a hierarchical scaling law.

2.6.1 Deterministic rule of mixtures

The rule of mixtures is the simplest model to predict the tensile strength of UD composites. For the majority of composite materials the failure strain of the reinforcing fibres (ε_f) is lower than the failure strain of the matrix (ε_m), which means that the fibres will fail first. Usually composite materials have a fibre volume

fraction (V_f) around 50 to 70% and, after the fibres fail, the matrix is not able to carry the stress. This means that the failure strain of the composite (ε_C) is equal to the failure strain of the fibres (ε_f). This assumptions translate into the following equation for the composite tensile strength (X_C^t):

$$X_C^t = V_f X_f^t + (1 - V_f) \frac{E_m}{E_f} X_f^t;, \tag{2.7}$$

where X_f^t is the fibres' tensile strength and E_f and E_m are, respectively, the fibre and matrix stiffness. According to the already reviewed influencing factors of the tensile strength, this model fails in two aspects. Firstly, it considers the fibre strength to be a deterministic one, which was already proven to not be realistic, as the tensile strength of fibres follow a statistical distribution. The second flaw is that the model doesn't consider interaction between components and therefore it fails to accurately predict the tensile strength of UD composites.

More advanced and accurate models are presented in the next sections.

2.6.2 Analytical fibre bundle models

Fibre bundle models (FBMs) consider a bundle of parallel fibres with stochastic tensile strength, but with the same elastic properties and loaded under uniaxial tension [36]. When the remote stress is high enough to make the weakest fibre fracture it breaks and the stress is redistributed towards the remaining intact fibres. If the stress concentration, due to this stress redistribution, is enough to make another fibre fail, it will fail and the stress is redistributed again, if not the remote stress is increased. This process is repeated until all fibres fail or until the material cannot withstand further load increments. FBMs have been developed for dry bundles (with no matrix) and for composite materials, considering the influence of the matrix. The matrix acts as a connector between fibres and alters the stress redistribution, affecting the ineffective length and the stress concentrations in the neighbouring fibres of a broken one. According to the stress distribution rule this models can be divided into global load sharing (GLS) models and local load sharing (LLS) models. The GLS models are able to predict the failure of a dry bundle where the interaction between the fibres is low [18]. The LLS models consider that there isn't a uniform stress redistribution due to the presence of the matrix.

Global load sharing models

The first fibre bundle model was developed by Daniels [37] and was later developed by several authors. This model considers a bundle composed of N fibres

with a defined length (l_r), and the fibre strength is considered to follow a Weibull distribution (Equation 2.1). He determined the following law relating the stress in the bundle (σ^∞) with the applied strain (ε^∞):

$$\sigma^\infty = E_f \varepsilon^\infty \cdot S_f\left(\sigma^f\right) \ , \tag{2.8}$$

where E_f is the fibre longitudinal modulus, σ^f is the stress actuating in the intact fibres and $S_r^f\left(\sigma^f\right)$ represents survival probability under the stress σ^f of a fibre with length l_r. In this equation the contribution of the matrix to the load carrying capacity has been neglected. This model allowed the conclusion that the tensile strength of a bundle with a large number of fibres can be represented by a normal distribution and the expected value for the strength of the bundle is given by:

$$X_r^b = \frac{\sigma_r^f}{m^{1/m} e^{1/m}} \qquad \text{where} \qquad \sigma_r^f = \sigma_0^f \left(\frac{l_r}{L_0}\right)^{-1/m} \ . \tag{2.9}$$

σ_0^f, m and l_0 are the characteristic parameters of the Weibull distribution and e is the base of the natural logarithm. As this model was developed for dry bundles it considers that a broken fibre is no longer able to carry load, which is not accurate in the presence of a matrix.

Rosen [27] considered the influence of the matrix trough a shear-lag model. This model considers that the stress is transferred, by the matrix, that is loaded in shear, back to the broken fibre. This means that there is a stress recovery in axial direction of the broken fibre. This leads to the definition of the ineffective length as the distance δ from the break where the fibre recovered the ability to carry a percentage ξ (e.g. 90%) of the remote stress. Using his model he derived the following expression for the ineffective length δ:

$$\delta = \frac{\phi_f}{2} \sqrt{\frac{1-\sqrt{V_f}}{\sqrt{V_f}} \frac{E_f}{G_m}} \ln\left[\frac{1}{1-\xi}\right] \tag{2.10}$$

where ϕ_f is the fibre diameter and G_m is the matrix shear modulus.

Rosen considered that a bundle with length l_r could be divided into a chin of bundles width lengths l_r/δ and that the longer bundle will fail as soon as one of the sub-bundles fails, according to the weakest link theory. As the strength distributions of the sub-bundles are given by Daniels' approach and, therefore, follow a normal distribution $F_\delta^b\left(\sigma^\infty\right)$. This assumptions mean that the bundle follows weakest link theory and the strength distribution for a bundle with length l_r can be calculated by:

$$F_r^b\left(\sigma^\infty\right) = 1 - \left[1 - F_\delta^b\left(\sigma^\infty\right)\right]^{l_r/\delta} \ . \tag{2.11}$$

For the particular case of a very large bundle ($n \to \infty$), the standard deviation of the sub-bundle strength equal to zero and Weibull fibre strength distribution, the most likely failure strength of the bundle with length l_r is given by:

$$X_r^b = \frac{\sigma_r^f}{m^{1/m} e^{1/m}} \qquad \text{where} \qquad \sigma_r^f = \sigma_0^f \left(\frac{\delta}{L_0}\right)^{-1/m} . \tag{2.12}$$

This equation is similar to the one presented for Daniels' model (Equation 2.9), except for the length correction in the Weibul distribution. This means that while Daniels' model considers the full length of the bundle (l_r), Rosen's model considers only the ineffective length (δ). Equation 2.12 is a simplification of the general model (Equation 2.11) and represents a deterministic model based of the average fibre strength, and therefore isn't able to capture size effects [4].

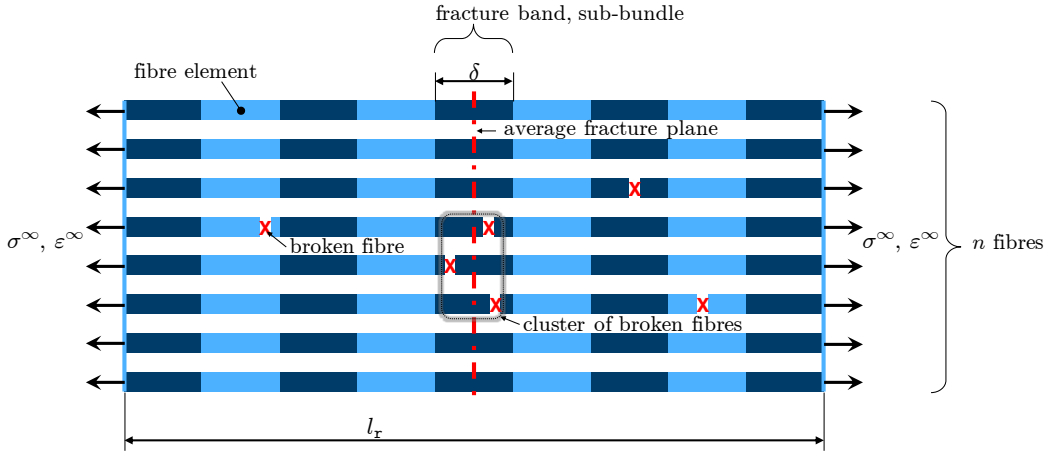

Figure 2.5: Diagram of a fibre bundle model [4].

Curtin [38] developed a fibre bundle model aimed for ceramic-matrix composites, that considers global redistribution of stress. This model considers a fracture band centred at the average plane of a bundle and for each remote stress σ^∞, a fraction of the bundle fibres χ are fractured at a random distance from the middle plane (see Figure 2.5). The fracture band as a length δ and each fracture is located at a distance l_{po} from the average plane. The broken fibres recover stress linearly, according to the shear lag model with a constant shear stress τ_{SL}. Being the undisturbed stress of a fibre σ^f, it is possible to define the fracture band length δ as:

$$\delta = \frac{\sigma^f \phi^f}{2\tau_{SL}} . \tag{2.13}$$

It is possible then to calculate the stress of a broken fibre at the average fracture plane (matrix crack) σ_{po}, which is given by:

$$\sigma_{po} = \frac{4 l_{po} \tau_{SL}}{\phi^f} . \tag{2.14}$$

With the Equations 2.13 and 2.14 one can relate the stress at the average fracture plane with the undisturbed stress, resulting in:

$$\frac{\sigma_{po}}{\sigma_f} = \frac{2l_{po}}{\delta} \ . \tag{2.15}$$

Considering a random distribution of fracture within a band, the average pull-out length will be $\delta/_4$ resulting in a average pull-out stress equal to $\sigma^f/_2$. Curtin assumes that the fraction of broken fibres within a bundle χ is given by a Weibull distribution (with parameters σ_0,l_0 and m), as follows:

$$\chi = \frac{\delta}{l_0}\left(\frac{\sigma^f}{\sigma_0}\right) \ , \tag{2.16}$$

which can be manipulated into

$$\chi = \left(\frac{\sigma^f}{\sigma_\delta^f}\right) \ , \qquad \text{where} \qquad \sigma_\delta^f = \left[\frac{2\left(\sigma_0\right)^m \tau_{SL} l_0}{\phi_f}\right]^{1/m+1} \ . \tag{2.17}$$

The parameter σ_δ^f is the key strength of the material. Considering the overall force equilibrium of the composite material and considering V_f as the fibre volume fraction, the composite tensile strength X_b^r results as:

$$X_r^b = V_f \sigma_\delta^f \frac{m+1}{m+2}\left(\frac{2}{m+2}\right)^{1/m+1} \ . \tag{2.18}$$

Curtin's model is an improvement over Rosen's model as it accounts the stress of broken fibres in the tensile strength and considers a characteristic length (δ) that isn't constant and scales with the applied stress [4]. The models presented in this section consider a global load sharing rule, which is considered not to be very accurate and therefore limits the application of this models.

Local load sharing models

The first person to address the non uniform redistribution of stress was Hedgpeth [39] in 1961. Considering a shear lag model and uniformly distributed parallel fibres he calculated the stress concentration factor in the neighbouring fibres as a function of the number of broken fibres r, resulting in:

$$K_r = \frac{4 \cdot 6 \cdot 8 \cdot \ldots \cdot (2r+2)}{3 \cdot 5 \cdot 7 \cdot \ldots \cdot (2r+1)} \ . \tag{2.19}$$

Later, Hedgepeth and Dyke [40] extended this model to a 2D arrangement of fibres.

At this point here is no universally accepted rule, although there has been many publications about this subject using different approaches: shear-lag models, FE analysis, variational mechanics, fracture mechanics. The stress redistribution, as already mentioned, affected by fibre packing, interaction between breaks, dynamic factors and others, and including a complex model for stress redistribution in a complex fibre strength model may lead to too complex models. Therefore, many models considers simplified stress redistribution models.

According to Pimenta [4] one of the most influential local load sharing fibre bundle model is the one developed by Harlow and Phoenix [41, 42]. This model considers a bundle composed of n fibres, with a length δ, in which the fibres strength is characterized by a Weibull distribution ($F^f(\sigma)$). They consider that the stress concentration due to a cluster of r broken fibres is $K_r = 1 + r/2$. The bundle probability failure ($F^b(\sigma)$) was obtained considering all the different sequences of fibre breaks leading to failure. Since the number of sequences is equal to 2^n, only bundles with less than nine fibres ($n < 9$) were considered. The main conclusions resulting from this model are:

- At high loads, the failure probability of the bundle follows the weakest link theory (WLT), leading to a Weibull distribution with same shape parameter as the fibre distribution: $f^b(\sigma) = 1 - \left[1 - F^f(\sigma)\right]^n$;
- At low loads, the failure probability follows a Weibull distribution with a higher shape parameter than the shape parameter for fibre distribution, resulting in less dispersion of the bundle strength: $m^b = n \cdot m^f$;
- As the bundle size increases, the asymptotic behaviours mentioned start governing the strength distributions;
- The size effects are lower in bundles with increasing number of fibres;
- The strength distribution for large bundles follows a Weibull distribution, within reasonable probabilities;
- It is possible to determine the equivalent single-fibre strength distribution through the WTL based on the strength distribution of a large number of fibres. The authors also noted that it is possible to estimate the strength of any large bundle with $n \geq 7$ following the WLT.

The results obtained by Harlow and Phoenix are exceptionally accurate and have been supported by more recent models and experimental results.

There are other LLS models that take into account other stress redistribution rules. One of this examples is the model developed by Ibnabdeljalil and Curtin [29] that considers the stress redistribution based on Green's function, whose parameters

can be adjusted to consider a certain level of local load sharing.

2.6.3 Micromechanical models based on Monte-Carlo simulations

Monte-Carlo simulations of micromechanical models have been used to predict the tensile behaviour of UD composites, some assisted by finite element analysis. These models consider a large number of fibres, that are divided in segments, to which is applied a probabilistic failure strength, normally based on a length scaling Weibull distribution. Models are ran with different fibre strength realisations to simulate cluster formations and stress redistributions. Large number of simulations are done until there is enough data to fully characterise the material's behaviour.

There are some challenges when developing a Monte-Carlo simulations based model. Firstly, one needs to calculate the stress fields around broken fibres. Secondly, one needs to be able to do progressive failure analysis of cluster growth.

These models are usually grouped into three groups [4]:

- **Single-step Spring-based models**, that are models based on simplified shear-lag redistribution of stress and consider stochastical strength of fibres.
- **Combined field-superposition and fibre bundle simulations**, that consider a simple superposition method of the stress fields around broken fibres. These stress fields are obtained for a single fibre break and superposition of fields is imposed. This fields are included in Monte-Carlo simulations of fibre bundles.
- **Two-scales finite element models**, which consider a macro model to be composed of several Unit Cells (UC). Using micromechanical simulations of the UCs, the stress fields with different number of fibre breaks are calculated. This stress fields are then used in the macro model using Monte-Carlo simulations.

Single-step spring-based models

Single-step spring-based models consider a lattice of nodes that are longitudinally connected by fibre springs and transversely by matrix springs (see Figure 2.6). The fibre springs can only support longitudinal load and their strength is stochastic. The matrix springs are considered to only being able to support shear stress. The movement of the nodes is limited to longitudinal displacement, which means that there is only one degree of freedom.

One of the most acknowledged single-step spring-based models is the one devel-

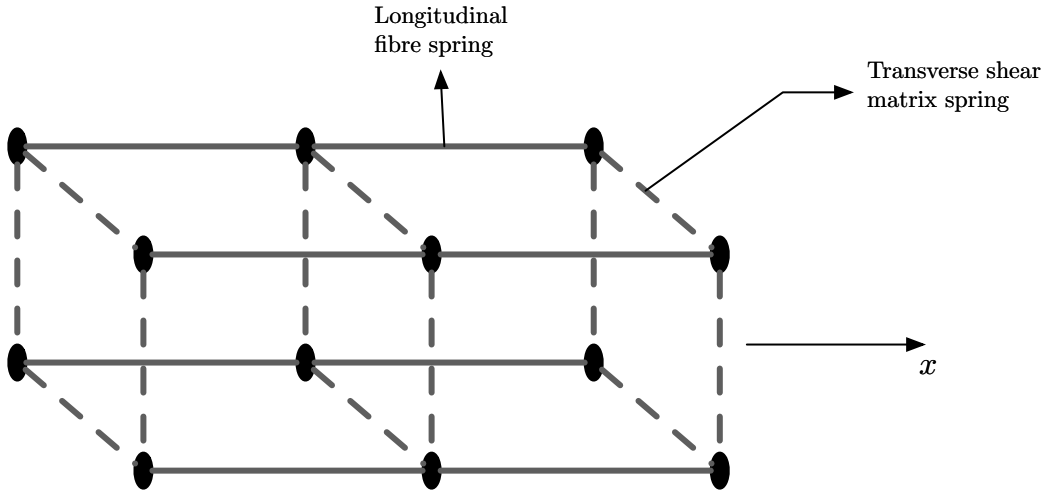

Figure 2.6: Representation of the node lattice of a single-step spring-based model.

oped by Okabe et al. [43, 44] and is named Spring Element Model (SEM). The SEM considers a hexagonal arrangement of nodes, connected longitudinally by N^f linear elastic fibre spring elements with a random strength Xf_l, stiffness E^f and length l. It is then possible to calculate the longitudinal stiffness matrix $\boldsymbol{K}^f$ as a function of the area, length, stiffness of the fibres and nodal connectivities. In the transverse plane the nodes are connected by N^m linear elastic shear matrix springs, which can be arranged into the stiffness matrix $\boldsymbol{K}^m$, as function of the matrix properties, including the thickness. The nodes have only longitudinal displacements which can be arranged in the matrix $\boldsymbol{u}$.

A fibre fails when the applied stress is equal to its tensile strength (which is stochastic). If a fibre fracture, it recovers stress linearly according to the shear lag models with perfectly plastic matrix. At a given stress state there are N_b^f broken fibre elements and N_{SL}^f fibre elements whose stress is lower than the applied stress due to a nearby break in that fibre. Therefore, the overall equilibrium for the model results in:

$$\left(\sum_{N_i^f} \boldsymbol{K}^f + \sum_{N^m} \boldsymbol{K}^m\right).\boldsymbol{u} + \sum_{N_{SL}^f} A^f \int_{x_i}^{x_i+l} \boldsymbol{B}^{f\intercal} \sigma_{SL}\left(x\right)\, \mathrm{d}x = \boldsymbol{f}\ , \tag{2.20}$$

where N_i^f is the number of intact fibre elements in the model, $\boldsymbol{B}^f$ is the deformation matrix of the fibre elements and $\boldsymbol{f}$ is the matrix with the nodal applied forces. Equation 2.20 can be computed and at each increment of applied stress/strain there is the need to determine if any fibre fractures, if so a new equilibrium needs to be calculated. This process is repeated until there is failure of the composite.

Combined field super-position and fibre bundle simulations

Combined field super-position and fibre bundle simulations models derive from the basic fibre bundle models (section 2.6.2), but consider more accurate stress redistribution rules. This models are composed by three components:

- A deterministic model for stress redistribution to the neighbouring fibres after a fibre breaks;
- A super-position rule to account the effect of multiple fibre breaks in the stress redistribution;
- A Monte-Carlo simulation of the fibre bundle model. Due to the complexity of the stress redistribution this models aren't purely analytical as the ones referred in section 2.6.2.

Several models have been presented using this kind of analysis, but considering different stress concentration factors and different super-position techniques [45–47]. The most recent model was developed by Swolfs [2]. This model uses FE to determine the stress redistribution profiles around a broken fibre. The FE model consisted of a circular RVE with a broken fibre in the center, with the remaining fibres arranged in a random packing. The stress concentration factors were studied as a function of distance to the broken fibre. It was studied the effects of matrix cracks [33], volume fraction, fibre/matrix stiffness ratio, isotropic vs anisotropic fibres [16] and others. In his studies he concluded that the stress concentrations depended mainly on the distance to the broken fibre and the other parameters only have a small influence.

The stress concentration profiles from FE were used to get trend-lines to be used in the FBM. The fibre bundle model considered a bi-modal Weibull fibre strength and a random fibre packing. The interaction between breaks was taken into account with a enhanced superposition method (Figure 2.7). This method firstly considers the linear superposition of stress fields due to the broken fibres, which doesn't guarantee the force equilibrium. In order to do so, the SCF that the broken fibres introduce in one another need to be redistributed. This redistribution is done proportionally to the original SCF in the linear superposition. Obtaining, therefore, a stress redistribution that guarantees the force equilibrium.

The stress redistributions are used as inputs to the FBM, based on Rosen's chain of bundles approach [27] (Figure 2.8), that are used to predict the material behaviour, which is considered to fail when, at least, 10% of the fibres have failed in the same axial segment with length 35 μm. This model considers typically 2000 fibres and are 10 mm long, divided into 35 μm segments to which is attributed a strength based on a Weibull distribution, at the beginning of each Monte Carlo

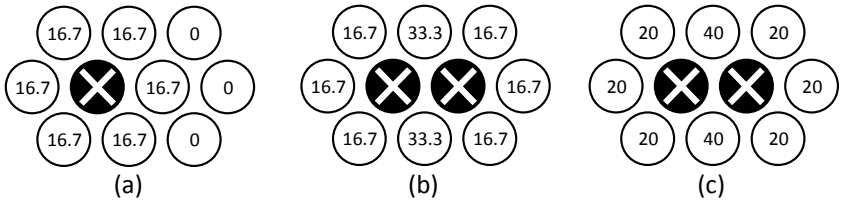

Figure 2.7: Schematics of the enhanced super-position stress redistribution: (a) stress concentration around a single break, (b) linear superposition results and (c) enhanced super-position [2].

simulation. This model was developed with the objective of incorporating different types of fibres in a RVE in order to study hybrid composites and his able to do so due to its versatility. According to the author [2] the discrepancies to the experimental data of this model are due to: (1) errors in the Weibull distribution, (2) neglecting dynamic stress concentrations and (3) averaging of the SCFs over the entire cross section of the fibre. Nonetheless, this model was used to predict the tensile behaviour and cluster formation in different composite materials with good results.

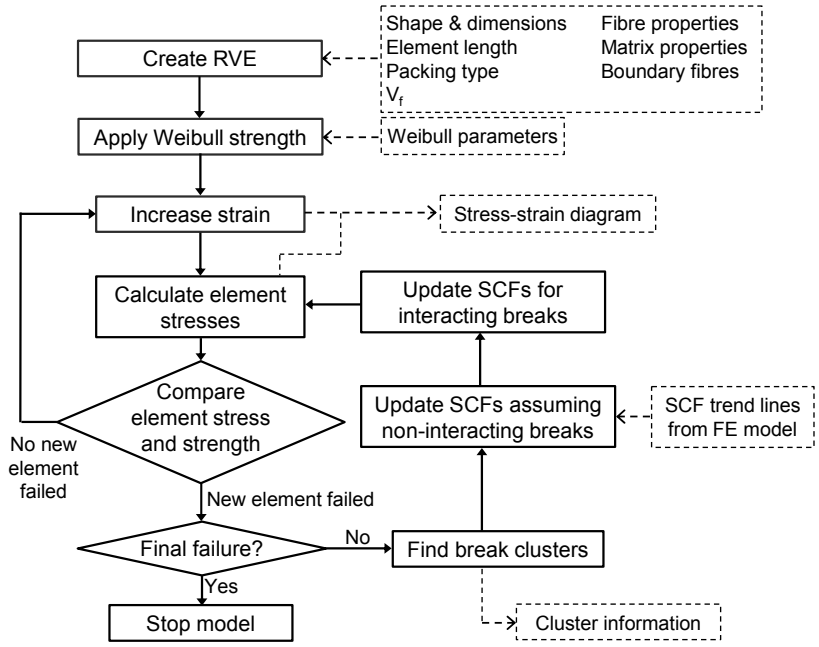

Figure 2.8: Flow chart of the model developed by Swolfs [2].

Two-scales FE models

Finite elements are extensively used in modelling composite materials, however, the prediction of micromechanical behaviour requires extremely refined meshes, mak-

ing the models computationally costly. This fine mesh is required in order to accurately capture the stress redistribution, especially when a random packing is considered. In order to avoid the use of such refined meshes in full scale models, coupled two-scale FE models have been developed [48, 49]. This separation of micro-macro scales allows the simulation of composites specimens with millions of fibres.

In the model developed by Thionnet et al. [49] the micro-scale model considers a Unit Cell (UC) with a length of 4 mm and 32 linear-elastic fibres arranged in a square packing. This UC are used to study the stress distribution due to different number of broken fibres (2,4,8 or 16 broken fibres). This micro-scales model are used to generate a library with the stiffness of the UC and the stress concentrations in the fibres for different damage states [4].

The macro-scale FE model is composed of several UCs with one integration point to which is attributed a fibre strength given by a Weibull distribution. The damage state of the UC is considered to evolve from no damage to 2, 4, 8, 16 and 32 broken fibres, and the library of micro-scale models is used to predict the stress concentrations and stiffness reduction as function of the damage.

It is considered that the specimen fails when there is a numerical instability, due to a rapid increase of the strain in constant stress. This model was used to predict the behaviour of UD composites under different loading conditions [49]. Also, it was considered the effect of time in the simulations, which lead the authors to conclude that time is an important factor due to visco-elastic behaviour of the matrix.

Monte-Carlo based models are extensively used in the literature, however they require a very fine mesh and large number of simulations in order to accurately capture the material response. Nonetheless, they are very versatile and allow to take into account several factors that most models aren't capable of.

2.6.4 Continuum damage mechanic based models

The failure mechanisms of UD composites can be described in the framework of continuum damage mechanics. This type of modelling uses simple definitions of internal damage variables, formulated in the framework of the thermodynamics of irreversible process [36]. These damage variables are then used to alter the mechanical properties of the constituents, namely the reduction of stiffness.

This type of modelling has been tackled by several authors and can be divided into three stages: (1) definition of a suitable norm for the damage variable, (2) definition of a damage criterion and (3) definition of the evolution law for the damage variable [5]. Matzenmiller et al. [50] developed a model that relates the effective elastic properties and the damage state of the composite material, and studied the

influence of the material parameters in the stress-strain diagrams.

More recently, Turon et al. [5] developed a progressive damage model based on fibre fragmentation for UD composites. This model proposes a degradation of composite effective stiffness based on fibre fragmentation. The fibre fragmentation model considers that the fibre strength follows a Weibull distribution, and when the applied stress reaches the fibres tensile strength it will break. A broken fibre is still capable of carrying stress, according to a shear lag theory, and therefore it can fracture again at a certain distance from the original fracture. A fibre will fracture into shorter fragments until the shear stress transfer across the interface is no longer able to cause another fracture (Figure 2.9).

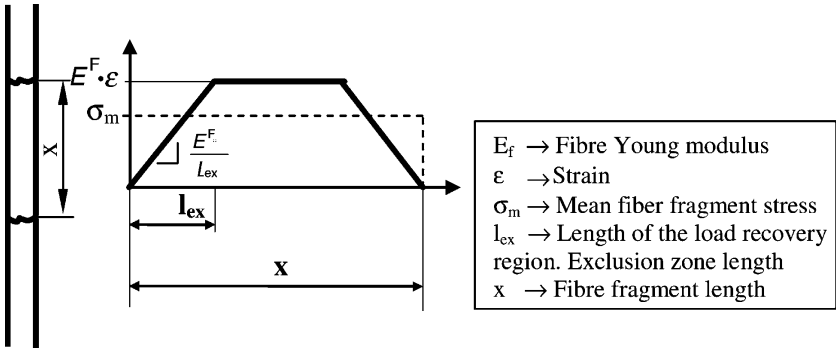

Figure 2.9: Stress profile in a fibre with multiple fractures, according to shear-lag model[5].

Based on the multiple fracture of the fibres, the authors formulate a damage model that considers a global load sharing rule and the influence of each component of the material is accounted for by using the mixity law. The authors used this model, implemented in a FE model to study the effect of several parameters on the stress-strain curve and were able to accurately capture the stiffness loss in UD composites.

2.6.5 Hierarchical scaling law for the strength of composite fibre bundles

Pimenta and Pinho [6] developed a model that considers a scaling law for composite strength. They consider the composite to be composed of bundles with different levels, and that a bundle of the level $i+1$ is composed of two level-i bundles (see Figure 2.10). The level-0 bundle is composed of a singular fibre (embedded in the matrix), which means that a level-i bundle has number of fibres n^i equal to 2^i.

The model firstly considers a level-1 bundle of length l_r which is remotely loaded with a tensile stress σ^∞. When both fibres are intact their stress is considered

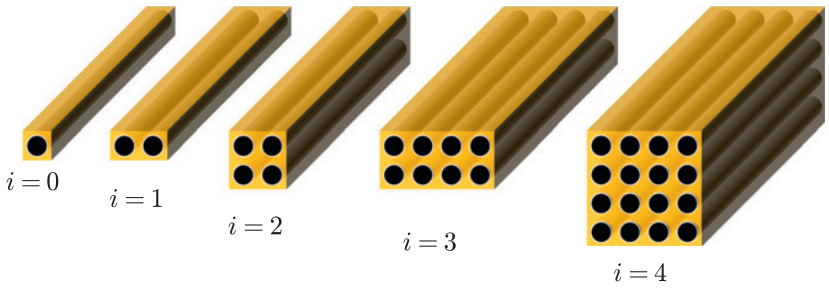

Figure 2.10: Hierarchical fibre bundles [6].

equal and equal to σ^{∞}. The strength of the fibres is consider to follow a Weibull distribution. When the weakest fibre in the level-1 bundle fails, the broken fibre is assumed to follow a perfectly-plastic shear-lag formulation, with shear strength τ_{SL} and, therefore, the broken fibre linearly recovers its capacity to carry load (in the length l_e). Has the broken fibre locally looses its ability to carry stress, there is a stress concentration in the remaining intact fibre, increasing its probability of failure. A level-1 bundle is considered to fail if both fibres fail in nearby locations, close enough to promote complete yielding of the matrix. Is so possible to define a control region, where if the second fibre breaks leads to the failure of the bundle (see Figure 2.11). This region has a length $l_c = 2l_e$.

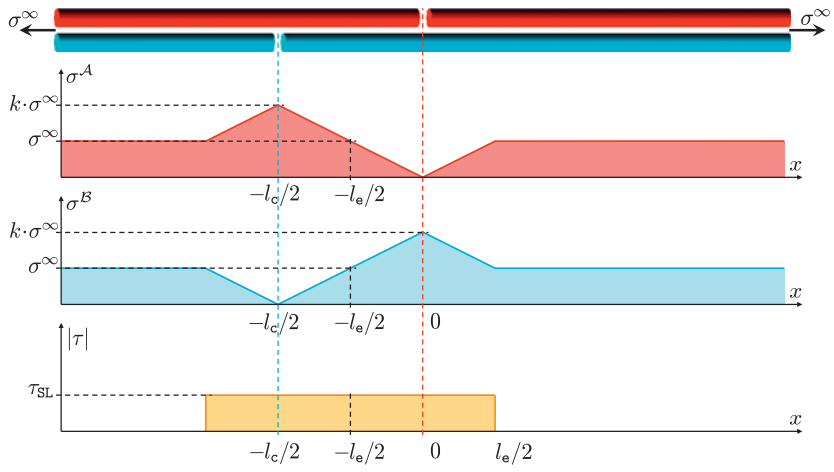

Figure 2.11: Definition of control region [6].

A level-1 bundle with length l_c survives an applied remote stress σ^{∞} in the following situations:

- If the stress σ^{∞} is lower than the strength of both fibres. Which means that the four elements with length L_e remain intact. If the survival probability of a level-0 bundle is $S^0_{U,e}$, then the survival probability of the four regions is $\left[S^0_{U,e}\right]^4$;

- If the weakest fibre fails in the stress σ^{∞} and the surviving fibre is able to support the stress concentration. The stress is the intact fibre (Figure 2.11) consists of half a length of constant stress and the other half with linear stress concentrations. If the surviving probability of a element with length l_e under linear stress concentrations is $S^0_{K,e}$, the probability of the bundle to survive in this conditions is given by: $2\left[1-\left(S^0_{U,e}\right)^2\right]S^0_{U,e}S^0_{K,e}$.

Considering both events, the failure probability of a level-1 bundle with length l_c, under the stress σ^{∞} can be expressed as

$$S^1_{U,c} = \left[S^0_{U,e}\right]^4 + 2\left[1-\left(S^0_{U,e}\right)^2\right]S^0_{U,e}S^0_{K,e}\ . \tag{2.21}$$

The authors consider a self-similar hierarchical failure process and generalise the failure events to higher order bundles, obtaining the following hierarchical scaling law:

$$S^{i+1}_{U,c} = \left[S^i_{U,e}\right]^4 + 2\left[1-\left(S^i_{U,e}\right)^2\right]S^i_{U,e}S^i_{K,e}\ , \tag{2.22}$$

where the probabilities with the superscript i refer to the failure modes of a level-i bundle, the same for the superscript $i+$. The subscript U refers to uniform stress in the bundle region and the subscript K to linear stress concentrations in that region.

The survival probability distributions $S^i_{U,e}$ and $S^i_{K,e}$ can be calculated analytically, taking into account that:

$$l^i_e = 2\frac{n^i A^f}{C^i \tau_{SL}\sigma^{\infty}} \qquad \text{and} \qquad l^i_c = l^{i-1}_e\ , \tag{2.23}$$

where C^i the shear-lag perimeter for a level-i bundle, τ_{SL} is the yielding strength of the matrix (or sliding resistance) and A^f is the area of a single fibre. It should be noted that the length of the damage zone increases, not only with the level of the bundle, but also with the applied stress. This means that the cluster of broken fibres has influence over a larger zone than a single fibre break.

This model is able to make predictions of tensile behaviour of composites with large number of fibres in short amount of time and is able to capture the size effects of composite materials.

2.7 Conclusion

In this chapter several models for tensile behaviour of UD composites have been presented, as well as the main influencing parameters in these materials' behaviour. It is well agreed that the failure of UD composites is a progressive one and that

fibre will fracture progressively forming clusters that will grow until a critical size is reached. This, in turn, results in an unstable propagation leading to failure. This process in governed mainly by the fibre strength statistics and the micromechanical stress redistribution, which has been proven to be affected by several parameters.

Several models, with different backgrounds and formulations, are able to accurately predict the behaviour of UD composites, however there are still improvements to be made. Most of the models don't include the increase in influence area of a cluster in relation that of a single broken fibre, which has been proven by experimental data [4]. Another aspect that most models fail to capture is the dynamic effects of the loading, which has been proven to affect the matrix properties. The dynamic effects are also present when a fibre fails, leading to dynamic stress concentrations that vary with time [39].

In the next chapter models will be presented for hybrid UD composites, and the main influencing factor in hybrid behaviour will be accessed.

Chapter 3

Hybridization-State-of-the-art

The previous chapter focused in understanding the mechanisms of failure in unidirectional composites. While it is important to understand the models and physical mechanisms of UD failure, the main goal of this thesis is the understanding of the failure mechanisms of hybrid unidirectional composites. To do so, it is necessary to understand the main aspects regarding hybrid composites and the main parameters that influence their behaviour.

In this chapter, the state-of-the-art of hybrid composites will be reviewed, firstly focusing on the general aspects of hybrid composites, including the main effects of hybridization under different loadings. Later on, the models for tensile failure of UD hybrid composites will be reviewed and conclusions will be drawn regarding the most influential parameters of their behaviour.

3.1 Hybrid composites

Fibre-reinforced composites play a fundamental role in aircraft structural applications, however their optimal use is still hampered partly due to the relatively low toughness they exhibit. Hybridisation is a strategy that can lead to improved composite properties.

Hybrid composites can be defined as a composite material that contains more than one of type of fibre and/or matrix system [51]. The main focus of this work will be in the hybrid composites with more than a single type of fibres, the so called fibre-hybrid composites.

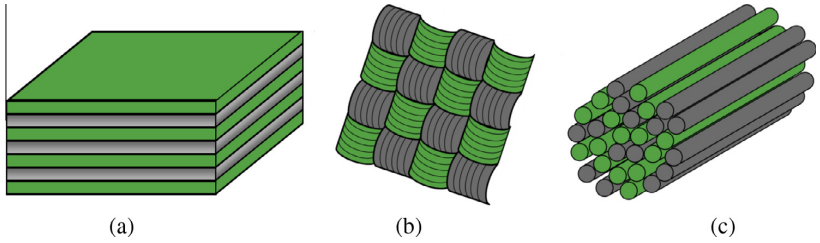

Figure 3.1: Hybrid configurations: (a) interlayer, (b) intralayer and (c) intrayarn configurations [7].

There are three main types of fibre-hybrid composites, defined according to the configurations of both fibre types:

- **Interlayer** or layer-by-layer hybrids have different types of fibres in different layers, being that each layer only has a single fibre type (Figure 3.1a);
- **Intralayer** or yarn-by-yarn hybrids have both types of fibres in a single layer (Figure 3.1b), layers that can be stacked in different configurations;
- **Intrayarn** or fibre-by-fibre hybrids have both fibre types in a single tow (Figure 3.1c). This type of configuration is the one that leads to a better dispersion of both fibre types.

The different types of hybridization will lead to different properties and different mechanisms of failure.

The study of hybrid composites started in the 70s. Due to the high price of the recently invented carbon fibres, cheaper fibres, like glass fibres, would be added to the carbon fibre composites in order to reduce the material's price and still take advantage of the better properties of carbon fibres. Afterwards, and with the reduction of carbon fibre prices, the hybridization of composite materials became a secondary topic and the focus became in modelling non-hybrid composites.

Nowadays the topic of hybridisation is growing in interest due to the fact that it allows the compensation of some of the disadvantages while maintaining part of the advantages of each fibre. This is valid in several loading cases, for instance, in flexural loadings it is advantageous changing the inner carbon layer for carbon fibres allows the reduction of the price of the material while maintaining its flexural properties [7].

In hybrid composite materials it is usual to refer the two types of fibres as: high elongation (HE) and low elongation (LE) fibres. The HE fibres are the ones that have the highest failure strain, while LE have the lowest. It should be noted that high and low are relative terms and that in a hybrid system glass fibres can be the

HE fibres while in another they can be the LE fibres.

In the topic of hybrid composites it is usual to refer to the hybrid effect, whose definition and characteristics are presented next.

3.1.1 Hybrid effect

The hybrid effect was firstly defined by Hayashi [52], in 1972, when he noticed that the apparent failure strain of the carbon fibres in a carbon/glass hybrid was enhanced in relation to that of the non-hybrid carbon composite. This experimental fact lead to the creation of the first definition of hybrid effect, defined as the apparent failure strain enhancement of the LE fibres in a hybrid composite compared to the failure strain of the LE fibress in the non-hybrid reference composite (Figure 3.2a). The application of this definition requires an accurate determination of the failure strain of the reference non-hybrid composite as this value is the baseline in the determination of the hybrid effect. The determination of the failure strain can be affected by the experimental set-up, namely the stress concentrations at the grips. These stress concentrations are usually higher for non-hybrids than for hybrid composites [7], leading to a reduction of the baseline failure strain, which can result in an overestimation of the hybrid effect.

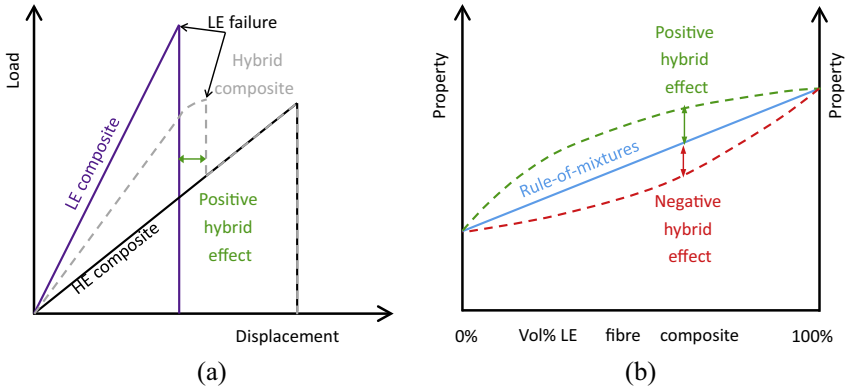

Figure 3.2: Diagrams for the definition of the hybrid effect: (a) first definition proposed by Hayashi and (b) general definition based on the rule-of-mixtures [7].

The definition proposed by Hayashi [52] for the hybrid effect refers only to the enhancement of apparent failure strain, however, hybridization introduces changes in other mechanical properties [53]. This lead to a new, more general definition for the hybrid effect. Hybrid effect was then defined has a deviation from the linear rule of mixtures [54]. This definition is more general and allows it to be applied to several mechanical properties and allows the existence of positive or negative hybrid effect (Figure 3.2b) if there is, respectively, an improvement or a deterioration of the property in question.

Although the second definition for hybrid effect presents an improvement in relation to the first proposed by Hayashi, it still has some flaws. Firstly, the rule-of-mixtures is not always linear, for instance, for the tensile strength the rule-of-mixtures is a bilinear one [53, 55]. Secondly, as noted by several authors [53, 56], the definition of a good parameter to define the hybrid composition and to be applied in the rule-of-mixtures is essential. This authors noted that a good parameter would be the relative HE/LE volume fraction, however this parameter is not always easy to determine [7]. And finally, not all properties can be describe with a rule-of-mixtures. While tensile elastic properties relate well with a linear rule-of-mixtures [52, 53, 56], to determine the flexural modulus one should use a more complex approach, such as classical laminate theory.

Several authors [13, 53, 57] noted that one essential parameter in the influence of hybridization in the mechanical properties of the hybrid composite was the dispersion of both fibre types (Figure 3.3). Dispersion can be defined has the reciprocal of the length of the smallest repeat unit of the composite [57]. Dispersion is, therefore, a characterization of how well mixed both fibre types are.

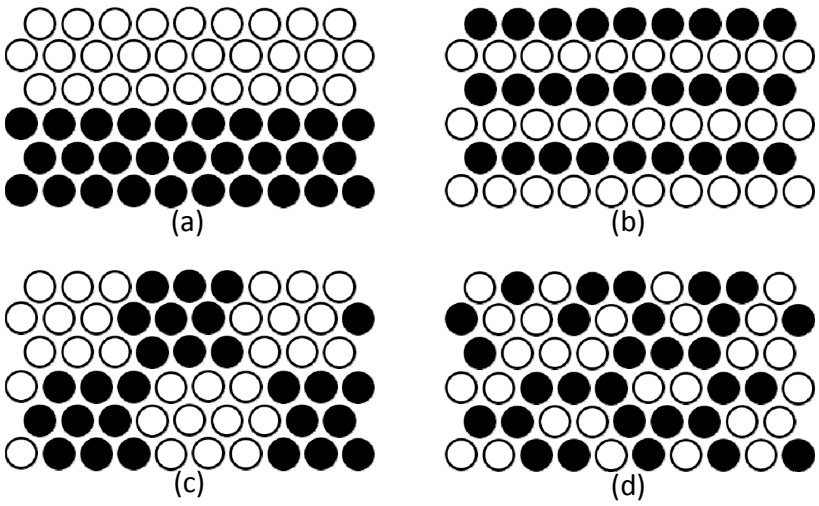

Figure 3.3: Dispersion in hybrid composites: the degree of dispersion increases from (a) to (d) [7].

The referred authors [13, 53, 57] noted that increasing the dispersion lead to an improvement in the mechanical properties. This means that the use of intrayarn (Figure 3.1c) hybridization instead of interlayer (Figure 3.1a) or intralayer (Figure 3.1b) may lead to better mechanical properties.

Throughout the years several explanations for the occurrence of the hybrid effect were proposed. Currently there are three hypotheses for the hybrid effect [7]: (1) thermal residual stresses, (2) changes in the damage development leading to final failure of the hybrid composite and (3) dynamic stress concentrations. These hy-

potheses will be further explained in the following sections. Another influencing parameter in hybrid effect is the scatter in fibre strength, which will be explained later on.

Residual stresses

Hybrid composite materials are composed of different types of materials, whose coefficients of thermal expansion (CTE) differ from each other. For instance, carbon fibres have a CTE ranging from -1 to $+1$ $10^{-6}\mathrm{K}^{-1}$ [2, 57], while in glass fibres it is around 5-10 $10^{-6}\mathrm{K}^{-1}$ [7, 57]. This difference of CTEs means that upon cooling the carbon fibres will remain almost the same size while glass fibres will tend to shrink. In a composite material, however, there is a third component, the matrix, that acts as a restraint to the free movement of the fibres. Therefore, the cooling stage of the fabrication of a hybrid composite material leads to residual stresses in the fibres. For instance, in a carbon/glass hybrid, the carbon fibres, whose CTE is close to zero, will be subject to compressive residual stresses and the glass fibres will be subjected to tensile residual stresses, maintaining the overall force equilibrium in the material. The compressive residual stresses in the carbon fibres will alter their tensile behaviour and change the apparent failure strain of the carbon fibres.

These residual stresses contribute effectively to the hybrid effect, however they do not sufficient to fully explain the hybrid effect [57, 58]. According to Zweben [58], in a carbon/graphite hybrid with epoxy resin the residual thermal stresses can account only for 10% of the increase in apparent failure strain of the carbon layers, which is insufficient to explain the total hybrid effect and that there are other mechanisms affecting the hybrid effect.

Damage development

As explained in the previous chapter (Ch. 2), failure of unidirectional composites is determined by the stochastic strength of fibres and the stress redistribution after fibre failure. Hybridizing a composite material significantly changes both these parameters.

As the composite is constituted by more than one type of fibres, their strengths will be represented by different distributions, meaning that the fibres will not fail at the same applied stress/strain which, by itself, changes strongly the behaviour of the composites under tensile loadings.

After a LE fibre fails, due to a lower failure strain, the stress that they previously carried has to be redistributed among the intact fibres. As the fibres have different

elastic properties the distribution won't depend only on the distance to the fibre break, as in non-hybrid UD composites [11, 16]. The hybridization not only changes the SCFs but also changes the ineffective lengths as the different type of fibres have different elastic properties, radius and different interface properties [58]. This changes in the stress redistribution will alter the cluster development and damage progression.

When loaded in the fibre direction, the LE fibres will fail first, however, as there are HE fibres mixed in the composite, there will be bridging points, provided by the HE fibres, that will hinder crack propagation and the cluster development, therefore, delaying the failure of the composite. Another aspect that can have effect in the damage development in hybrid materials are the size effects [1, 59].

The strength of a fibre decrease with increasing the sample size. As hybrid effect is defined in comparison with a LE fibres non-hybrid composite, and in this material the volume of LE fibres is higher, the introduction of another fibre type (HE) in the material will cause an increase in the expected strength of the LE fibres, because their overall volume is lower, which may affect the hybrid effect[2].

Dynamic stress concentrations

Failure of a composite material is a dynamic process. When a fibre breaks energy is released and the fibre acts as a spring and a stress wave propagates in its axial direction. This phenomena was first reported by Hedgepeth [39] and later confirmed by several authors [60, 61]. Hedgepeth limited his study to the dynamic stress concentrations in the fracture plane and reported an increase of 15 to 27% in relation to the static SCF, however he used a shear-lag model that has limitations in the study of dynamic phenomena [2].

Hedgepeth model was later extended by Xing et al. [61], that reached similar conclusions for the SCFs outside the plane of fracture.

Xia and Ruiz [60] studied the dynamic stress concentrations in carbon and glass composites and predicted that they were 20% higher for glass composites. This means that stress wave, that propagates axially in the intact fibres after another breaks, behaves differently according to the material. According to Xing et al. [61], the phase and amplitude of the stress wave are dependent on the elastic properties of the fibres, thus changing with the material.

Xing et al [62] extended this dynamic model to hybrid composites. With this theoretical model, the authors were able to capture two waves propagating in the LE and HE fibres.

Since the waves in the different fibres are out-off-phase, the stress concentrations in the composite are lower and, therefore, improve the overall resistance of the material. Strictly from the point of view of dynamic stress concentrations the hybrid effect will always be positive as it always leads to lower SCFs [2].

This earlier models were able to give some insight off the dynamic effects in fibre composites and hybrid fibre composites, however more advanced dynamical models should be used to support these conclusions.

3.2 Mechanical properties of hybrid composites

The previously described effects alter the response and failure development in hybrid composites.

An brief review on the effects of hybridization on the mechanical properties of composites will be presented in the following sections.

3.2.1 Tensile properties

Tensile modulus

The longitudinal tensile modulus can be accurately predicted by a linear rule-of-mixtures:

$$E^* = E_{f1}V_{f1} + E_{f2}V_{f2} + E_mV_m \ , \tag{3.1}$$

where E_{f1} and E_{f2} are the longitudinal tensile modulus of both fibres, E_m the matrix elastic modulus, and V are the volume fractions of the respective component.

Since the longitudinal tensile modulus can be predicted by a linear rule-of-mixtures, hybrid effects are not expected for this property. In the transverse direction, however, hybrid effect may occur[63].

Failure strain

In regard to the failure strain, it is expected that hybrid effect occurs. In fact, the first definition of hybrid effect was done regarding failure strain enhancement [52]. This enhancement regards the failure strain of LE fibres in hybrid composites in comparison with non-hybrids. Kretsis [53] reviewed the mechanical properties of hybrid composites in 1987, later compiled by Swolfs et al. [7]. For failure strain the

typical range for hybrid effect is 10-50%. In figure 3.4 data of failure strain hybrid effect is compiled.

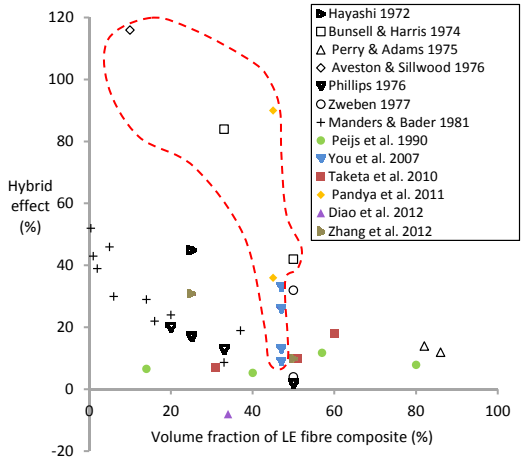

Figure 3.4: Hybrid effect for tensile failure strain. Information in Black was gathered by Kretsis and information in colour by Swolfs. The information inside the red line should be interpreted with care, due to errors [7].

According to Swolfs et al. [7] the values inside the red line in Figure 3.4 should be treated with care because of improper testing, definition of the reference failure strain or definition of the hybrid effect.

Tensile strength

The hybrid effect for tensile strength should determined based on a bilinear rule-of-mixtures (Figure 3.5a). As tests are based on iso-strain conditions and LE fibres are the first to fail. If the HE fibre content is low the composite strength reaches its maximum when the LE fibres fail (Figure 3.5b). However, if the HE volume fraction is high enough the composite may still able to carry stress after the LE fibres fail and, therefore, the tensile strength is dominated by the HE fibres (Figure 3.5d).

Several authors have found a positive hybrid effect for tensile strength [7], concluding that the bilinear rule-of-mixtures does not accurately predict the effects of hybridization on the tensile strength.

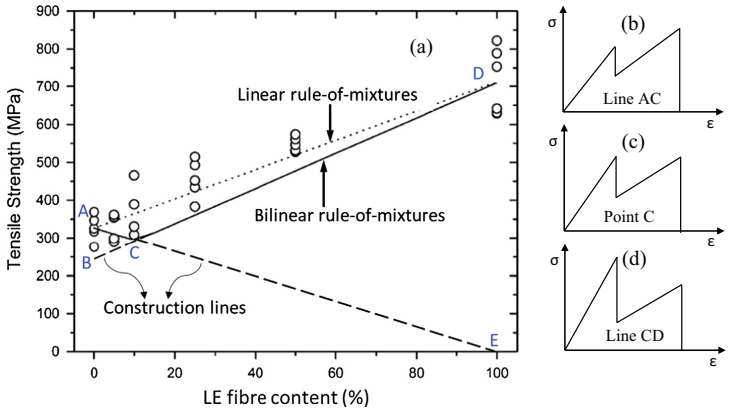

Figure 3.5: Bilinear rule-of-mixtures for tensile strength. Experimental data for carbon/glass hybrids [7].

3.2.2 Flexural properties

The effect of hybridization in flexural properties cannot be determined based on the volume fraction of both fibre types since the layup configuration is essential. This is due to different stress states in different positions relatively to the neutral axis/plane, which makes the prediction of the flexural hybrid effect harder than for tensile properties. The hybrid effect in flexural properties is due to different material behaviour in tension and in compression, for instance, glass fibres have a tensile to compressive strength ratio of 0.73, while for carbon is 0.37 [64].

Dong et al. [8, 65] studied the effects of hybridizing carbon fibre composites with glass fibres, concluding that replacing the carbon fibres by glass fibres in the compressive side of the specimen would increase the flexural properties of the material (Figures 3.6 and 3.7).

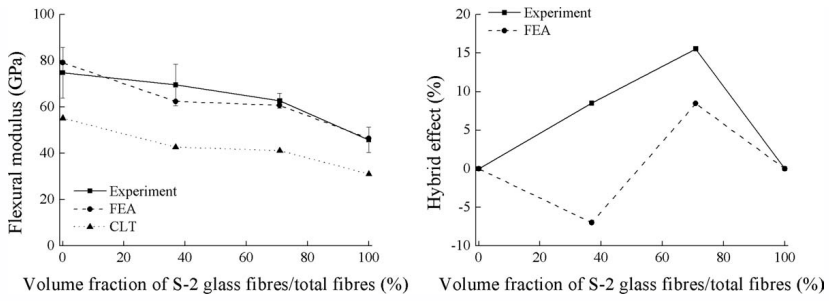

Figure 3.6: Effects in the flexural modulus of hybridizing carbon fibre composites with glass fibres in the compressive layers [8].

Dong et al. [8, 65] results show positive hybrid effects for flexural modulus and strength, which can not be accurately predicted by classical laminate theory nor by

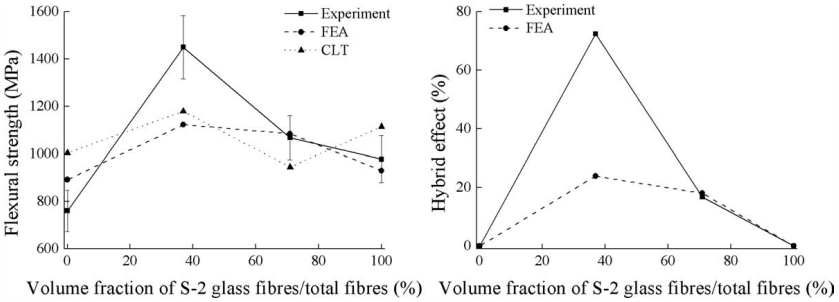

Figure 3.7: Effects in the flexural strength of hybridizing carbon fibre composites with glass fibres in the compressive layers [8].

simple FE analysis. Other authors [66] reached similar conclusions in hybridizing carbon composites with glass fibres. These results mean that an symmetrical layup may not be optimal when there are flexural loads and that there is an optimal hybrid ratio to improve flexural properties wich, according to Dong et al.[65], is 12.5% of glass fibres.

3.2.3 Impact resistance

One of the main goals of hybridizing fibrous composites is improving the toughness of these materials, making impact resistance properties important, as they are related with the toughness of the material. Impact resistance can be characterized by three parameters: (1) energy absorbed during penetration impact, (2) damaged area after a non-penetrating impact and (3) post impact properties. These parameters are governed by different mechanisms and hybridization may affect differently each one of them [7]. In impact tests, the material behaviour is highly dependent on the ply configuration and, therefore, hybridizing different plies will have different influence in the impact resistance. Similarly to the other mechanical properties, the dispersion of both fibres types is important in impact resistance, in this case due to changes in the damage mechanisms [2].

For interlayer hybrids,the positioning of the layers is important because it not only changes the flexural properties (as seen in Section 3.2.2), but also the damage mechanisms to dissipate the impact energy.

Sayer et al. [67] tested asymmetric interlayer carbon/glass hybrids. With this asymmetric laminate it was possible to study the effect of having the LE in the impact side or in the other side of the laminate, which is subjected to tensile loadings. The authors found that if the carbon fibres (LE) were on the impacted side, the impact resistance was increased by 30%.

Jang et al. [68] studied several hybrid composites with different fibre types. For a two-layer carbon/aramid hybrid, the dependence of which layer is in the compressive side was reduced, fact that was attributed to similar impact behaviour of the aramid and carbon reference composites. However, replacing the carbon fibres with polyethylene (PE) resulted in diferent behaviours if the aramid fibres were on the compressive or tensile side of the impact. If the PE fibres (HE fibres) were on the compressive side, the impact resistance increase by 50% in comparison with the aramid fibres in the compressive side, which suggests that HE preform better when in the tensile side of the impact. These results contradict the ones of Sayer et al. [67], however thheys can be attributed to differences in the damage mechanisms which are related to fibre and fibre/matrix interface properties [2].

Naik et al. [69] tested the impact behaviour and post-impact properties of carbon/glass symmetrical hybrids and reported that the compression-after-impact strength of the hybrid material was higher than that of both reference composites (non-hybrid).

As seen, the positioning of the different plies affects the impact properties of the material however dispersion also influences these properties.

Sarasini et al. [70] tested glass/basalt hybrid composites and concluded that the well dispersed specimens showed smaller damaged area and higher post-impact flexural strength, which was attributed to the presence of high amount of small delaminations in the well dispersed composites compared to extensive fibre breaks and delaminations in the less dispersed ones. De Rosa et al. [71] got similar results for the same hybrid material.

Park and Jang [72] studied aramid/polyethylene hybrids and observed that the interlayer hybrids had a higher penetration impact resistance than the intralayer hybrids, which means that less dispersed composites had better impact resistance. In terms of damaged area it was found that intralayer hybrids presented a smaller damaged zone and therefore should have better post-impact properties (which were not determined).

3.2.4 Fatigue resistance

Although fatigue resistance is an important property for many applications, the effects of hybridization in this property have not been extensively studied [7]. In principle, hybridization should lead to improved fatigue properties, as HE can act as bridging points in a crack and stop crack propagation.

Wu et al. [9] studied the fatigue properties of several materials, including hybrid composites.

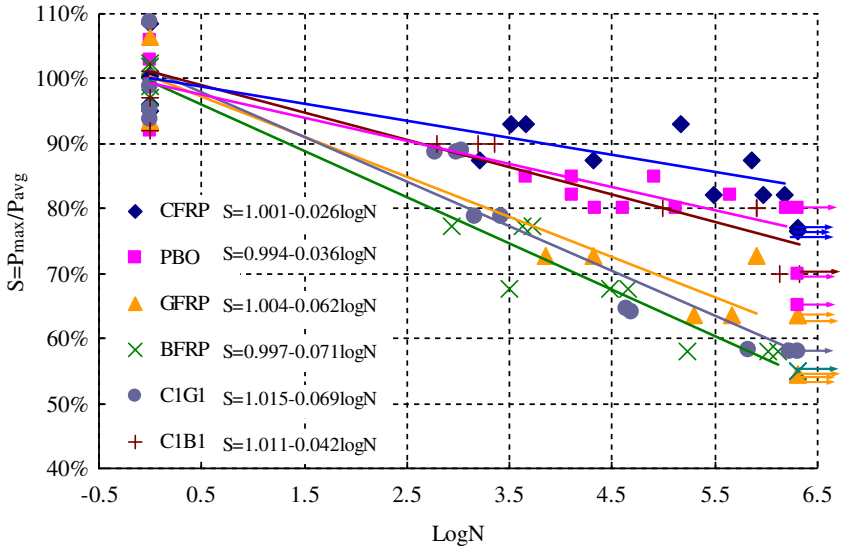

Figure 3.8: Fatigue response of several fibre reinforced composites [9].

As one can see in Figure 3.8 for the in the same conditions (same fraction of maximum and medium loads), the addition of carbon fibres, whose base behaviour is represented by CFRP, in a basalt composite (BFRP) increases the number of cycles to rupture of the hybrid material (C1B1). The authors justified this increase with the reduction of the stress in the basalt fibres due to the addition of the carbon fibres, that have a higher modulus, improving the fatigue life of the basalt fibres. The addition of carbon to a glass composite (GFRP) didn't have the same effect as the previous material (see Figure 3.8-C1G1), which was attributed to the superficial properties of glass fibres.

Peijis and de Kok [73] studied the fatigue resistance of PE/carbon hybrids and found that hybridization resulted in flatter S-N curves, meaning that the fatigue life of the material was improved. They also reached the conclusion that hybrid composites have a less scattered fatigue life and that increasing the dispersion improves it.

3.2.5 Pseudo-ductile behaviour

Fibrous composites are widely used, however, the longitudinal failure of this material is catastrophic and without any previous warning. Another problem is that the material can be damaged in its interior without it being noticeable in the outer layers. This can lead to mechanical properties lower than expected, leading to a premature failure of the component.

Hybridization can tackle some of these challenges by developing a more gradual

failure of the material. The usual behaviour of a composite material is showed in Figure 3.9a, which represents a catastrophic failure. Hybridization leads to a diagram like the on in Figure 3.9b but, if the material is designed correctly, a pseudo-ductile behaviour can be achieved (Figure 3.9c), which is considered to be the ideal response of a hybrid composite [74].

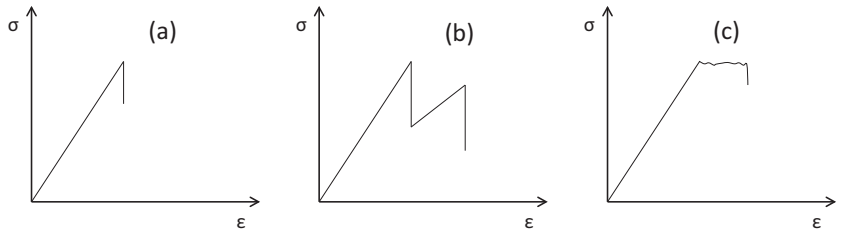

Figure 3.9: Schematic stress-strain diagrams for: (a) non hybrid composites, (b) typical hybrid composites and (c) pseudo-ductile hybrid composites [2].

The increase in interest in a pseudo-ductile behaviour can be attributed to the high safety factors that are used in composite materials, which can be reduced if the materials showed a pseudo-ductile behaviour (like in metals) [2].

Czél et al. [75] and Jalalvand et al. [10] achieved a pseudo-ductile behaviour for carbon/glass hybrid with thin plies. The authors considered carbon/glass hybridization due to: the compatibility between materials, the existence of ultra-thin carbon prepregs, the difference in failure strain of the considered materials allows the alteration of the reference properties by hybridization and the transparency of the glass allows the detection of failure mechanisms in the ultra-thin carbon layer. The authors [10, 75] presented both experimental and numerical evidence of the pseudo-ductile behaviour. It was noted that the pseudo-ductile behaviour was closely connected with the failure mechanisms and that the total and relative thickness of the layers lead to different behaviours (see Figure 3.10).

It was noted that when there was multiple fragmentation of the carbon layer the material showed a pseudo-ductile behaviour. This multiple fragmentation could be achieved when the carbon layer thickness was small (see Figure 3.10).

Other authors have tackled the pseudo-ductile topic. Jones and Dibenedetto [74] demonstrated pseudo-ductile behaviour of carbon/glass and carbon /aramid composites when each carbon fibre was surrounded by carbon or aramid fibres, reducing the interaction between the carbon fibres. Liang et al. [76] demonstrated some degree of pseudo-ductility in carbon/glass rods when the glass fibres were all put in the core of the rod. However, the stress-strain diagram is more close to the one from Figure 3.9b than the pseudo-ductile one in Figure 3.9c. Czél et al. demonstrated a pseudo-ductile behaviour in unidirectional discontinuous carbon/glass fibre composites [77] and for composites with discontinuous carbon fibres and continuous glass

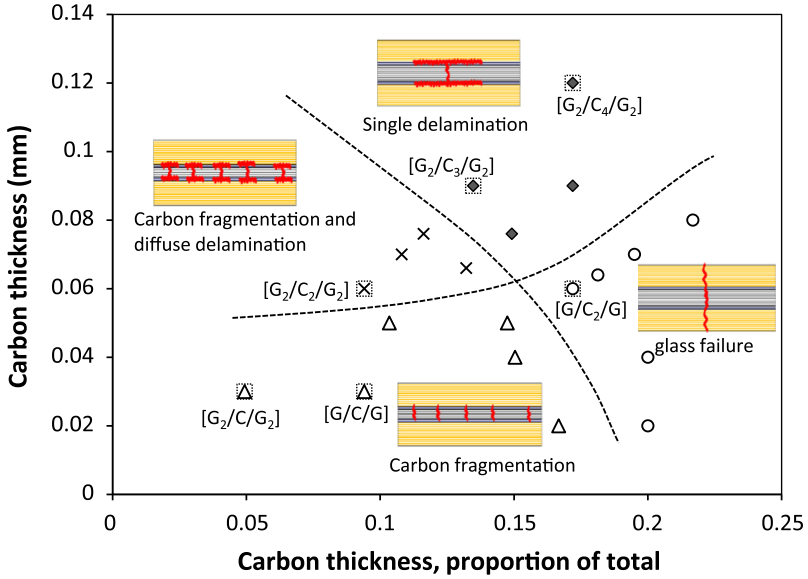

Figure 3.10: Failure modes as a function of absolute and relative layer thickness in carbon/glass hybrid composites [10].

fibres [78]. Swolfs et al. [79] also demonstrated that pseudo-ductility can be achieved by controlling the failure mechanisms in composites. This was done for carbon fibre and self-reinforced polypropylene composites and the pseudo-ductility was achieved when the carbon fibre layers were able to fracture in multiple locations before the failure of the composite. Yu et al. [80] also achieved a pseudo-ductile behaviour for hybrid carbon/glass composites with highly aligned discontinuous fibres. This hybridization was done at the ply level and each ply was constituted by both types of fibres (intralayer hybridization).

Overall, the pseudo-ductile behaviour has only been achieved for low fractions of LE fibres (e.g. carbon fibres) and therefore their mechanical properties are reduced. New strategies need to be developed to achieve this behaviour in higher LE fibre fractions [7].

3.3 Failure development and stress redistribution in UD hybrid composites

The failure development of hybrid composites follows the same guide lines of non-hybrid composites (presented in chapter 2). The same base principles can be applied: (1) the strength of the fibres is not deterministic and (2) the stress previously carried by a broken fibre is redistributed among the intact ones in a complex manner.

As in a hybrid composite, there is presence of two fibre types (HE and LE), the

failure development will be more complex than in non-hybrid composites. As the LE fibres have a lower mean failure strain, they will break first, causing stress concentrations in the remaining fibres. The failure of the LE fibres causes the initiation of cracks in the matrix, which will extended with increasing applied stress. As the HE fibres have a higher failure strain, they will act as crack arresters, bridging the cracks formed by broken LE fibres [2, 74, 81]. This will lead to a delay in damage development and failure of hybrid composites. Nonetheless, the increase in applied strain/stress will cause the creation of clusters of broken fibres, constituted by LE and HE fibres. These clusters will grow and, when they reach a critical size, the failure of the composite will occur.

As previously stated for non-hybrid composites, the stress redistribution after a fibre breaks is crucial to understanding the behaviour of UD composites under tensile loadings. Swolfs et al. [11] did an extensive study of stress redistribution in hybrid composites. Using a 3D FE model with a random fibre packing with a broken LE fibre (in this case carbon) in the middle, the authors were able to study the effects of several parameters in the stress redistribution in hybrid composites.

Firstly, Swolfs et al. [11] studied the effect of the having fibres with different radii in the SCFs and ineffective lengths (see Figure3.11). They considered the carbon to have a radius of 3.5 μm and the glass fibres to have a radius of 3.5 or 6 μm.

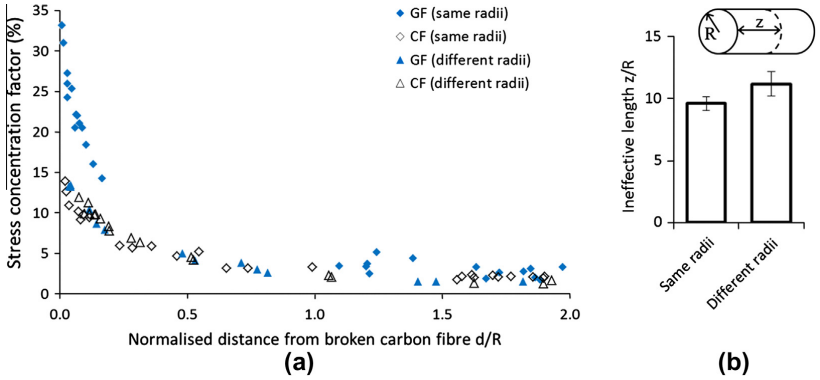

Figure 3.11: Stress redistribution in hybrid composites with 50% carbon and glass fibres: (a) SCFs in both fibre types, considering the same and different radii; (b) ineffective length of the broken carbon fibre considering fibres with the same and different radii [11].

The authors concluded that having fibres with different radius affects both the SCFs and the ineffective length. For the model with different fibre radii the SCFs, in the carbon and glass fibres follow the same trend-lines. This was attributed to the fact that considering glass fibres with higher diameter causes the SCFs to decrease due to an increase in cross section, compensating, therefore, the difference in the stiffness of the fibres. In terms of ineffective length, the authors attribute the

increase of ineffective length in the model with fibres with different radii to the fact that, in packings with different radii, there is less fibrous material surrounding the broken fibre, reducing the homogenized shear stiffness of the material in this region of the composite. As the stress is transmitted to the broken fibre in shear, reducing the homogenized shear stiffness causes an increase of the ineffective length.

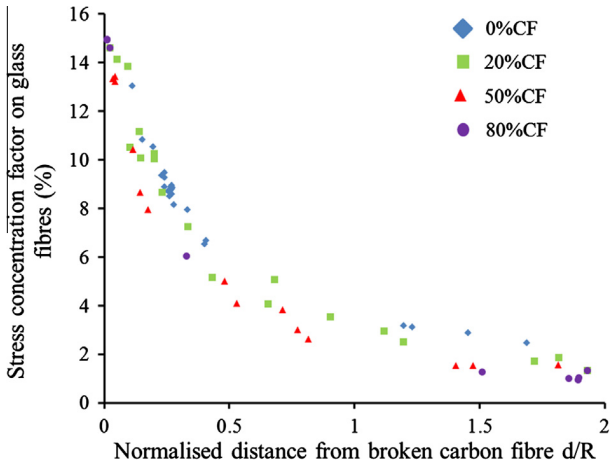

Figure 3.12: Stress concentration factors in glass fibres as a function of the distance from the broken fibre [11].

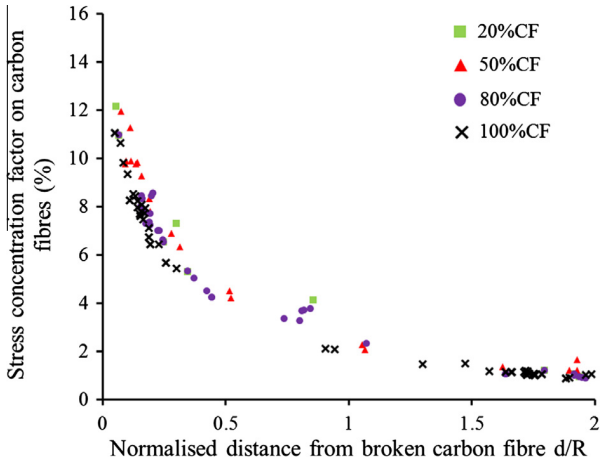

Figure 3.13: Stress concentration factors in carbon fibres as a function of the distance from the broken fibre [11].

Swolfs et al. [11] also studied the effect of hybrid volume fraction in the stress redistribution, for carbon/glass hybrids. By analysing Figure 3.12 and 3.13 one can see that the hybrid volume fraction has a low influence in the SCFs in both fibre types, however, increasing the volume of carbon fibres, slightly decreases the SCFs due to an increase in the composite longitudinal stiffness. The influence of the hybrid

volume fraction in the ineffective length is similar to that in the SCFs (see Figure 3.14), the increase of the carbon volume content slightly decreases the ineffective length.

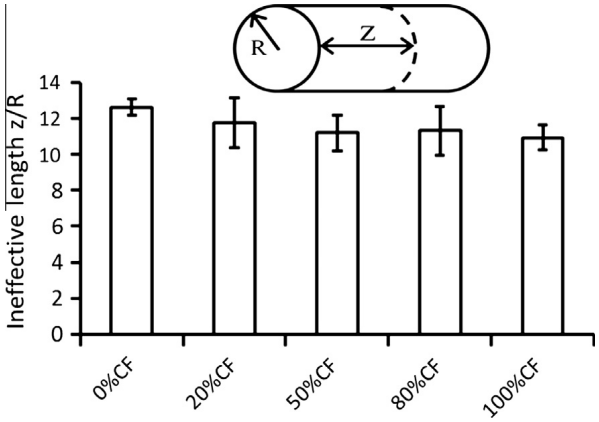

Figure 3.14: The ineffective length of carbon–glass hybrids for different hybrid volume fractions. The error bars indicates the 95% confidence interval based on five realisations[11].

Swolfs [2] also presented the results for SCF and ineffective length for carbon hybrids hybridized with HE fibres with different stiffnesses. HE concluded that increasing the stiffness of the HE fibres increased the SCF in these fibres. However, the effect is opposite in the SCFs in the carbon fibres, but this effect is reduced. The effect of the stiffness of HE fibres in the ineffective length can be seen in Figure 3.15. As one can see, increasing the stiffness of the HE fibres slightly reduces the ineffective length of a broken carbon fibre, but increases that of a broken HE fibre.

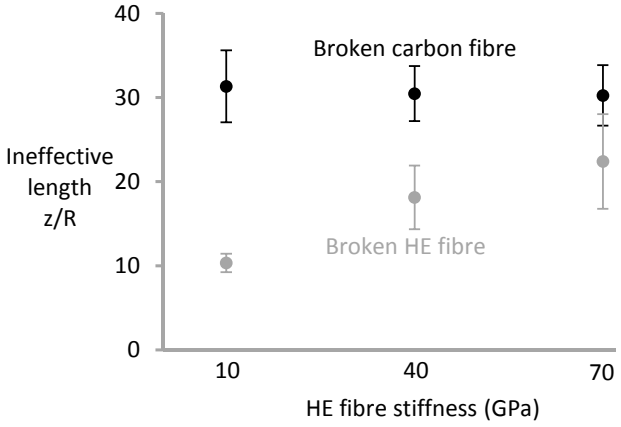

Figure 3.15: The ineffective length in carbon and HE fibres as a function of HE stiffness[2].

The cluster development in composite materials is affected by hybridization. Swolfs et al. [13] studied the how the hybrid ratio affected the cluster develop-

ment, concluding that, increasing the volume fraction of HE fibres would lead to an delay in the cluster formation. This means that to achieve the same level of clusters of broken fibres the applied strain needs to be higher. The authors also found a relation between the critical cluster size and the hybrid ratio, concluding that increasing the volume fraction of HE fibres leads to a reduction of the critical cluster size.

Due to theses results in the stress redistribution, Swolfs et al. [11] concluded that bridging of the broken carbon fibres by the intact hybridisation fibres is the major contribution to the hybrid effect.

3.4 Modelling the tensile failure of UD hybrid composites

The first author to model the tensile failure of hybrid composites was Zweben [58], in 1997, with the intention of predicting the hybrid effect for failure strain. Zweben extended a shear-lag model for UD hybrid composites and considered local-load-sharing for stress redistribution after a fibre break. This model considered a 1D fibre packing with alternating HE and LE fibres (Figure 3.16b) which represents a simplification of the complex geometry of hybrid composites. The hybrid composite behaviour was compared with the non-hybrid composite composed only with LE fibres (Figure 3.16a) to determine the hybrid effect.

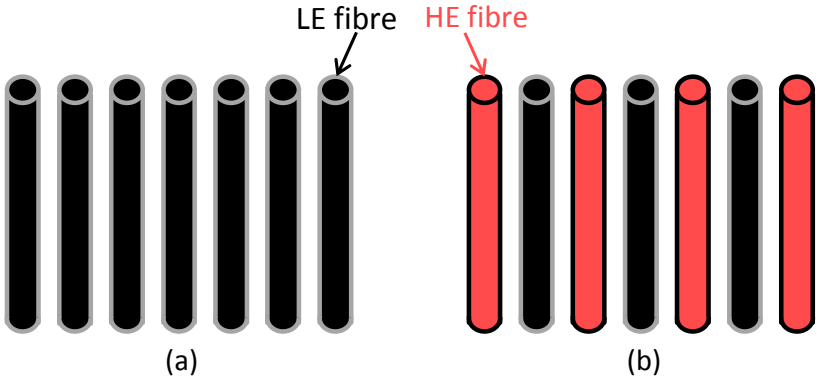

Figure 3.16: Representation of the fibre packings used in Zweben's model : (a) non-hybrid LE composite and (b) hybrid composite with alternating LE and HE fibres [2].

As the model considered fibres with different cross sections and elastic modulus, Zweben considered that when a LE fibre breaks the neighbouring HE fibres would be subjected to a strain concentration, rather than a stress concentration. The strain concentration factor can be defined as the ratio between the strain in a fibre next

to a single broken fibre over the applied strain. Zweben also considered that after a fibre breaks there is a length at which the fibre is not capable of fully carry stress (ineffective length) and derived analytical expressions for both strain concentration factors and ineffective length for hybrid and non hybrid composites. For non-hybrid composite, the strain concentration factor (k_{LE}) is equal to 1.293 and for hybrid composites the strain concentration factor (k_h) only depends on ρ, which is the ration of normalised stiffness of both fibres:

$$\rho = \frac{E_{LE}A_{LE}}{E_{HE}A_{HE}}\,, \tag{3.2}$$

where E_{LE} and E_{HE} are the Young's modulus of the low elongation (LE) and high elongation (HE) fibres, and A_{LE} and A_{HE} are the cross-sectional areas of both fibre types.

The ineffective lengths for the non-hybrid (δ_{LE}) and hybrid composite (δ_h) can be determined as:

$$\delta = N\left(\frac{E_{LE}S_{LE}d_m}{G_m t_m}\right)^{1/2}\,, \tag{3.3}$$

where G_m is the matrix shear modulus, t_m and d_m are, respectively the matrix thickness and the fibre spacing. the factor N is equal to 1.531 for non-hybrid composites and is a function of ρ for the hybrid ones.

Zweben considered that the hybrid composite fails when the first HE fibre breaks, resulting in a lower bound for composite strength [58]. Zweben assumed that the failure of a HE fibre would trigger the unstable failure of all the other LE fibres, therefore, the failure strain used to determine the hybrid effect is according to the definition of hybrid effect presented by Hayashi [52] and explained in Section 3.1.1. Combining the equations for ineffective length, strain concentration factors and the Weibull distributions for fibre strain, Zweben derived the following expression for the hybrid effect (R_{hyb}):

$$R_{hyb} = \sqrt{\frac{\varepsilon_{HE}}{\varepsilon_{LE}}}\left[\frac{\delta_h\left(k_h^m - 1\right)}{2\delta_{LE}\left(k_{LE} - 1\right)}\right]^{-1/2m}\,, \tag{3.4}$$

where ε_{LE} and ε_{HE} are the mean failure strains of the LE and HE fibres at the considered gauge length and m is the Weibull modulus of the fibres, which was considered to be equal in both fibre types.

According to Swolfs [2] the main conclusions to draw from this model are:

- The strain concentration factor depends only on the normalised stiffness ratio of the two fibres (ρ), which means that in the case of a hybrid composite with both fibres with the same factor [$E \times A$], the stress concentration in the hybrid and non-hybrid composite will be the same;

- The most influential parameter in Zweben's model is the ratio of failure strains, meaning that hybrid effect should be more effective with fibres with very high failure elongation;
- As the Weibull modulus are usually over 5, the exponent $-1/(2m)$ will be small, meaning that the strain concentration factors and ineffective lengths have a small influence in the hybrid effect;
- Fibres with small Weibull modulus (high strength/strain dispersion) should lead to higher hybrid effects as comproved by Fukunaga et al. [82].

In 1984 Fukuda [83] modified the model developed by Zweben [58] according to three flaws he encountered in that model. Firstly, Fukuda considered that the first failure of a HE fibre, which was the failure criteria used by Zweben, is not an accurate failure criteria for hybrid composites and is not in accordance with the hybrid effect definition proposed by Hayashi [52]. Secondly, Zweben focused on the failure of a HE fibre next to a broken LE fibre and said that represented the lower bound for composite failure strain. According to Fukuda [83], that will represent the lower bound for non-hybrid composites but may not be true for hybrid ones, because, after a LE fibre breaks, it is expected that the nearest LE fibre will break next, instead of the HE fibre in the middle of those, due to the difference in failure strains. The failure of the two LE fibres causes an higher stress concentration in the HE fibre that is in the middle of the broken LE fibres than the one predicted by Zweben. Lastly, Fukuda [83] considered that the SCFs and the ineffective lengths used in Zweben's model were not accurate as, in a non-hybrid composites, the model predicted smaller SCFs than the ones of Hedgpeth shear-lag model [39].

Taking into account these three shortcomings of Zweben's model [58], Fukuda [83], proposed the following equation for the hybrid effect:

$$R_{hyb} = \left[\frac{\delta_h \left(k_h^m - 1\right)}{2\delta_{LE}\left(k_{LE} - 1\right)}\right]^{-1/2m} . \tag{3.5}$$

This equation is very similar to the one of Zweben's model (Equation 3.4), however it was developed using more accurate values for the SCFs. Comparing equations 3.5 and 3.4 one can see that in Fukuda's model the failure strain ratio of both fibre types doesn't affect the hybrid effect, as proposed in Zweben's model.

Zweben [58] did experimental work to determine the hybrid effect in a carbon/aramid hybrid composite and concluded that the hybrid effect for this material was 4%. For this material Zweben's model [58] predicted a hybrid effect of 22% and Fukuda's model [83] predicted a hybrid effect of 13%, which is closer to the experimental value. Both authors compared their results with a multi-directional

composite material, however, these 1D models may not be accurate to predict the complex failure of multi-directional composites.

According to Swolfs [2], there are others limitations of Zweben's model. Firstly, the 1D fibre packing is a simplification of the complex 2D micro-structure of the hybrid composite materials and leads to a overestimation of the SCFs in the fibres [11]. Secondly, the dispersion of both fibre types is maximized in the alternating HE and LE fibres for a hybrid ratio of 50%. Lastly, Zweben's model does not allow the study of the hybrid ratio, which has been proved to affect the hybrid effect [53].

More recently, Mishnaevsky and Dai [84] developed a 2D numerical fibre bundle model with a random fibre packing. Using Monte-Carlo method, random properties are given to the fibres according to a Weibull distribution. The authors used this model to study the failure of a carbon/glass hybrid, and concluded that fibre mixing had a negative effect on the critical stress of the composite. However they considered that the critical stress occurred when the composite stiffness was reduced by 50% and considered a fibre volume fraction of 25%.

Pimenta and Robinson [12] extended the hierarchical bundle model, previously developed [6], to hybrid composites. This model was the first 2D shear-lag model for hybrid composites and considers a square arrangement of fibres with stochastic strength values. The model is able to study the effect of dispersion and hybridization ratio (N^B) by changing the construction parameters of the unit cells (see Figure 3.17)

With this model, Pimenta and Robinson [12] were able to demonstrate the influence of the carbon/glass fibre volume ratio and the effect of dispersion in the hybrid effect, which increases with increasing dispersion. According to Swolfs [2] the main drawback in this model is the stress concentrations that were considered are unrealistic and, therefore, so are the results for failure development.

Swolfs [2] extended his model, presented in section 2.6.3, to hybrid composites. Some adaptations were made from the original model. Firstly, the hybrid model considers an hexagonal arrangement of fibres instead of a random one which, according to the author, was done to allow the study of dispersion of both fibre types in hybrid composites. The stress redistribution around a broken fibre was also altered to consider a very local load sharing, which means that the stress, previously carried by a broken fibre, is redistributed only to the six closest fibres (Figure 3.18). Fibres that were considered to have de same radius.

In figure 3.18 one can see the SCFs in both fibre types. The difference in SCFs is due to the difference in stiffness of both fibres. If the broken fibre is a carbon fibre, the nearest carbon fibres have a SCF of 7/6 and the glass fibres have a SCF equal to

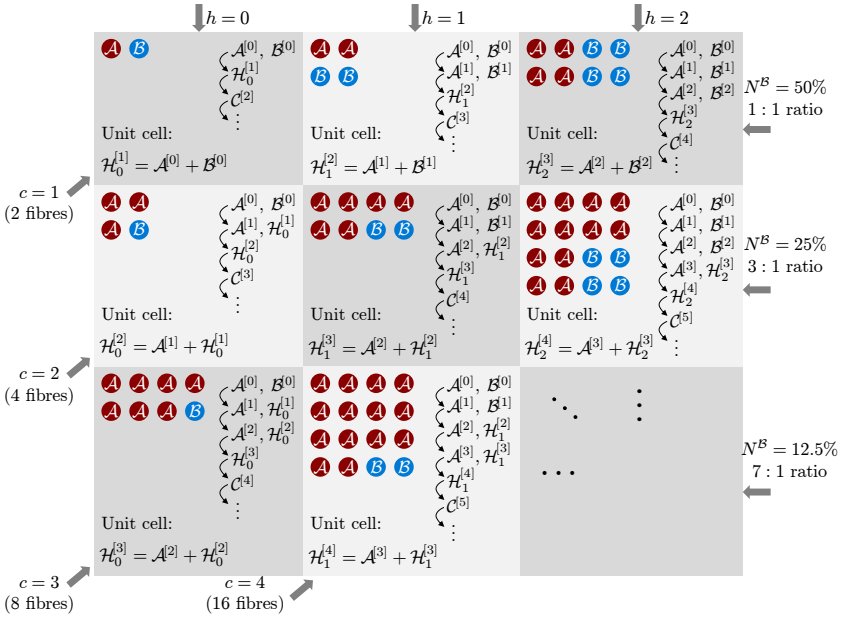

Figure 3.17: Hybrid unit-cells with different hybridization ratios (N^B) and hybridization degrees [12].

$1 + 1/6 \cdot 230/70 = 1.548$ where 70 and 230 GPa are the Young's moduli of the glass and carbon fibres, respectively. The same strategy is used for a broken glass fibre, where the nearby glass fibres have a SCF equal to7/6 and the carbon fibres equal to $1 + 1/6 \cdot 70/230 = 1.051$. To further simplify the original model, the stress recovery in a broken fibre is assumed to be linear. The ineffective lengths were determined using FE analysis.

The model considers 2000 breakable fibres and 250 boundary fibres (unable to break), to which is attributed a strength according to a Weibull distribution. This model was used to study the hybrid effect and cluster formation of carbon/glass hybrids.

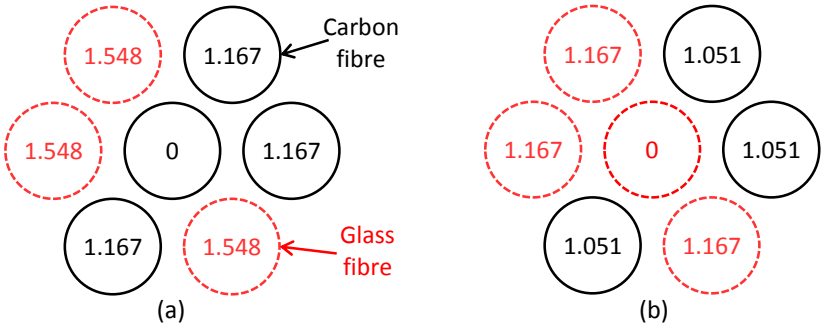

Figure 3.18: Stress concentration factors, according to very local load sharing, around (a) a broken carbon fibre and (b) a broken glass fibre [2].

3.5 Influencing parameters in the strength of hybrid composites

The models for predicting the failure of hybrid UD composites have been presented, however, the most influencing parameters in the hybrid composite behaviour are yet to be accessed. There is a large amount of parameters that can influence the behaviour of hybrid composites and some will be presented in this section. As most authors focus their attention on the parameters that influence the failure strain enhancement of the LE fibres (hybrid effect), most of this data will be related to that effect.

3.5.1 Failure strain ratio

As presented in Section 3.4, Zweben's model [58] considers the ratio of the failure strains of both fibres to be the most influential parameters in the hybrid effect. Fukuda [83] contradicted the results of Zweben's model and considered that the failure strain ratio has no influence on the hybrid effect. This difference is due to the models considering different failure definitions for the hybrid composite. More recently, Swolfs [2] addressed this issue and concluded that the failure strain ratio affects the hybrid effect, however, for failure strain ratios above 2 this influence is reduced (see Figure 3.19). This results were obtained for the same failure strain of the LE fibres.

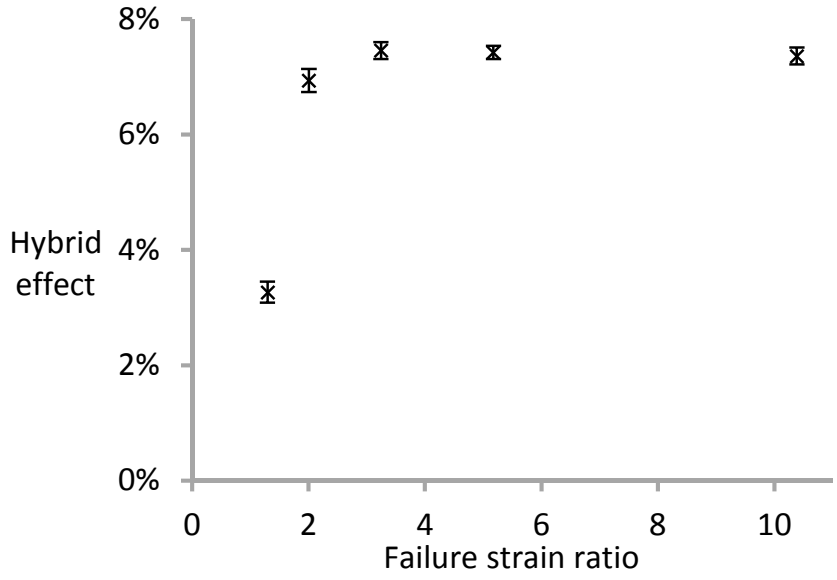

Figure 3.19: Influence of failure strain ratio in the hybrid effect, for a hybrid composite with 50% of each fibre type [2].

Swolfs [2] attributed this results to the delay of HE fibre breaks, delaying the development of clusters of broken fibres. Nonetheless, Swolfs says that there are three limitations to his conclusions. Firstly, the model assumes that the failure occurs when a critical cluster of broken LE fibres is developed. In this situation, most of the HE fibres are still intact and able to carry load, which means that, especially for high contents of HE fibres, the composite may not fail at this point. Secondly, the model considers the elastic properties of the HE fibres remain the same with increasing their failure strain, which may not be accurate since higher failure strain is usually associated with higher compliance. Thirdly, the author considers that the threshold of failure strain ratios of 2 may be affected by the Weibull modulus of both fibre types.

Although the model developed by Swolfs [2] isn't able to consider the residual load carrying capabilities of the HE fibres, he considers that this may be an important factor to achieve pseudo-ductility in hybrid composites.

3.5.2 Hybrid volume fraction

Hybrid volume fraction represents the relative amount of both fibre types and has been shown to have a large effect in the hybrid composite behaviour [2, 53]. Increasing the volume content of HE fibres has been shown to increase the hybrid effect [53]. The earlier models for hybrid composites were not able to study this effect due to the limitations in fibre packing. Recent models [2, 12, 74] have been able to do so, concluding that increasing HE fibre content increases the hybrid effect. Swolfs [2] reported that, for carbon/glass fibres, increasing the HE fibre content lead to a delay of the development of clusters of broken fibres. On the other hand, they found that increasing the volume fraction of HE fibres reduced the critical cluster size (size of a cluster of broken fibres that leads to failure of the composite), which will counteract, in part, the delay in cluster development, as the composite will fail when a smaller critical cluster develops.

3.5.3 Elastic properties of the fibres

The elastic properties of the fibres are important in the stress distribution in the hybrid composite. They affect the three hypotheses for hybrid effect [2], as they affect the static SCFs [11, 58, 83], the dynamic stress concentrations [62], the ineffective lengths [2, 11] and the residual thermal stresses. According to the results presented by Swolfs [2], increasing the stiffness of the HE fibres (maintaining same properties for the LE fibres) leads to a small increase of the hybrid effect, which is attributed to a decrease in the SCFs in the LE fibres with the increase of the HE fibres' stiffness.

3.5.4 Fibre strength distribution

Both Zweben's [58] and Fukunga's [83] models consider the fibre strength distribution to have a large influence on the hybrid effect and concluded that, increasing the dispersion of the strength of the fibres, by decreasing the Weibull modulus, increases the hybrid effect. Swolfs [2] adressed this issue and reached the same conclusions as the previous authors, stating that reducing the Weibull modulus from 4.8 to 3 increased the hybrid effect to the double. These conclusions are important because, lower quality fibres, may have a higher potential for hybrid effects. Manders [85] even stated that "the hybrid effect arrises from a failure to realise the full potential strength of the fibres in all-carbon fibre composites, rather than from an enhancement of their strength in the hybrids", which means that if the fibres had a deterministic strength, their full potential would already be realised in non-hybrid composites and the hybrid effect wouldn't exist.

3.5.5 Fibre dispersion

Fibre dispersion is a measure of how well mixed the fibres are in a hybrid composite. Several authors have, experimentally demonstrated that this is an important factor in the behaviour of hybrid composites [57, 86].

The earlier models that considered 1D arrangements of fibres were not capable of addressing this topic. Recently, Mishnaevsky and Dai [84] addressed this topic and reported that increasing dispersion lead to to slower internal damage development for displacement-controlled models but faster damage development for load-controlled models. Pimenta and Robinson[12] reported that clustering the carbon fibres decreased both the failure strength and strain of the hybrid composites (for the same hybrid fibre ratio), which means that dispersion the carbon fibres in the HE fibres leads to better properties.

Swolfs et al. [13] extensively studied this topic. The authors considered a RVE with around 2000 breakable fibres and considered three different types of mixing of both fibre types: in bundles (Figure 3.20a), in layer (Figure 3.20b) and random dispersion.

In this study, the authors concluded that increasing dispersion, by either reducing bundle size or reducing layer thickness, increased the hybrid effect. However, the authors found that layer-by-layer dispersion with layers of 1 fibre thickness, lead to the maximum hybrid effect, even higher than random dispersion (for a hybrid volume fraction of 50%). This was attributed to a reduced number of possible paths for a crack to grow in the LE fibre layers. Random dispersion, however, showed higher hybrid effect than that possible with bundle-by-bundle dispersion, but the

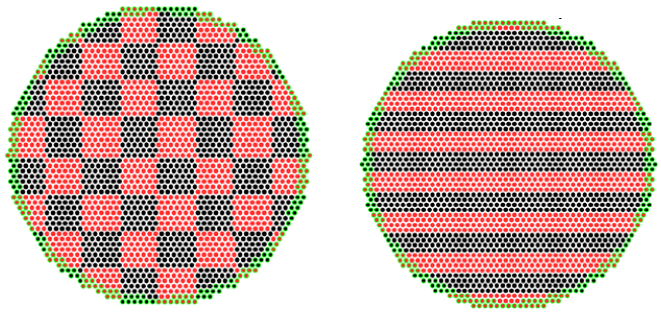

(a) (b)

Figure 3.20: Illustration of the (a) bundle-by-bundle and (b) layer-by-layer dispersion considered by Swolfs et al. (Adapted from[13]).

authors didn't study the limit case of bundles with just one fibre. The authors also reported that dispersion had a small influence in the critical cluster size.

3.5.6 Matrix properties

Has in non-hybrid composites, the matrix properties are only expected to have a secondary effect in the composite properties, by influencing the SCFs and the ineffective lengths. The matrix shear modulus has an influence on the ineffective length, however its effect on the SCFs is usually not represented in the models due to shear-lag assumptions.

3.6 Conclusion

Hybrid composites are attracting an ever growing attention from both academia and industry, due to their potential. The interactions between the components in hybrid composites are hard to predict, however they may lead to better resulting properties that those of the non-hybrid composites of reference, leading to the existence of positive hybrid effects. This hybrid effects have been reported under several loading conditions and in several hybrid materials.

Modelling the tensile behaviour of hybrid composites has been shown to be a difficult task. The earlier model to do so was Zweben's model [58], which considered a 1D packing of fibres. This model was able to predict the existence of hybrid effect, but due to its simplicity wasn't able to fully predict the full composite's behaviour, nor fully justify the hybrid effect. Other models have since then been presented, however there is still no model that is able to fully predict the hybrid composite's behaviour up to failure.

The models and the experimental work done in this area allow us to determine the main influencing parameters in the behaviour of hybrid composites, being the most important the dispersion of the fibres, the hybrid volume fraction and the fibre strength distributions.

Chapter 4

Model for the tensile failure of dry tows

Failure of UD composites under tensile loading is a phenomena mainly dominated by the fibres, which means that fibres and fibre tows are fundamental entities in composite materials.

The tensile testing of dry tows (bundles of fibres without the presence of the matrix) is important to determine the strength distributions of the fibres [18]. This is a more adequate testing method than single fibre testing, because it is more representative as there is no selection of the fibres and the results are obtained from the average behaviour of a large number of fibres [87].

As fibre strength is of high importance in UD composites and hybridization implies an interaction between fibres that present different distributions of strength, the study of hybrid dry bundles is important. This study will allow the understanding of the effects of tow hybridization and the main parameters controlling the tow's behaviour.

4.1 Model development

To study the tensile failure of hybrid tows, a model based on the works of Calard and Lamon [18] was developed. The model was firstly implemented for non-hybrid tows (tows with a single type of fibres), and it considers a bundle composed of N_t parallel fibres with radius R_f and length L. The fibre strengths are considered to follow a Weibull distribution:

$$P(\sigma) = 1 - \exp\left[-\frac{L}{L_0}\left(\frac{\sigma}{\sigma_0}\right)^m\right] , \tag{4.1}$$

where $P(\sigma)$ is the failure probability of a fibre with length L when subjected to a tension σ. L_0 is the reference length at which the Weibull parameters σ_0 and m were calculated.

The Weibull distribution for fibre strength leads to an average fibre strength ($\langle\sigma\rangle$) given by

$$\langle\sigma\rangle = \sigma_L \Gamma\left(1 + \frac{1}{m}\right) , \tag{4.2}$$

where $\Gamma()$ is the gamma function, that can be defined as:

$$\Gamma(x) = (x-1)! , \tag{4.3}$$

if x is a positive integer, or

$$\Gamma(x) = \int_0^\infty t^{x-1} e^{-t}\, \mathrm{d}t , \tag{4.4}$$

if x is an complex number with positive real part. σ_L is the reference tension at gauge length L and is related to σ_0 and L_0 by:

$$\sigma_L = \sigma_0 \left(\frac{L_0}{L}\right)^{1/m} . \tag{4.5}$$

The model assumes global-load-sharing of the stress after a fibre breaks, meaning that there is no interaction between fibres, as there is no presence of a matrix and it is considered that there is no friction between the fibres. The load previously carried by a broken fibre is equally redistributed among the remaining fibres. The model assumes strain-controlled conditions and the strain is incremented from zero with a pre-defined value of $\Delta\varepsilon$. The stresses in the fibres are calculated and compared to the tensile strength assigned to each fibre. This assignment is done by generating a random number (X) between 0 and 1 for each fibre that represents the failure probability $P()$ in Equation 4.1. The strength of the fibre is then calculated by the following expression:

$$\sigma_f = \sigma_0 \left[-\frac{L_0}{L}\ln(1-X)\right]^{1/m} . \tag{4.6}$$

If the stress in a fibre (i) reaches the fibre's strength (σ_f^i) that fibre breaks and the number of broken fibres (N_f) is incremented. The force and strain can be related by the following expression:

$$F = \varepsilon (N_t - N_f) S_f E_f \tag{4.7}$$

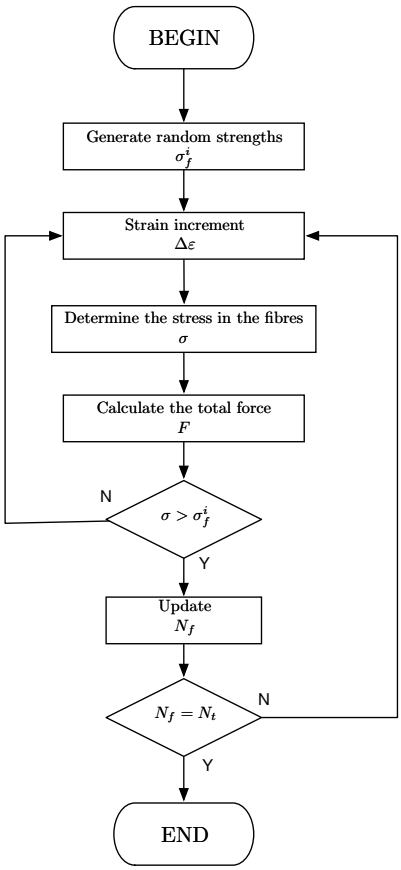

Figure 4.1: Flowchart of the model for dry bundle failure.

where ε is the applied strain, S_f is the fibre sectional area and E_f is the Young modulus of the fibres. The simulation is concluded when all fibres have failed. The algorithm of the model is shown in Figure 4.1.

4.2 Non-hybrid tow behaviour

In this section a parametric study will be done in order to determine the influence of the Weibull distribution parameters on the tow behaviour. As the fibre strengths are calculated using a random distribution at least 10 simulations are performed for each case, in order to obtain an average response.

As base information for fibre properties, the AS4 carbon fibres will be considered. These fibres have a mean radius (R) of 3.5 μm, Young's modulus (E) equal to 234 GPa and the parameters for the Weibull distribution are: $\sigma_0 = 4275$ MPa and $m = 10.7$ at $L_0 = 12.7$ mm [88]. This values will serve as a baseline for the parametric study of the effect that the strength distributions of the fibres have in

the tow behaviour. In this study the tow is considered to have 500 fibres with a length (L) equal to 75mm, unless other parameters are specified.

One of the statistical parameters of the Weibull distribution is the Weibull strength scale parameter (σ_0), which relates linearly with the average fibre strength (Equation 4.2). Figure 4.2 shows the effect that varying σ_0 has in the failure strength of the fibres. It can be seen that varying the scale parameter translates the curves horizontally, which means that the average fibre strength is modified but the strength dispersion is constant.

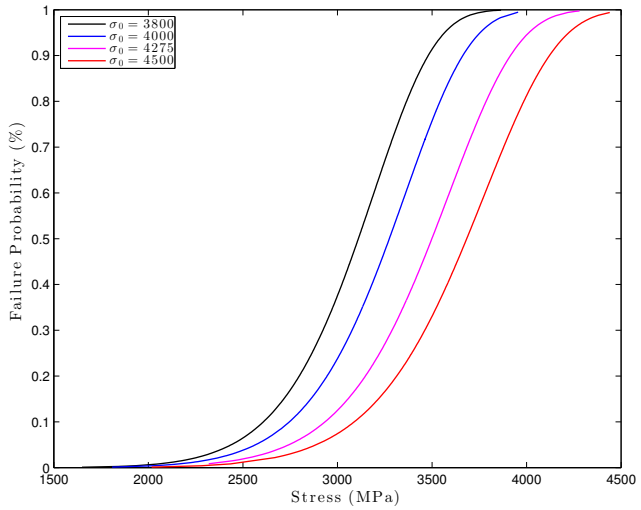

Figure 4.2: Effect of the scale parameter (σ) in the strength of the fibres.

Figure 4.3 shows the stress-strain diagrams for the Weibull distributions with different scale parameters, with the same shape parameter. It is observed that reducing the shape parameter leads to a reduction in the maximum load that the tow can withstand. The curves, however, seem to be very similar, as it is expected, due to the same dispersion of fibre strength. The key parameters for the characterization of the tow behaviour are presented in Table 4.1. It is possible to see a direct relation between the scale parameter (σ_0) and the maximum load in the load-strain diagrams. As the elastic modulus of the fibres was not altered, increasing the scale parameter results in an increase of the tow's strength and failure strain (strain at maximum force).

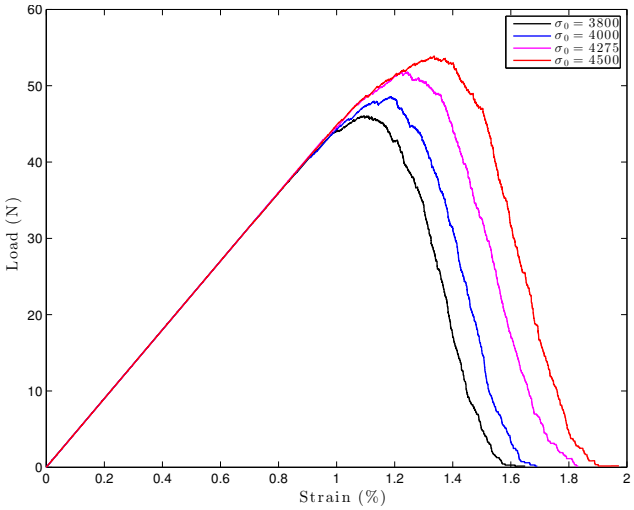

Figure 4.3: Force-Strain diagrams for tows of fibres with different scale parameters (σ).

Table 4.1: Effect of the shape parameter (m) in some reference properties.

σ_0 (MPa)	m	$\langle\sigma\rangle$ (MPa)	Maximum load (N)	Strain at max. load (%)
3800	10.7	3070.9	45.8	1.11
4000		3232.5	48.0	1.16
4275		3454.7	51.2	1.24
4500		3636.6	53.9	1.3

The second Weibull distribution parameter is the shape parameter (m), that is a measure of the dispersion of fibre strength, influencing the width of the distribution. As one can see in figure 4.4, increasing the shape parameter will lead to a wider distribution of fibre strengths, however, the shape parameter will also change the average failure probability, which is expected from Equation 4.2.

This modification of the fibre strength will translate into different stress-strain diagrams (Figure 4.5). As one can see, as the average failure strength of the tows is reduced, by reducing the shape parameter, so is the maximum load in the stress-strain diagram. Another effect of the reduction of the shape parameter is that the strain at which the first fibres fail is reduced, which can be seen in Figures 4.4. This translates into the tow behaviour in Figure 4.5, where the non-linear behaviour starts at lower strains if the shape parameter is reduced. This is the result of a earlier failure of the weakest fibres, which reduces the tow's effective stiffness. At higher values of m this non-linear behaviour is reduced as the majority of the fibres

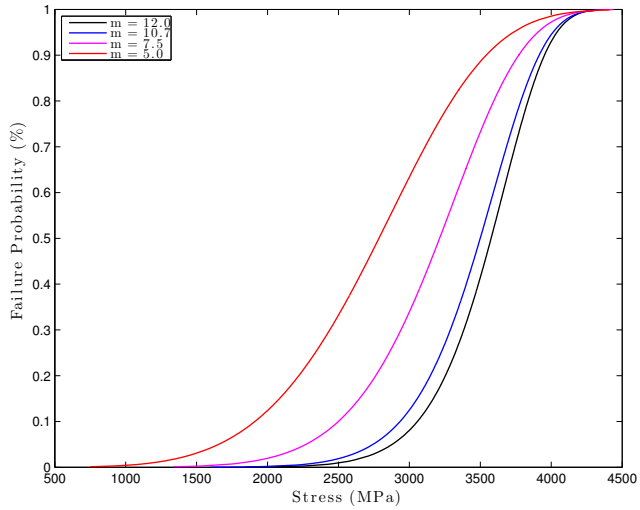

Figure 4.4: Effect of the shape parameter (m) in the strength of the fibres.

breaks in a small range of strains, due to a reduced dispersion.

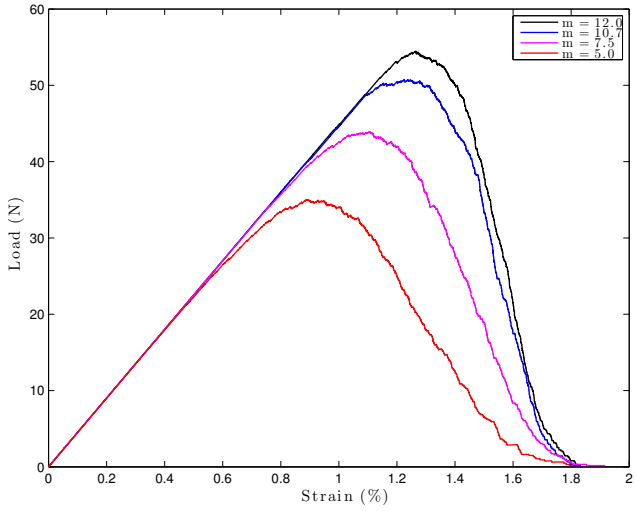

Figure 4.5: Force-Strain diagrams for tows of fibres with different shape parameters (m).

Table 4.2, presents the relation between the Weibull shape parameter and the tow's average failure strength ($\langle\sigma\rangle$), the maximum load and the strain at maximum load.

As explained in the previous paragraphs, changing σ_0 changes the average failure strength of the fibres without changing the dispersion of this parameter, however, changing the shape parameter (m), not only changes the dispersion, but also the average strength of the fibres. To study the effect that dispersion has in the behaviour of the tows it is necessary to change both the shape and scale parameter, in

Table 4.2: Effect of the shape parameter (m) in some reference properties.

σ_0 (MPa)	m	$\langle\sigma\rangle$ (MPa)	Maximum load (N)	Strain at max. load (%)
4275	12.0	3533.1	53.4	1.29
	10.7	3454.7	51.5	1.24
	7.5	3167.0	44.0	1.10
	5.0	2751.7	34.7	0.93

order to have the same average failure strength, as given by Equation 4.2. Taking as the baseline the combination $\sigma_0 = 4275$ MPa and $m = 10.7$, which gives an average failure strength ($\langle\sigma\rangle$) equal to 3454.7 MPa, and varying the both the shape and scale parameter we obtain several distributions. The main results are presented in Table 4.3.

Table 4.3: Effect of dispersion in some reference properties (distributions with the same average strength).

σ_0 (MPa)	m	$\langle\sigma\rangle$ (MPa)	Maximum load (N)	Strain at max. load (%)
4180.1	12.0	3454.7	52.2	1.3
4275.0	10.7	3454.7	51.2	1.2
4663.4	7.5	3454.7	47.8	1.2
5367.1	5.0	3454.7	43.5	1.2

The strength distribution for the fibres are presented in Figure 4.6 and it can be seen that the average failure strength (strength at a failure probability of 50%) is the same in all distributions, but the dispersion is different, resulting in broader distributions if the shape parameter is reduced.

The effect of dispersion in the tow's behaviour is shown in Figure 4.7. Increasing the dispersion, by reducing m, reduces the strain at which the first fibres will fail but increases the failure at which the last fibres will fail. This leads to a reduced maximum force but creates a broader stress-strain diagram. Another aspect that can be concluded from analysing the results in Figure 4.7 and Table 4.3 is that, as the average failure strength is the same in all distributions, the strain at maximum strength will be identical in all distributions, the differences are due to the random generation of the vector of fibre failure probabilities.

As seen in Chapter 2, the tensile strength of brittle fibres is dominated by surface

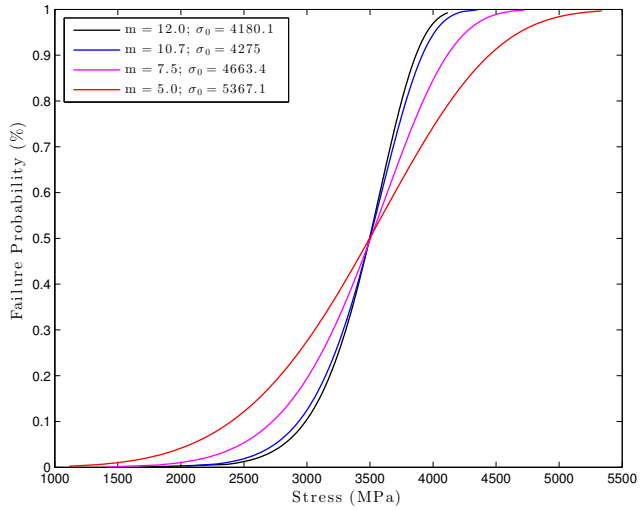

Figure 4.6: Effect of dispersion in the strength of the fibres, maintaining the same average strength.

or volume flaws [15] and exhibits weak-link characteristics, therefore, the length of the fibres will affect the strength distribution of the fibres (Equation 4.1). The size effects in composite materials are, not only affected by the size effects of the strength distributions, but also other parameters such as manufacturing and testing.

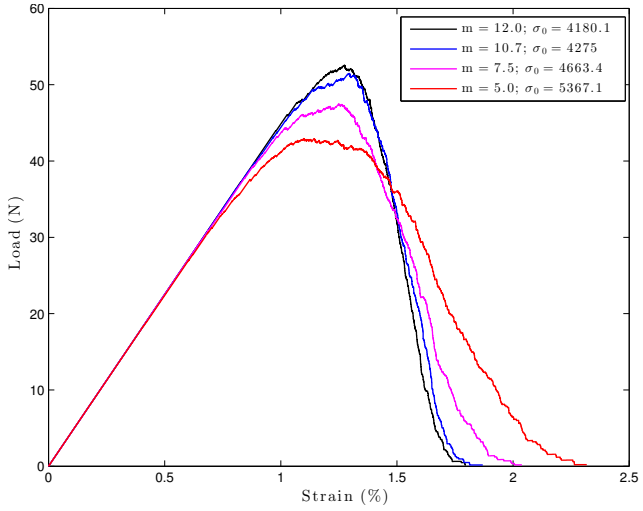

Figure 4.7: Force-Strain diagrams for fibres with different dispersions, but same average strength.

It is important to understand the effect that the gauge length (L) has in the behaviour of a tow whose fibre strengths are considered to follow a Weibull distribution. To do so, the fibres were considered to have the following reference parameters: $\sigma_0 = 4275$ MPa and $m = 10.7$ at $L_0 = 12.7$ mm. The length of the tow was varied

from 5 to 100 mm, which translates in the fibre strength distributions present in Figure 4.8. It can bee seen that the effect of the gauge length in the strength distribution of the fibres is similar to that of the scale parameter (σ_0), which is expected as the reference strength changes with the gauge length.

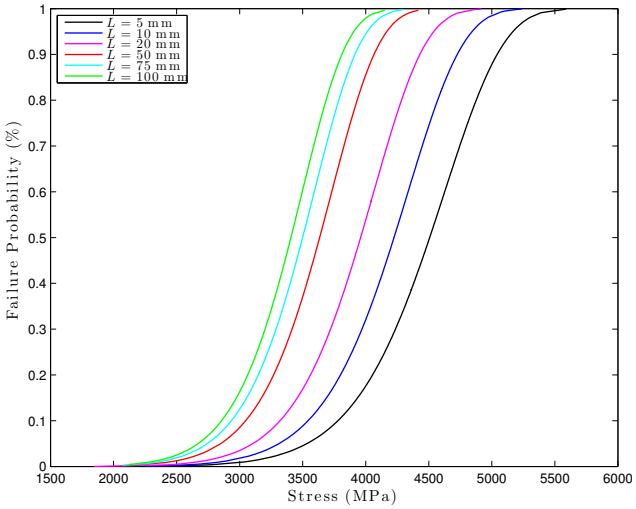

Figure 4.8: Effect the gauge length (L) in the strength of the fibres.

Changing the tow's length has the same effect as changing the scale parameter, as can be seen in Figure 4.9 and Table 4.4.

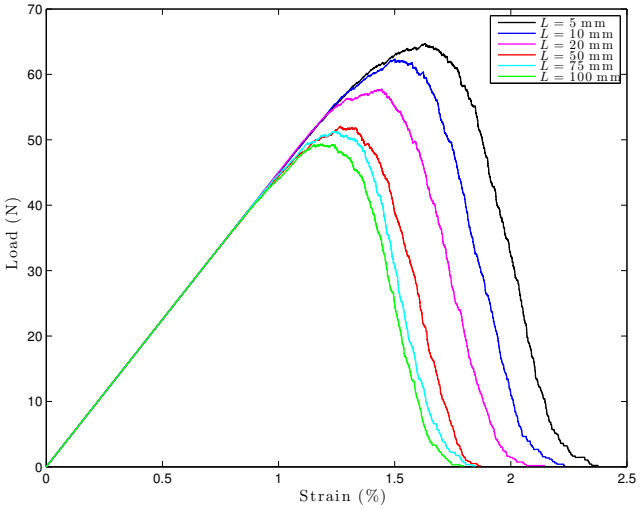

Figure 4.9: Force-Strain diagrams for tows of fibres with lengths (L).

As seen the these results, the characteristic parameters of the Weibull distribution drastically change the tow behaviour, as the strength distributions are modified by these parameters. The Weibull scale parameter (σ_0) as an effect on the average failure strength of the fibres, while the shape parameter (m) changes both the average failure strength and the dispersion of the strength. This motivated the study

Table 4.4: Effect of the gauge length (L) in some reference properties.

σ_0 (MPa)	m	L_0 (mm)	$\langle\sigma\rangle$ (MPa)	Maximum load (N)	Strain at max. load (%)
4275	10.7	5	4449.7	65.9	1.6
		10	4170.6	61.9	1.5
		20	3909.0	58.0	1.4
		50	3588.2	53.3	1.3
		75	3454.7	51.1	1.2
		100	3363.1	49.9	1.2

of the effect of the fibre dispersion by changing both m and σ_0 in order to get the same average failure strength ($\langle\sigma\rangle$) for different shape parameters. It was concluded that the dispersion changes the initiation of failure, which will affect the maximum force of the tow, as more fibres will fail at lower forces. Increasing the strength dispersion, by reducing the shape parameter, leads to a broader stress-strain curve. The gauge length (L) as similar effects as the scale parameter (σ_0) by changing the average failure strength, which affects both the maximum force and failure strain of the tow.

4.3 Hybrid tow behaviour

The previous section focused on the effects that changing the Weibull parameters for fibre strength have on the tow's tensile behaviour. This section will study the effects of hybridization on the tensile behaviour of tows.

When dealing with more than one type of fibres it is important to note that not only the strength distributions, but also the elastic properties and fibre radius affect the tow's behaviour. In order to better compare both fibre distributions, the Weibull distribution will be considered in terms of strain, given by:

$$P(\varepsilon) = 1 - \exp\left[-\frac{L}{L_0}\left(\frac{\varepsilon}{\varepsilon_0}\right)^m\right] , \tag{4.8}$$

where $\varepsilon_0 = \sigma_0/E$. This distribution is used to generate two random vectors failure strains, one for each type of fibre, with the respective parameters.

As the elastic properties and sectional area of the fibres may not be the same, Equation 4.7 needs to be modified as follows:

$$F = \varepsilon\left[(N_{t1} - N_{f1})\, S_{f1}E_{f1} + (N_{t2} - N_{f2})\, S_{f2}E_{f2}\right] , \tag{4.9}$$

where the subscripts 1 and 2 refer to each of the fibre types.

As seen in Equation 4.9, the load depends on the sectional area of both fibres. As the total tow sectional area may vary with the hybrid volume fraction, due to fibres with different radii and, to better relate the results for different tows, the load-strain diagrams were substituted by stress-strain diagrams, where the stress is given by:

$$\overline{\sigma} = \frac{F}{S_{\text{tow}}} \ . \tag{4.10}$$

The tow's area (S_{tow}) is expressed as function of the hybrid volume fractions (F_{fi} as:

$$S_{\text{tow}} = N_t \left(S_{f1} V_{f1} + S_{f2} V_{f2} \right) \ . \tag{4.11}$$

Note that $V_{f1} + V_{f2} = 1$ as dry tows are considered. One of the objectives of studying hybrid composites, as explained in Chapter 3, is the possibility of a pseudo-ductile behaviour, which represents a gradual failure of the composite material. To compare the behaviour of different hybrids, a metric for the pseudo-ductility has to be established. H. Yu et al. [80], defined the pseudo-ductile strain (ε_d) as the difference between the strain at which the specimen looses is integrity ($\varepsilon_{\max}$) and the elastic strain (ε_{E0}), at the same stress level as $\varepsilon_{\max}$ but based on the initial young modulus (E_0), as illustrated in Figure 4.10.

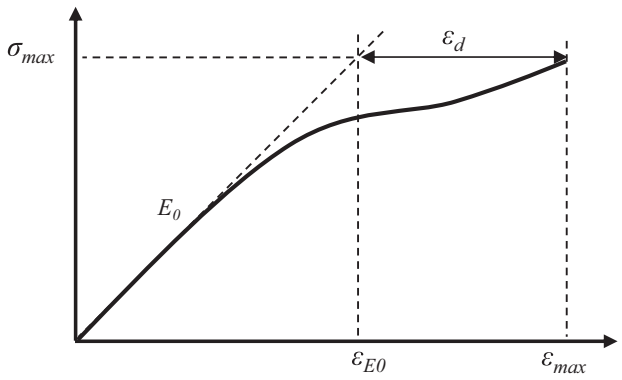

Figure 4.10: Diagram of pseudo-ductile strain.

ε_{E0} can be calculated as $\varepsilon_{E0} = \sigma_{\max}/E_0$, where E_0 can be estimated by the linear rule-of-mixtures as:

$$E_0 = V_{f1} E_{f1} + V_{f2} E_{f2} \ . \tag{4.12}$$

This metric will allow the comparison of the pseudo-ductile behaviours of different composites or tows.

In the next sections the behaviour of different hybrid tows will be studied. The sections will be divided by the type of fibres that constitute the tow (e.g. carbon-carbon, carbon-glass). As in Section 4.2, the tows will be constituted by 500 fibres with a length of 75 mm.

4.3.1 Carbon-Carbon hybridization

Table 4.5: Mechanical properties for carbon fibres.

Material	Reference	σ_0 (MPa)	L_0 (mm)	m	E (GPa)	R (μm)	$\langle\varepsilon\rangle$ @75mm (%)
HTS carbon	Beyerlein 1996 [89]	4493	19	4.8	230	3.5	1.34
X5 fibers	Nakatani 1999 [90]	2500	25	6.1	520	5.05	0.37
AS4 carbon	Curtin 1998 [88]	4275	12.7	10.7	234	3.5	1.48
T300	Curtin 1998 [88]	3170	25	5.1	232	3.5	1.01
T300	R Mili 1996 [87]	3200	30	5.5	232	3.5	1.08
T300-B4C	R Mili 1996 [87]	3150	30	5.4	232	3.5	1.06
700°C	Tanaka 2014 [91]	1400	10	11	55	3.3	2.02
1000°C	Tanaka 2014 [91]	4500	10	4.5	240	2.9	1.09
T800G	Tanaka 2014 [91]	6800	10	4.8	295	2.75	1.39
M30S	Tanaka 2014 [91]	6400	10	4.6	295	2.8	1.28
M40S	Tanaka 2014 [91]	4900	10	5.2	380	2.7	0.81
M50S	Tanaka 2014 [91]	4600	10	9	480	2.65	0.73

In this section we will study the tow hybridization with multiple types of carbon fibres. For that we need the properties given in Table 4.5. The fibres strength is considered to be characterized by a Weibull distribution (Equation 4.1). For HTS carbon fibres distribution, the authors [89] consider a modified Weibull distribution with $\alpha = 0.6$, however, we will consider $\alpha = 1$ and, therefore, a traditional Weibull

distribution.

The distributions for fibre strength of carbon fibres are represented in Figure 4.11 in terms of failure strain. As one can see, the failure distributions are quite diverse for the different types of carbon fibres. This variety can lead o interesting behaviours when different carbon fibres are mixed in a hybrid tow.

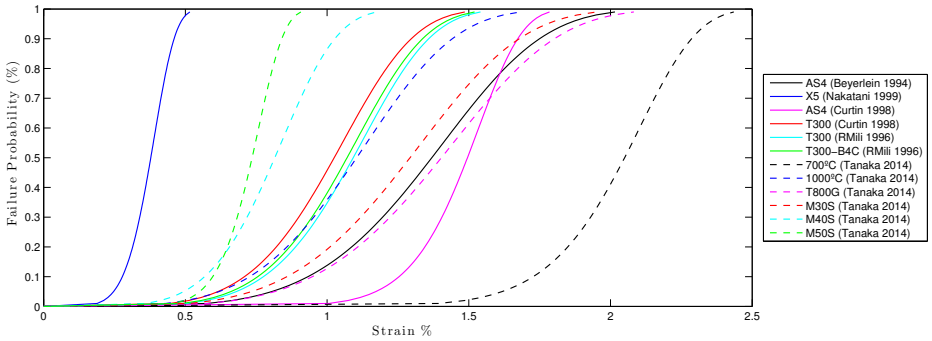

Figure 4.11: Failure strain distributions for different carbon fibres.

AS4/T300 carbon hybridization

In this section the hybridization between the AS4 and T300 [88] carbon fibres, whose properties can be found in Table 4.5, will be analysed. The T300 fibres, in this case, are the LE fibres and the AS4 the HE fibres. Figure 4.12 shows the stress-strain diagrams for the hybrid tows at various hybrid volume fractions.

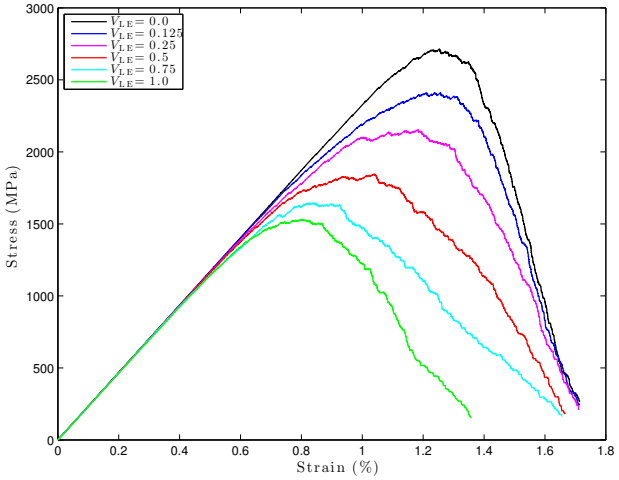

Figure 4.12: Stress-strain diagrams at various hybrid volume fractions for AS4/T300 hybridization.

It is observe in Figure 4.12 that when the volume content of LE fibres is increased,

the failure strain is reduced and, as the fibres have similar elastic moduli, so is the maximum load. These parameters can be found in Table 4.6. The maximum pseudo-ductile strain is achieved for a volume fraction of T300 fibres equal to 0.25, however, the tow's behaviour does not represent a pseudo-ductile behaviour, as there is no gradual failure. The pseudo-ductile strain is, mainly, due to the non-linearity cause by the failure of the weakest fibres.

Table 4.6: Stress-strain reference properties for AS4/T300 hybridization.

V_{LE}	Maximum stress (MPa)	Strain at max. stress (%)	ε_d (%)
0	2657.05	1.24	0.11
0.125	2387.96	1.22	0.20
0.25	2152.55	1.17	0.24
0.5	1813.23	0.98	0.20
0.75	1650.80	0.85	0.14
1	1551.89	0.82	0.15

AS4/M40S carbon hybridization

Figure 4.11 shows the failure strain distributions for the AS4 [88] and the M40S [91] are quite different. The M40S fibres are, in this case, the LE fibres. The stress-strain curves for several hybrid volume fraction are presented in Figure 4.13.

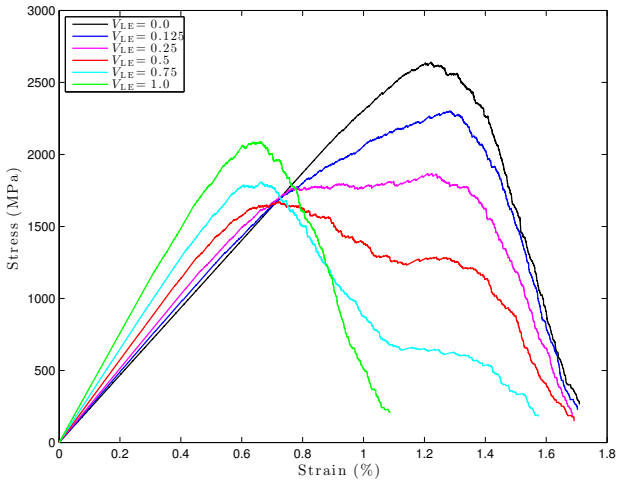

Figure 4.13: Stress-strain diagrams at various hybrid volume fractions for AS4/M40S hybridization.

In Figure 4.13 it can be seen that for a LE fibre volume fraction of 0.25, there

is a pseudo-ductile behaviour and a gradual failure of the tow. The values of the pseudo-ductile strain and other properties are shown in Table 4.7.

Table 4.7: Stress-strain reference properties for AS4/M40S hybridization.

V_{LE}	Maximum stress (MPa)	Strain at max. stress (%)	ε_d (%)
0	2650.92	1.25	0.12
0.125	2260.18	1.24	0.35
0.25	1889.69	1.23	0.53
0.5	1688.61	0.73	0.18
0.75	1807.68	0.67	0.14
1	2023.12	0.66	0.12

In this table it is possible to note that the pseudo-ductile strain ε_d is higher for a LE fibre volume fraction of 0.25 and is equal to 0.53%, which is expected from the interpretation of the Figure 4.7. For a LE fibre volume fraction of 0.125 there is a reduction of stiffness when the LE fibres start to fail, which leads to a second almost linear ($0.75 < \varepsilon > 1.22$) behaviour until the rupture of the tow.

This type of hybridization may have potential in composite materials as some degree of pseudo-ductility is already present in the dry tow behaviour. The pseudo-ductile behaviour comes at a cost of strength, as the maximum force the tow can withstand is reduced, from 2651 MPa in the AS4 carbon tow to 1889 MPa for a M40S fibre volume fraction equal to 0.25.

AS4/M50S carbon hybridization

As the AS4 and M50S failure strain distributions are quite different (see Figure 4.11), the results of their hybridization may be interesting. Figure 4.14 shows the stress-strain curves for AS4/M50S carbon hybrids.

Table 4.5 shows that the difference of average failure strain $\langle\varepsilon\rangle$ between the AS4 and M50S fibres is higher than that between AS4 and M50S fibres. This, in addition to the differences in the elastic properties, leads to the different behaviours found in Figures 4.13 and 4.14.

Table 4.8 shows that for LE fibres volume fraction of 0.25 the pseudo-ductile strain is maximum and equal to 0.58%. However, analysing Figure 4.14, one can see that there is a drop in load bearing capacity of the tow when the LE fibres fail, resulting in a load drop. For a LE volume fraction of 0.125 there is an increase in

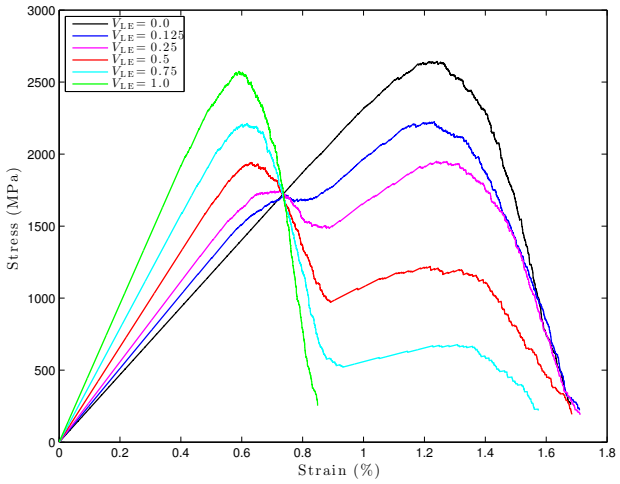

Figure 4.14: Stress-strain diagrams at various hybrid volume fractions for AS4/M50S hybridization.

Table 4.8: Stress-strain reference properties for AS4/M50S hybridization.

V_{LE}	Maximum stress (MPa)	Strain at max. stress (%)	ε_d (%)
0	2647.83	1.26	0.13
0.125	2266.18	1.24	0.38
0.25	1904.89	1.23	0.58
0.5	1887.11	0.63	0.10
0.75	2182.22	0.62	0.10
1	2603.82	0.61	0.07

ductility in relation to the non-hybrid composites, with a pseudo-ductile strain equal to 0.38% without having the load drop that is present in the composite with a LE fibre volume fraction of 0.25.

Analysis of the results

From the previous sections it is concluded that hybridizing dry tows can lead to a drastic changes in the tow's behaviour under tensile loadings, even for hybridizations using only carbon fibres. To understand the behaviours previously presented for the tows, it is necessary to understand the difference in failure strain distributions (Figure 4.15).

The AS4 fibres are present in the three hybridizations studied and should be

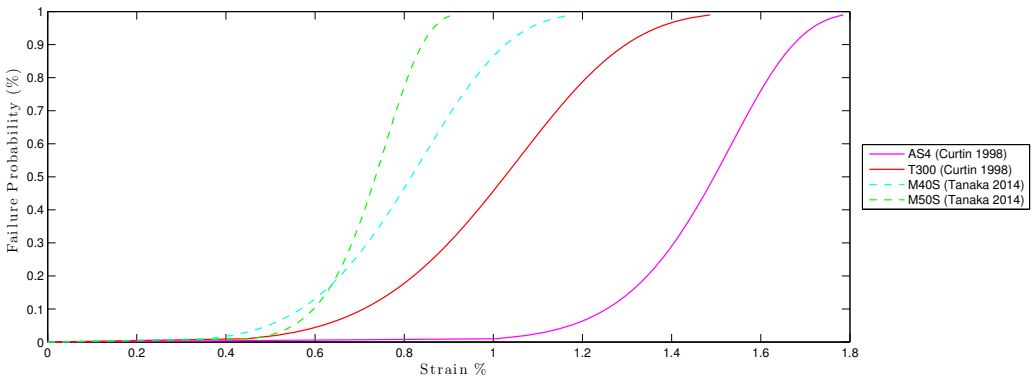

Figure 4.15: Failure strain distributions for the carbon fibres used for hybridization.

used as reference. The T300 carbon fibres have the most similar failure strain distribution to that of the AS4 carbon fibres. This leads to a behaviour like the one shown in Figure 4.12, where it can be seen a more gradual failure with the hybridization, however, it is far from the desired pseudo-ductile behaviour. As the distributions between the hybridized fibres are further apart, it is shown that there is a less catastrophic failure (Figures 4.13 and 4.14). For the AS4/M50S hybridization, the distributions are the furthest apart and there is no continuity in fibre failure, leading to a load drop, as seen in Figure 4.14 for $V_{LE} = 0.25$ or $V_{LE} = 0.5$. For the AS4/M40S hybridization there is a continuity in the fibre failure and there is a more gradual failure, leading to a pseudo-ductile behaviour.

4.3.2 Glass-Glass hybridization

The previous section analysed the hybridization of tows only with carbon fibres. This section will a similar study for glass fibre hybrid tows, whose fibre properties are in Table 4.9. These properties result in the failure strain distributions present in Figure 4.16. The main objective of this study is to verify whether the phenomena observed in the carbon-carbon hybridization can also be found in glass-glass hybrids. It is also important to understand that the conclusions, from the study of the carbon-carbon hybrid tows, still hold for the glass hybrids. As it was mentioned in the previous section, the separation in the strain failure distributions may be necessary for the existence of a pseudo-ductile behaviour, therefore, the first hybridization to be studied will be the High Performance (HP) and High Dispersion (HD) AR glass fibres [92] hybridization.

Table 4.9: Mechanical properties for glass fibres.

Material	Reference	σ_0 (MPa)	L_0 (mm)	m	E (GPa)	R (μm)	$\langle\varepsilon\rangle$ @75mm (%)
E-Glass	T.Okabe 2001 [43]	1550	24	6.34	76	6.5	1.59
E-Glass	Feih 2005 [93]	1649	20	3.09	66.9	7.8	1.44
E-Gkass	Pauchard 2002 [94]	2300	10	3.6	70	5	1.69
AR-HP	Foray 2012 [92]	1363	60	9.6	70	7	1.81
AR-HD	Foray 2012 [92]	876	60	4.8	70	7	1.09

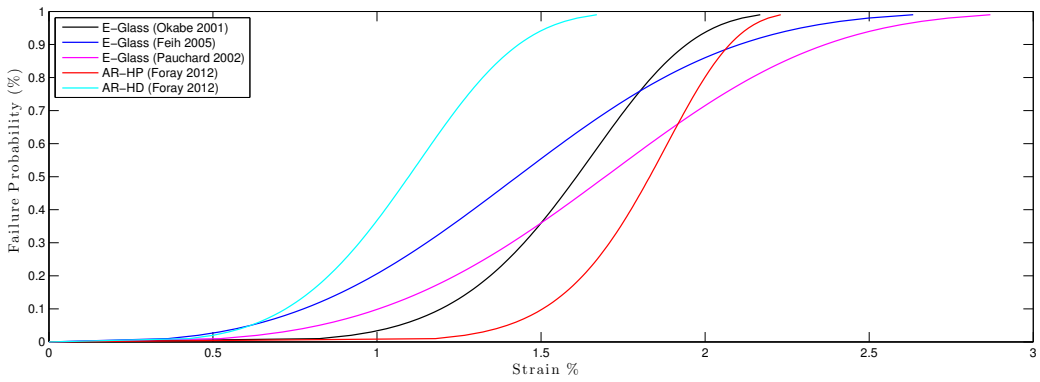

Figure 4.16: Failure strain distributions for several glass fibres.

HD/HP AR glass hybridization

The HP fibres have a higher average failure strain ($\langle\varepsilon\rangle$) and will referred as HE fibres, while the HD fibres as the LE fibres. The stress-strain diagrams for this type of hybridization can be seen in Figure 4.17.

The fibres in study in this section have the same elastic moduli and the same radii, therefore, the difference in behaviour due to hybridization may only be attributed to the differences in strength distributions. In this hybridization it is possible to see a progressive failure, which results in a maximum pseudo-ductile strain equal to 0.4%. However, the behaviour seen in Figure 4.17 is quite different of that for the AS4/M40S carbon (Figure 4.13). This may be attributed to the glass fibres having the same elastic properties and radii, while in the carbon hybridization the elastic modulus of the AS4 carbon (HE fibres) is inferior to that of the M40S carbon.

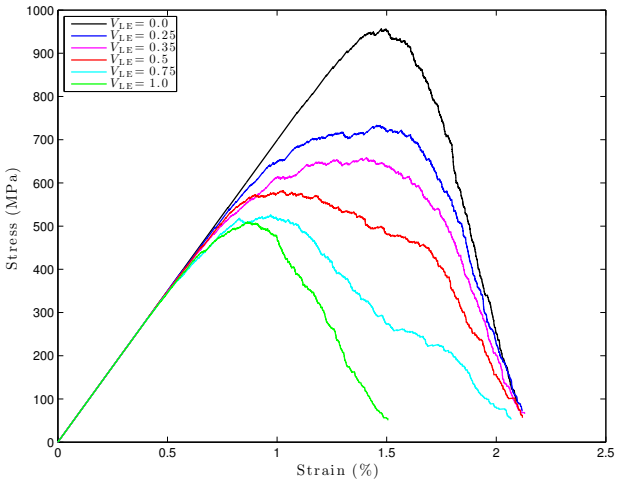

Figure 4.17: Stress-strain diagrams at various hybrid volume fractions for HD/HP AR glass hybridization.

Table 4.10: Stress-strain reference properties for HD/HP AR glass hybridization.

V_{LE}	Maximum stress (MPa)	Strain at max. stress (%)	ε_d (%)
0	953.24	1.50	0.14
0.25	738.89	1.45	0.40
0.35	660.87	1.34	0.40
0.5	588.33	1.07	0.23
0.75	528.39	0.94	0.18
1	498.60	0.89	0.18

Trying to hybridize a tow with any other two types of glass fibres (from those in Table 4.9) results in a tow behaviour similar to that of Figure 4.12, meaning there is no pseudo-ductile behaviour. Analysing the fibre failure strain distributions (Figure 4.16) it is possible to reinforce what was concluded in Section 4.3.1: to have a pseudo-ductile behaviour there has to be a continuity in fibre failure and the start of failure of the HE fibres must be for strains close to the failure strains of the strongest LE fibres. The Feih [93] and Pauchard [94] E-glass strength distributions have a high dispersion and their hybridization shows high values for pseudo-ductile strain, however, there is no pseudo-ductile behaviour. The high dispersion of fibre strengths leads to a high non-linearity in the tow's tensile behaviour, justifying the high results of the pseudo-ductile strain.

4.3.3 Kevlar-Kevlar hybridization

Kevlar fibres are polymeric fibres used in technical composites. The fibre properties and strength distributions are shown in Table 4.11 and Figure 4.18. This section presents the study of the influence of hybrid tows based on kevlar fibres.

Table 4.11: Mechanical properties for kevlar fibres.

Material	Reference	σ_0 (MPa)	L_0 (mm)	m	E (GPa)	R (μm)	$\langle\varepsilon\rangle$ @75mm (%)
Kevlar 29	Naito 2013 [95]	3445.8	25	11.8	85.3	6.895	3.52
Kevlar 49	Naito 2013 [95]	4083.3	25	8.2	149.1	5.135	2.26
Kevlar 119	Naito 2013 [95]	3101.2	25	11.8	61.4	5.46	4.41
Kevlar 129	Naito 2013 [95]	3433	25	10.3	99	5.79	2.97

This fibres have, in general, an average failure strain superior to that of carbon and glass fibres.

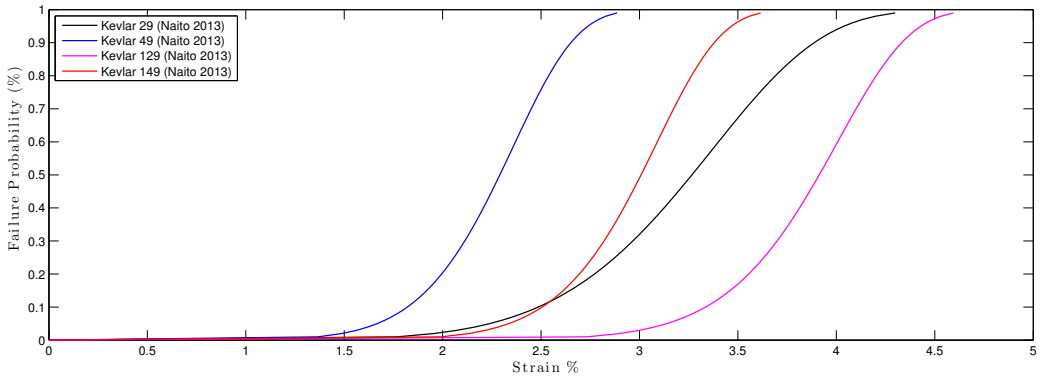

Figure 4.18: Failure strain distributions for several kevlar fibres.

Kevlar 49/119 hybridization

The hybridization of Kevlar 49 and Kevlar 119 is the hybridization between the Kevlar fibres with the highest and lowest average failure strain, among the data found. The stress-strain diagrams for this hybridization can be found in Figure 4.19 and the most significant properties in Table 4.12.

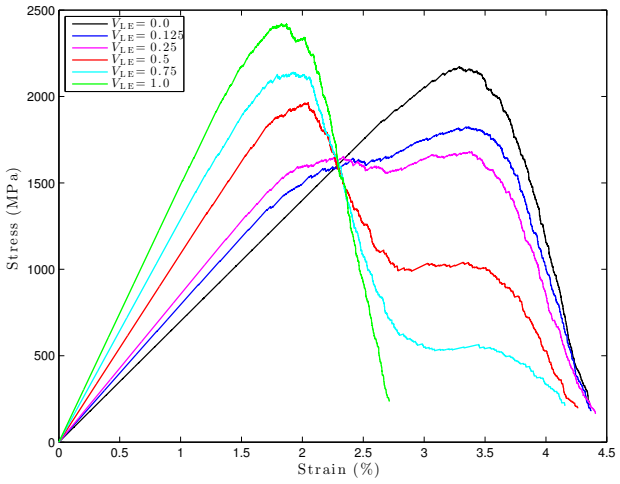

Figure 4.19: Stress-strain diagrams at various hybrid volume fractions for kevlar 49/119 hybridization.

Table 4.12: Stress-strain reference properties for kevlar 49/119 hybridization.

V_{LE}	Maximum stress (MPa)	Strain at max. stress (%)	ε_d (%)
0	2120.98	3.27	0.24
0.125	1853.77	3.27	0.95
0.25	1704.65	3.23	1.24
0.5	1905.42	1.96	0.22
0.75	2183.09	1.91	0.22
1	2457.20	1.87	0.22

As it can be seen from the data presented this hybridization shows a high value for the pseudo-ductile strain ($\varepsilon_d = 1.24\%$), and the failure strain distributions show a similar behaviour as the previous ones whose behaviour as pseudo-ductile like (the failure of the stronger LE fibres coincide with the beginning of failure of the HE fibres). The higher pseudo-ductile strain, in comparison with the carbon-carbon and glass-glass hybridization may be related to the higher failure strain of the Kevlar fibres.

Kevlar 119/129 hybridization

The Kevlar 119 and 129 fibres have failure distributions whose average failure strains are less apart than that in the Kevlar 49/119 hybridization. This hybridization results in the stress-strain curves and major properties in Figure 4.20 and Table

4.13.

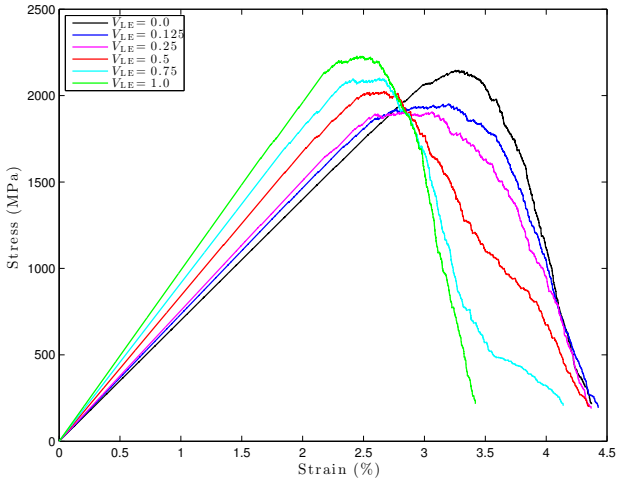

Figure 4.20: Stress-strain diagrams at various hybrid volume fractions for kevlar 119/129 hybridization.

It can be seen that the failure of this hybrid tow is more catastrophic than that of the previous hybridization. This leads us to similar conclusions to those from carbon-carbon and glass-glass hybridization: to achieve a pseudo-ductile behaviour in tow failure the HE fibres need to start failing near the end of the failure of the LE fibres. This causes a progressive failure of the fibres leading to an pseudo-ductile behaviour.

Table 4.13: Stress-strain reference properties for kevlar 119/129 hybridization.

V_{LE}	Maximum stress (MPa)	Strain at max. stress (%)	ε_d (%)
0	2118.78	3.27	0.24
0.125	1984.39	3.01	0.32
0.25	1957.57	2.87	0.28
0.5	2023.90	2.65	0.25
0.75	2115.10	2.56	0.25
1	2251.12	2.48	0.21

4.3.4 Carbon-Glass hybridization

In the previous sections the effects of hybridizing tows with fibres of the same type were studied. As previously stated in Chapter 3, the hybridization of composite materials started between carbon and glass fibres,with the objective of achieving a

reduced price of the composite while maintaining some of the desired properties of the carbon fibres.

The hybridization between fibres of different materials enables the creation of a wider range of material properties, that can be tuned to a specific application.

In the next sections, with the aim of maximizing the pseudo-ductile behaviour, the hybridization of tows with fibres of different materials will be studied. Some different behaviours are expected due to a more diverse range of fibre properties. This section is dedicated to carbon-glass hybrids, whose properties are presented in Tables 4.5 and 4.9.

T300 carbon/AR-HP glass hybridization

The T300 carbon fibres [88], whose elastic modulus is $E = 232$ GPa and Weibull parameters are $\sigma_0 = 3170$ MPa and $m = 5.1$ at $L_0 = 25$ mm, was hybridized with the AR-HP glass fibres [92], whose elastic modulus is $E = 70$ GPa and Weibull parameters are $\sigma_0 = 1363$ MPa and $m = 9.6$ at $L_0 = 60$ mm. In this hybridization, the T300 carbon fibres are the LE fibres, while the AR-HP glass are the HE fibres. The stress-strain diagrams for several hybrid volume fractions are presented in Figure 4.21.

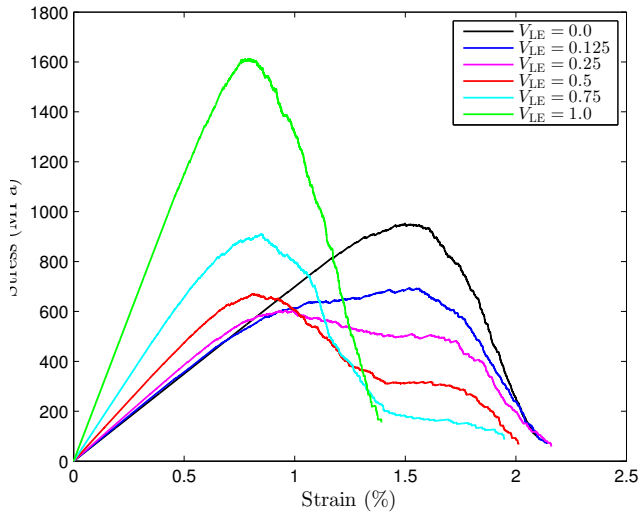

Figure 4.21: Stress-strain diagrams at various hybrid volume fractions for T300 carbon and AR-HP glass hybridization.

As it is possible to see in Table 4.14, the maximum value for the pseudo-ductile strain is equal to 0.74% and is achieved at a volume fraction of the LE fibres equal to 0.125. This pseudo-ductility comes at the cost of the maximum stress that the tow can withstand, as it is reduced from 1552 MPa, for full carbon, to 685 MPa

Table 4.14: Stress-strain reference properties for T300 carbon and AR-HP glass hybridization.

V_{LE}	Maximum stress (MPa)	Strain at max. stress (%)	ε_d (%)
0	955.86	1.52	0.15
0.125	685.19	1.49	0.74
0.25	603.03	0.96	0.41
0.5	677.67	0.88	0.43
0.75	917.28	0.81	0.33
1	1551.64	0.80	0.13

for a LE volume fraction of 0.125, value that is lower that that of full AR-HP glass ($V_{LE} = 0$).

1000°C carbon/AR-HP glass hybridization

Another carbon/glass hybridization was studied, maintaining the same glass fibres (AR-HP) and changing the T300 carbon fibres to the 1000°C carbon fibres [91], whose properties are: $E = 240$ GPa and $\sigma_0 = 4500$ MPa, $m = 4.5$ at $L_0 = 10$ mm.

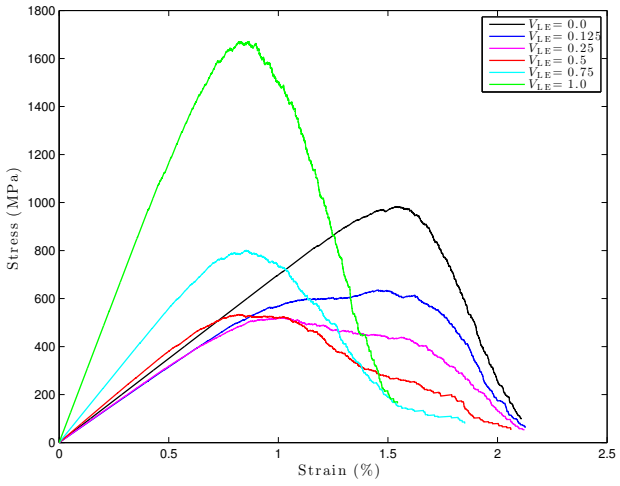

Figure 4.22: Stress-strain diagrams at various hybrid volume fractions for 1000°C carbon and AR-HP glass hybridization.

This hybridization is very similar to the one presented previously, as the fibre strength distributions are very similar. The maximum pseudo-ductile strain occurs

Table 4.15: Stress-strain reference properties for 1000°C carbon and AR-HP glass hybridization.

V_{LE}	Maximum stress (MPa)	Strain at max. stress (%)	ε_d (%)
0	959.20	1.51	0.14
0.125	613.90	1.37	0.70
0.25	524.97	1.08	0.61
0.5	565.80	0.91	0.54
0.75	806.46	0.89	0.48
1	1679.96	0.88	0.18

at a low LE fibre volume fraction and results in a reduction in the maximum stress in the tow. Similar results can be achieved with other carbon/glass hybridizations. In the present hybridization, the difference between the maximum stress in the tow, for 100% carbon, and the maximum stress when the maximum pseudo-ductile strain occurs is higher, than in the AR-HP/T300 hybridization, which can be attributed to a higher difference in the elastic moduli of the hybridizing fibres.

4.3.5 Carbon-Kevlar hybridization

This section is dedicated to the study of the tow hybridization with carbon and kevlar fibres. These fibres have very different properties. The carbon fibres are stiffer and have a lower failure strain, while the kevlar fibres have lower stiffness but higher failure strain, meaning that the failure stress of both types of fibres is similar.

AS4 carbon/Kevlar 49 hybridization

From the analysis of Figure 4.23 and Table 4.16 it is possible to not that the maximum pseudo-ductile strain that can be achieved with this hybridization is low and equal to 0.53%, however, the reduction of the maximum stress in the tow is very low, from 2672 MPa at 100% kevlar to 2034 MPa at a carbon volume fraction of 0.125, at which the pseudo-ductile strain is maximum. This behaviour is very different of the ones in the carbon/glass hybridization (Section 4.3.4), where the hybridization lead to a large reduction in maximum stress in the tows.

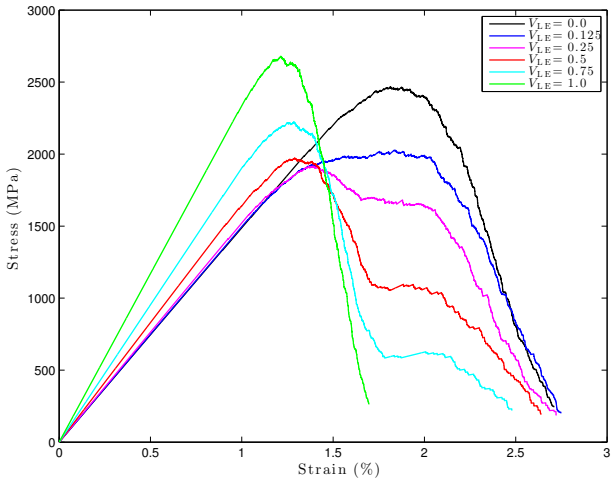

Figure 4.23: Stress-strain diagrams at various hybrid volume fractions for AS4 carbon and kevlar 49 hybridization.

Table 4.16: Stress-strain reference properties for AS4 carbon and kevlar 49 hybridization.

V_{LE}	Maximum stress (MPa)	Strain at max. stress (%)	ε_d (%)
0	2460.55	1.84	0.19
0.125	2033.85	1.80	0.53
0.25	1916.97	1.40	0.27
0.5	1982.74	1.31	0.28
0.75	2218.15	1.29	0.24
1	2671.80	1.24	0.10

M40S carbon/Kevlar 49 hybridization

In this hybridization the kevlar 49 were used, as in the previous section, but the AS4 carbon fibres were replaced by M40S carbon fibres [91]. These fibres are stiffer than the AS4 carbon but have a lower average failure strain. The M40S fibres have a elastic modulus of 380GPa and strength distribution parameters $\sigma_0 = 4900$ MPa and $m = 5.2$ at $L_0 = 10$ mm. Figure 4.24 shows the stress-strain diagrams for different hybrid volume fractions, the LE fibres are the M40S carbon fibres.

As the difference between failure distributions of these fibres is higher, than that of the AS4/Kevlar 49 hybridization, the resulting stress-strain diagrams are quite different. The maximum pseudo-ductile strain is achieved at a carbon volume fraction of 0.25 and is equal to 1.18%. This value is higher than that of the AS4/Kevlar

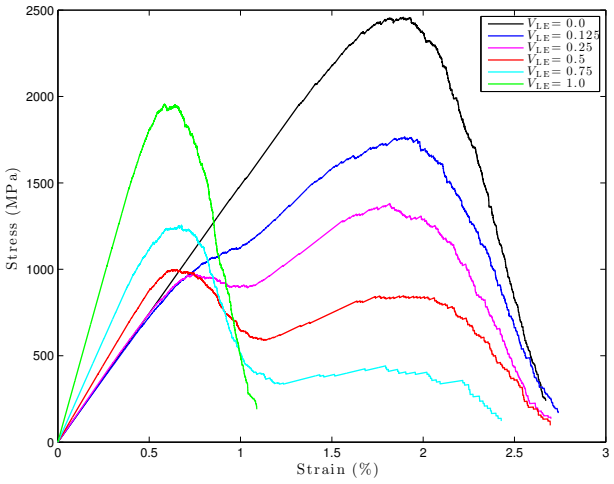

Figure 4.24: Stress-strain diagrams at various hybrid volume fractions for M40S carbon and kevlar 49 hybridization.

Table 4.17: Stress-strain reference properties for M40S carbon and kevlar 49 hybridization.

V_{LE}	Maximum stress (MPa)	Strain at max. stress (%)	ε_d (%)
0	2482.55	1.88	0.21
0.125	1788.63	1.88	0.88
0.25	1391.80	1.85	1.18
0.5	1024.64	0.70	0.31
0.75	1296.00	0.67	0.27
1	2014.17	0.64	0.11

49 hybridization, however, the reduction of the maximum stress is higher in the M40S/Kevlar 49 hybridization. The main difference between the behaviour of the tows in the AS4/Kevlar 49 and the M40S/Kevlar 49 hybridizations (Figures 4.23 and 4.24) is the reduction of the stress carrying capacity of the tow after the carbon fibres fail in the M40S hybridization. This reduction is due to a higher difference in failure strains and in elastic moduli of the hybridizing fibres.

M30S carbon/Kevlar 119 hybridization

This hybridization is the one where the hybridizing fibres have the highest difference between the average failure strains, for the carbon/kevlar hybridizations. The average failure strain of the M30S carbon [91] is 1.29% and of the kevlar 119 is

4.41%. The M30S carbon as elastic modulus $E = 295$ GPa and Weibull scale and shape parameters $\sigma_0 = 6400$ MPa and $m = 4.6$ at $L_0 = 10$ mm, while the kevlar 129 properties are: $E = 61.4$ GPa, $\sigma_0 = 3101.2$ MPa and $m = 11.8$ at $L_0 = 14$ mm. The results of this hybridization are presented in Figure 4.25 and Table 4.18.

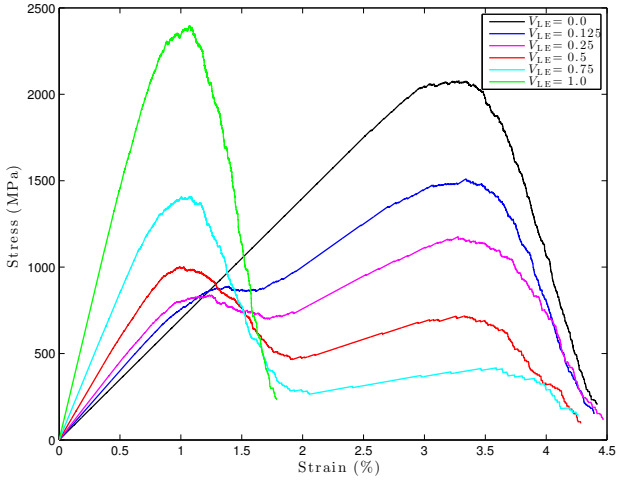

Figure 4.25: Stress-strain diagrams at various hybrid volume fractions for M43S carbon and kevlar 119 hybridization.

Table 4.18: Stress-strain reference properties for M30S carbon and kevlar 119 hybridization.

V_{LE}	Maximum stress (MPa)	Strain at max. stress (%)	ε_d (%)
0	2126.60	3.29	0.25
0.125	1521.70	3.30	1.74
0.25	1172.38	3.31	2.38
0.5	1041.73	1.08	0.51
0.75	1418.30	1.06	0.46
1	2409.27	1.01	0.20

The gap between the fibre strength distributions causes the stress drop seen for all hybrid volume fractions in Figure 4.25 but, as the kevlar fibres have a higher failure strain, at low LE fibre volume fractions, the tow is still able to carry stress after the failure of the LE fibres. Adding M30S carbon fibres to the Kevlar 119 tow, causes the pseudo-ductile strain to increase however, the stress-strain diagrams, are not exactly what is expected from a pseudo-ductile behaviour, as there is not a progressive failure. There is a drastic failure of the carbon fibres followed by a drastic failure of the kevlar fibres at a higher strain, which is the usual behaviour

of hybrid composites (see Chapter 3). This, in addition, to the remaining results, allows us to conclude that, in order to achieve a pseudo-ductile behaviour at the tow level, there needs to be a separation between the fibre strength distributions. However, if the separation is two high, the resulting tow will behave like in Figure 4.25 where there is no interaction between the failure of both fibre types.

4.4 Conclusion

A model for predicting the failure of dry tows of fibres under tensile loadings was developed. This model was based in the fact that the fibre strengths can be described by a Weibull distribution and that there is no interaction between the fibres, as there is no matrix connecting them.

This model allowed the study of the effects that different Weibull distributions have in the behaviour of the tow. The scale parameter is directly related with the average failure strength of the fibres and increasing it causes the tow to have a higher failure load and strain, as the average fibre is capable of carrying a higher stress before breaking. The shape parameter influences, not only the dispersion of fibre strength, but also the average failure strength. Therefore, changing this parameter drastically changes the tow's tensile response. In order to study the effect of the dispersion of fibre strength, the shape and scale parameters were changed, maintaining the same average failure strength. This changes lead to the conclusion that higher dispersion leads to a earlier failure of the tow, as there are more weak fibres, which cause the tow to have a more pronounced non-linear behaviour. This earlier failure of the weakest fibres cause the maximum force in the tow to be reduced as, at that point, more fibres have failed.

The second part of this chapter consisted in the hybridization of tows and understanding the interactions between fibres with different properties. The hybridization was done to understand and quantify the pseudo-ductile behaviour. This behaviour can be characterized by a gradual failure of the material, instead of the catastrophic one usually associated with composite materials. The parameter used for characterizing the pseudo-ductility was the pseudo-ductile strain, as defined by H. Yu [80]. Several hybridizations were performed, including hybridizations between fibres of the same type and different types.

The main conclusion that can be withdrawn from this study is that to achieve a pseudo-ductile behaviour at the tow level, there needs to be a separation between the strength distributions of both fibre types. This separation needs to be such that there is a continuity in the failure of the LE and HE fibres, which leads to a gradual failure of the composite and, therefore, a pseudo-ductile behaviour.

Chapter 5

Progressive damage model for hybrid composites

The effects of fibre hybridization on the tensile response of dry tows were studied in the previous chapter. In the dry tows there is no matrix and the fibres are not connected, which does happen in composite materials. The presence of the matrix changes the material's behaviour and this needs to be taken into account in a model to predict the tensile failure of composite materials.

The present chapter aims to extend the progressive damage model for unidirectional fibre-reinforced composites based on fibre fragmentation, developed by Turon et al. [5] to hybrid composites. The model will be used to predict the tensile behaviour of hybrid fibre reinforced composites to understand the factors controlling the pseudo-ductile behaviour of hybrid composites.

5.1 Model development

The model developed by Turon et al. [5] is based on the multiple fragmentation of the fibres in single fibre fragmentation tests, whose mechanisms are present in the failure of multiple fibre composite materials.

5.1.1 Fibre break density

The failure probability of the fibres is considered to follow a Weibull distribution [17], given by

$$P(\sigma) = 1 - \exp\left[-\frac{L}{L_0}\left(\frac{\sigma}{\sigma_0}\right)^m\right] , \tag{5.1}$$

where $P(\sigma)$ is the failure probability of a fibre with length L when subjected to a tension σ. L_0 is the reference length at which the Weibull parameters σ_0 and m were determined.

From Equation 5.1 it is possible to show that the number of breaks in a fibre follows a Poisson distribution, therefore, it is possible to determine the average number of breaks ($\langle N \rangle$) in a fibre as a function of the applied stress:

$$\langle N \rangle = \frac{L}{L_0} \left(\frac{\sigma}{\sigma_0} \right)^m . \tag{5.2}$$

This equation is not fully accurate as some defects will be located in the stress recovery region of the fibres, where the stress is lower than the applied stress, which is not taken into account by Equation 5.2.

If the number of breaks in a fibre follows a Poisson distribution then the distance between fibre breaks can be described by an exponential law:

$$f(x) = \Lambda e^{-\Lambda x} , \tag{5.3}$$

where Λ is the number of breaks per unit length, given by

$$\Lambda = \frac{\langle N \rangle}{L} = \frac{1}{L_0} \left(\frac{\sigma}{\sigma_0} \right)^m . \tag{5.4}$$

With the presented equations, the fibre break distribution, as a function of the applied strain, is fully characterized.

5.1.2 Fibre stress

As previously mentioned, a broken fibre does not loose the totality of the capacity to carry stress. After a fibre breaks, the matrix is loaded in shear and is able to transfer the stress back to the broken fibre, which will cause the fibre to have a stress profile similar to the one in Figure 5.1, described by the shear-lag theory.

The length recovery region (l_{ex}), distance from the fibre break to the location where the fibre is fully able to carry stress, can be defined as:

$$l_{ex} = \frac{R_f}{\tau} \frac{E_f \varepsilon}{2} , \tag{5.5}$$

where τ is the interfacial shear strength, R_f the fibre radius, E_f the elastic modulus of the fibre and ε is the applied strain.

The average stress in a fibre of length L can be computed by integrating the axial stress in all the fibre fragments along the fibre length:

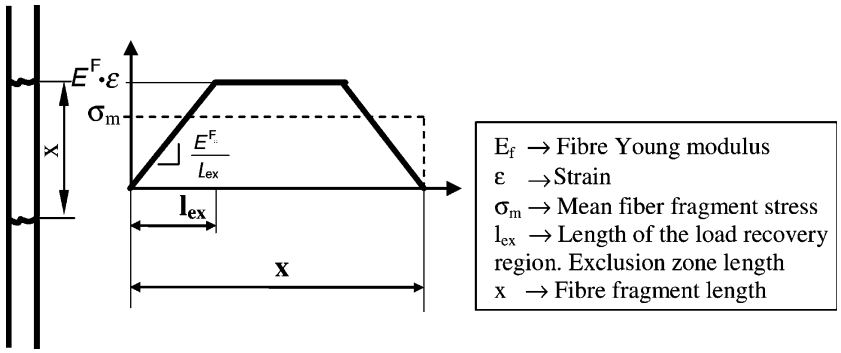

Figure 5.1: Stress profile in a fibre with multiple fractures, according to shear-lag model [5].

$$\sigma_m = \langle N \rangle \frac{1}{L} \int x \Sigma(x) f(x) \, \mathrm{d}x \,, \tag{5.6}$$

where $f(x)$ is the fragment length distribution function (Equation 5.3) and $\Sigma(x)$ is the average stress in a fragment of length x.

The average stress in a fragment will be dependent on the relation between the fragment length (x), the fibre length (L) and the recovery region length (l_{ex}), and three cases are possible:

1. The fragment length is lower than two times the recovery region (Equation 5.7a);
2. The fragment length is higher than two times the recovery region but lower than the fibre length (Equation 5.7b);
3. The fragment length is higher than the fibre length (Equation 5.7c).

As there are different cases for the average stress in a fragment, the function $\Sigma(x)$ can be described as a piecewise function given by:

$$\Sigma(x) = \begin{cases} E_f \varepsilon \dfrac{x}{4 l_{ex}} \,, & x \leq 2 l_{ex} \quad (5.7a) \\ E_f \varepsilon \left(1 - \dfrac{l_{ex}}{x}\right) \,, & 2 l_{ex} \leq x \leq L \quad (5.7b) \\ E_f \varepsilon \,, & x \geq L \quad (5.7c) \end{cases}$$

Using Equations 5.4 and 5.7 in Equation 5.6, the average stress in a fibre can be written as:

$$\sigma_m(\varepsilon) = E_f \varepsilon \Lambda \left(\int_0^{2 l_{ex}} \frac{x^2}{4 l_{ex}} f(x) \, \mathrm{d}x + \int_{2 l_{ex}}^{L} (x - l_{ex}) f(x) \, \mathrm{d}x + \int_L^{\infty} x f(x) \, \mathrm{d}x \right) . \tag{5.8}$$

The analytical solution of the previous equation gives the average stress in a fibre as a function of the applied strain (ε) and is given by:

$$\sigma_m(\varepsilon) = E_f \varepsilon \left(\frac{1 - e^{-2l_{ex}\Lambda}}{2l_{ex}\Lambda} + \Lambda l_{ex} e^{-L\Lambda} \right) . \tag{5.9}$$

In this type of models, based on fibre fragmentation, it is usual to define the critical strength parameter (σ_c) [96] . This critical strength relates the statistical parameters for fibre strength and the matrix properties. Imagine that the composite material is loaded with an applied stress (σ_i), which causes the fibres to fracture. If the spacing between the fibres is greater than twice the recovery region length (l_{ex}), then there are locations where the stress in the fibres is equal to the far field stress (σ_i), therefore the fibres are still able to fracture into smaller fragments, by increasing the applied stress. The critical stress (σ_c) is defined as the stress that causes the average fragment spacing to be equal to twice the recovery region and is equal to:

$$\sigma_c = \left(\frac{\sigma_0^m \tau l_0}{R_f} \right)^{1/1+m} . \tag{5.10}$$

In order to better relate the different types of fibres, with different elastic moduli, it is better to define the critical strain:

$$\varepsilon_c = \frac{\sigma_c}{E_f} = \frac{1}{E_f} \left(\frac{\sigma_0^m \tau l_0}{R_f} \right)^{1/1+m} . \tag{5.11}$$

5.2 Composite damage model

To develop the damage model for the composite material it is necessary to define how a fibre failure affects the loads in the remaining intact fibres and how to assemble the mechanical behaviour of the constituents in the composite. The model considers global load sharing (GLS) and, therefore, the stress is equally distributed among the intact fibres after one fails. This causes some limitations to the model as the longitudinal failure of UD composites is caused by the propagation of a cluster of broken fibres, which the model is not able to predict. The second aspect is resolved considering the rule-of-mixtures [5]. In order to avoid some physical incompatibilities the damage model is developed in the framework of the thermodynamics of irreversible processes. The free ernergy of the model is obtained by adding the free energy of the constituents as:

$$\psi = (1 - d_{f1})\, \psi_{f1}^0(\varepsilon_{f1})\, V_{f1} + (1 - d_{f2})\, \psi_{f2}^0(\varepsilon_{f2})\, V_{f2} + (1 - d_m)\, \psi_m^0(\varepsilon_m)\, V_m , \tag{5.12}$$

where d_N is the damage variable, V_N the volume fraction and ε_N the strain of the constituent N, with N equal to $f1$, $f2$ or m depending on the constituent (type one fibre, type two fibre or matrix). The variable ψ_N^0 represents the free energy of the undamaged material given by:

$$\psi_N^0 = \frac{1}{2}\varepsilon_{ij}^N C_{ijkl}^N \varepsilon_{kl}^N \,, \tag{5.13}$$

where C_{ijkl} is the constitutive tensor of the constituent N. Equation 5.13 is a function of the strains in the constituent in cause, however it is necessary to define the damage model as a function of the composite deformation. To do so is necessary to resort to the rule of mixtures considering a serial-parallel behaviour [97]. This allows to define the influence tensors T_{ijkl} as:

$$\varepsilon_{ij}^N = T_{ijkl}\varepsilon_{kl} \,, \tag{5.14}$$

where ε_{ij}^N is the strain in the constituent N and ε_{kl} is the strain of the composite. Using Equation 5.14 it is possible to determine the free energy as a function of the composite strains as

$$\psi_N^0 = \frac{1}{2}\varepsilon_{mn} T_{mnij}^N C_{ijkl}^N T_{klop}^N \varepsilon_{op} \,. \tag{5.15}$$

The rate of dissipation Ξ can be written as:

$$\Xi = \sigma_{ij}\dot{\varepsilon}_{ij} - \dot{\psi} = \left(\sigma_{ij} - \frac{\partial \psi}{\partial \varepsilon_{ij}}\right)\dot{\varepsilon_{ij}} - \sum \frac{\partial \psi}{\partial d_N}\dot{d_N} \geq 0 \,. \tag{5.16}$$

The constitutive equation for the damage model can be written as:

$$\sigma_{mn} = \frac{\partial \psi}{\partial \varepsilon_{mn}} = \left[\sum (1 - d_N)\, T_{mnij}^N C_{ijkl}^N T_{klop}^N\right] \varepsilon_{op} \,. \tag{5.17}$$

With the derivatives of the free energy respect to the damage variables and respect to the strains it is possible to write Equation 5.16 as:

$$\Xi = V_{f1}\psi_{f1}^0 \dot{d}_{f1} + V_{f2}\psi_{f2}^0 \dot{d}_{f2} + V_m \psi_m^0 \dot{d}_m \geq 0 \,. \tag{5.18}$$

From this equation is can be shown that, in order to guarantee the thermodynamic consistency, the derivatives of the damage variables must be positive: $\dot{d}_{f2} \geq 0$, $\dot{d}_{f2} \geq 0$ and $\dot{d}_m \geq 0$

As we are interested in studying the longitudinal failure of UD composites the model can be simplified by considering only the stresses in the longitudinal direction

due to an applied longitudinal strain. The constitutive equation, for the simplified case, can be written as:

$$\sigma(\varepsilon) = \left(\sum (1 - d_N) E_N V_N\right) \varepsilon \,, \tag{5.19}$$

where E_N, V_N and d_N are, respectively, the elastic modulus, volume fraction and damage variable of the constituent N. N can be the matrix or the fibres and there can be more than one type of fibres.

The damage variables for the constituents can be obtained from different damage models. For the fibres it was considered the damage variable that results from Turon's et al. model [5], given by:

$$d_f = 1 - \left(\frac{1 - e^{-2 l_{ex} \Lambda}}{2 l_{ex} \Lambda} + \Lambda l_{ex} e^{-L\Lambda} \right) \,. \tag{5.20}$$

As the longitudinal failure of the composite is a fibre dominated process the damage in the matrix was not considered, therefore, the damage variable for the matrix d_M is considered 0 for all the applied strains.

5.3 Non-hybrid composite behaviour

To better understand the effects of hybridization on the longitudinal failure of UD composites, it is important to understand the effects that the fibre and matrix properties have in the material response. In this section, the composite materials are considered to have a fibre volume fraction (V_f) of 60 % and a gauge length (L) of 75 mm. As base information for fibre properties, the AS4 carbon fibres will be considered. These fibres have a mean radius (R) of 3.5 μm, Young's modulus (E) equal to 234 GPa and the parameters for the Weibull distribution are: $\sigma_0 =$ 4275 MPa and $m = 10.7$ at $L_0 = 12.7$ mm [88]. This values will serve as a baseline for the parametric study of the effect that the strength distributions of the fibres have in the tow behaviour. The matrix is considered to have a elastic modulus (E_m) equal to 7 GPa and the maximum shear stress in the fibre-matrix interface is considered to be 40 MPa. The presented parameters should be considered unless other parameters are specified in the specific sections.

5.3.1 Matrix properties

The matrix is considered to have a secondary influence in the longitudinal failure of UD composites, however, the interfacial shear strength (τ) affects the recovery length of the fibres, therefore, affecting the average stress in the fibres. The influence

influence of the matrix elastic modulus (E_m) is very reduced, as the fibres are the main load carrying constituent.

The effects of the interfacial shear strength in the longitudinal response of the composite is shown in Figure 5.2 and Table 5.1. The parameter $\langle\sigma\rangle$ is the average failure strength of the fibres.

Table 5.1: Effect of interface shear strength (τ in some reference properties.

σ_0 (MPa)	m	$\langle\sigma\rangle$ (MPa)	τ (MPa)	Maximum load (N)	Strain at max. load (%)
4275	10.7	3454.73	10	2487.08	1.89
		3454.73	20	2638.83	2.01
		3454.73	40	2799.88	2.13
		3454.73	60	2898.62	2.21

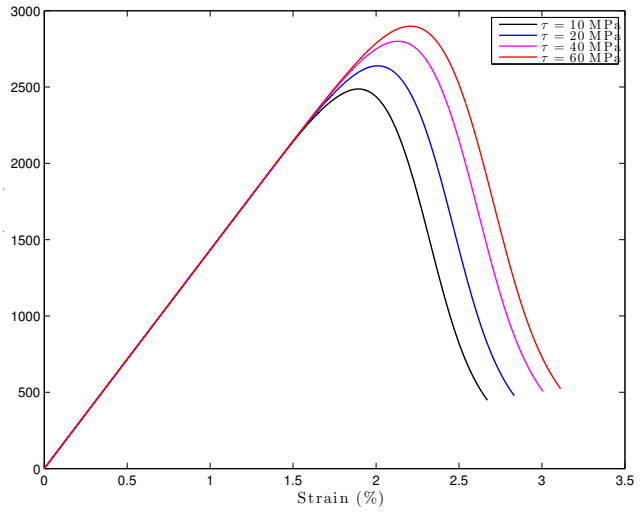

Figure 5.2: Stress-Strain diagrams for composites with different interfacial shear strength (τ).

From the analysis of Figure 5.2 and Table 5.1 it is possible to understand that increasing the interfacial shear strength has a positive effect in the composite strength. This can be attributed to a reduced recovery length of the fibres, which will decrease the length of the region where the fibre is not fully able to carry load and, therefore, increase the average stress in the fibres. As the elastic properties of the fibres remain the same, as the composite strength increases, so will the failure strain.

5.3.2 Weibull scale parameter

The effects of the scale parameter (σ_0) of the Weibull distribution, which is a measure of the average fibre strength, is shown in Figure 5.3 and the principal results from the composite response are presented in Table 5.2.

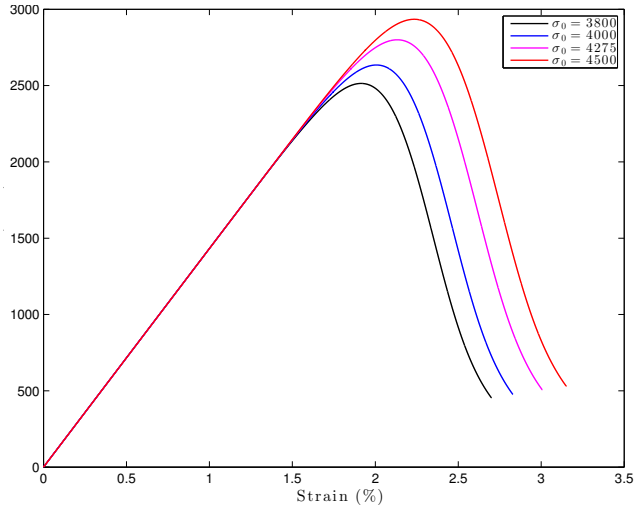

Figure 5.3: Stress-Strain diagrams for composites with fibres with different scale parameters (σ).

Table 5.2: Effect of the scale parameter (σ) in some reference properties.

σ_0 (MPa)	m	$\langle\sigma\rangle$ (MPa)	Maximum load (N)	Strain at max. load (%)
3800	10.7	3070.9	2514.0	1.91
4000		3232.5	2634.7	2.01
4275		3454.7	2799.9	2.13
4500		3636.6	2934.4	2.24

As expected, the scale parameter affects the average failure strength of the composite material. As the average failure strength of the fibres is increased by increasing the scale parameter, so is the failure strength of the composite material. This results are similar to the ones from Chapter 4.2.

5.3.3 Weibull shape parameter

The Weibull shape parameter (m) affects the dispersion of the strength of the fibres, however, as previously stated, it also affect the average failure strength of the

fibres (see Equation 4.2). Having as base the AS4 carbon fibre properties and varying the shape parameter results in the stress-strain curves shown in Figure 5.4.

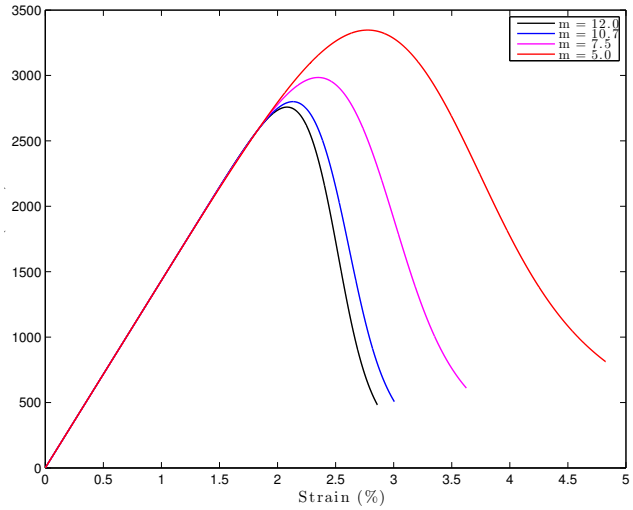

Figure 5.4: Stress-Strain diagrams for composites with fibres with different shape parameters (m), with $\tau = 40$ MPa.

Table 5.3: Effect of the shape parameter (m) in some reference properties, with $\tau = 40$ MPa.

σ_0 (MPa)	m	$\langle\sigma\rangle$ (MPa)	Maximum load (N)	Strain at max. load (%)
4275	12.0	3533.13	2758.15	2.08
	10.7	3454.73	2799.88	2.13
	7.5	3167.01	2984.57	2.35
	5.0	2751.74	3346.93	2.78

The results present in Figure 5.4 and Table 5.3 are not in accordance with those from the model for the dry tows (Chapter 4.2). It was expected that, as we increased the Weibull shape parameter, the failure of the composite would start at lower strains, the stress-strain curve would be wider and the materials resistance would be reduced. With this model the results show that increasing the shape parameter leads to a wider stress-strain curve, but also increases the composite strength. This increase in composite strength can partially be explained by an increase of the fibre strength, however this effect is higher for composite materials than for the dry tows, meaning that the increase in fibre strength does not fully explain the increase in the strength of the composite material.

As the interfacial shear strength has an influence in the composite strength, it may also affect the results from the influence of the Weibull shape parameter.

Changing the interface shear strength from 40 to 10 MPa changes the results from the influence of the Weibull parameter. These results are shown in Figure 5.5 and Table 5.4.

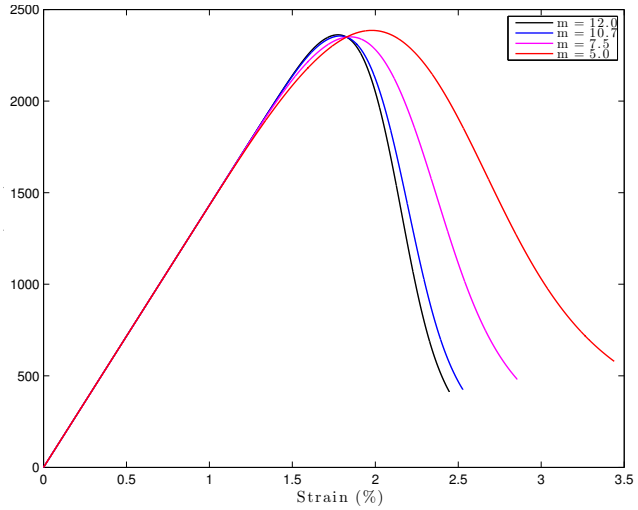

Figure 5.5: Stress-Strain diagrams for composites with fibres with different shape parameters (m), with $\tau = 10$ MPa.

Table 5.4: Effect of the shape parameter (m) in some reference properties, with $\tau = 10$ MPa.

σ_0 (MPa)	m	$\langle\sigma\rangle$ (MPa)	Maximum load (N)	Strain at max. load (%)
4275	12.0	3533.13	2362.04	1.77
	10.7	3454.73	2355.68	1.79
	7.5	3167.01	2350.82	1.85
	5.0	2751.74	2386.03	1.98

As it is possible to see, for the Weibull shape parameters from 12 to 7.5 the results are similar to the ones from the dry tow failure, decreasing the shape parameter increases the dispersion of the fibre strength, which leads to an earlier failure of the weaker fibres, reducing material's resistance, but leading to a wider stress-strain curve. For the case of $m = 5.0$ the results differ and the decrease of the shape parameter leads to a higher failure strength of the composite material.

5.3.4 Fibre strength dispersion

As previously stated, changing the Weibull shape parameter also changes the average failure strength of the fibres. In order to study the effect of the fibre strength

dispersion in the composite behaviour it is necessary to change both the shape and scale parameters. Using the same shape parameters as in the previous hybridization, the scale parameters were changed in order to obtain the same average fibre failure strength, as seen in Table 5.5. The respective stress-strain curve for the composite materials with the different fibre properties is shown in Figure 5.6.

Table 5.5: Effect of the fibre strength dispersion in some reference properties.

σ_0 (MPa)	m	$\langle\sigma\rangle$ (MPa)	Maximum load (N)	Strain at max. load (%)
4180.1	12.0	3454.7	2701.6	2.0
4275	10.7	3454.7	2799.9	2.1
4663.4	7.5	3454.7	3222.6	2.5
5367.1	5.0	3454.7	4045.6	3.4

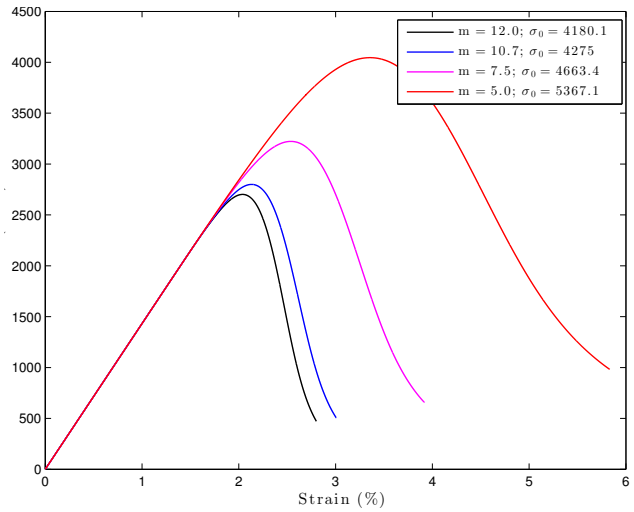

Figure 5.6: Stress-Strain diagrams for composites with fibres with different with different dispersion and the same average failure strength.

As one can see, the results from changing the dispersion, but maintaining the same average failure strength are very similar to the ones where only the shape parameter is changed. The reduction of the shape parameter (increase of the fibre strength dispersion) leads to a higher composite strength. The results will be similar when the interface shear strength (τ) is reduced to 10 MPa.

As the composite strength is related to the critical strength (σ_c) it is important to study the effects of varying the shape parameter (m) but maintaining the same critical strength (see Table 5.6). The resulting stress-strain curves are shown in Figure 5.7. As expected the average failure strain of the composite material is similar for all the different fibres, but the width of the curves is different. Similarly to the study

Table 5.6: Effect of the Weibull shape parameter (m) for composites with same critical strength (σ_c).

σ_0 (MPa)	m	$\langle\sigma\rangle$ (MPa)	σ_c (MPa)	Maximum load (N)	Strain at max. load (%)
4416.8	12.00	3650.3	5778	2842.5	2.1
4275	10.70	3454.7		2799.9	2.1
3759.3	7.50	2785.0		2664.5	2.1
3032.3	5.00	1951.8		2513.9	2.1

of fibre dispersion in dry tows (Chapter 4.2), the reduction of the shape parameter increases the strength dispersion. This leads to an earlier beginning of failure which causes the decrease of maximum strength. The dispersion also causes a delay in the failure of the stronger fibres and, therefore, for high strains the composites that have a higher dispersion also have a higher load carrying capability.

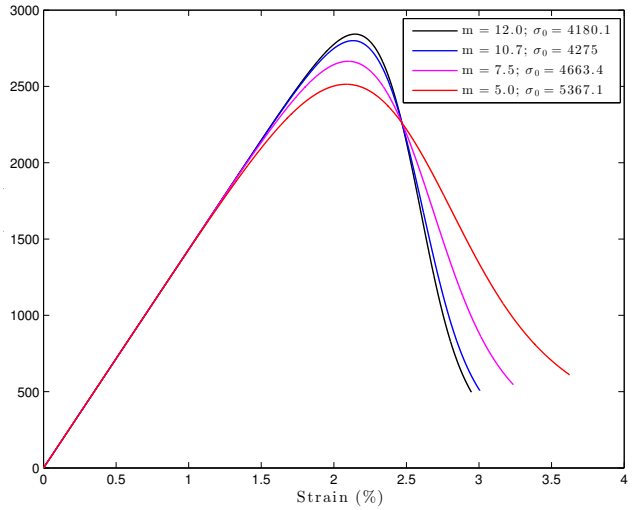

Figure 5.7: Stress-Strain diagrams for composites with fibres with different Weibull shape parameter (m) and same critical strength (σ_c).

5.3.5 Conclusions

In this section the effects of changing the parameters that characterize the fibre strength distribution were studied. The results from the model used differ from those for dry tow (Chapter 4). The model for dry tow failure does not take into account the existence of the matrix, while the model used in this chapter does, which might explain some of the differences observed.

The results from changing the Weibull scale parameter (σ_0) for fibre strength are similar to those obtained for dry tows. Increasing this parameter leads to an increase on composite strength and, as the fibre strength dispersion remains constant, the width of the stress-strain curves is similar for all the scale parameters.

When considering the effects of the fibre strength dispersion the results start to differ. As shown in Equation 4.2 the average failure strength of the fibres scale with the shape parameter, which means that, for the same scale parameter, the fibre strength increases with increasing the shape parameter and this leads to an increase in composite strength (Figure 5.4). In order to avoid this scaling of the strength, the shape and scale parameters were modified in order to obtain fibres with the same average failure strength and different dispersions. The results from this section are not what was expected, as increasing the dispersion lead to an increase in the composite strength (Figure 5.5). In order to understand these results another study was performed. As the composite strength is related with the critical strength (σ_c), the effect of changing the Weibull parameters, but maintaining the same critical strength was studied. This study lead to conclude that the critical strength is the parameter that controls the composite's strength and that the effects of the fibre strength dispersion are similar to those for dry tows. Increasing the shape parameter leads to a wider stress-strain curve but, as the critical strength remains constant, the failure strain of the material remains constant. The increased with of the stress-strain curves leads to a decrease in the resistance of the composite material. This is an important conclusion that might help explain the effects of hybridizing composite materials.

5.4 Hybrid composite behaviour

The previous section focused on the study of the effects of the fibre strength distributions in the tensile behaviour of the composite materials. This section focuses on the study of hybridizing composite materials and studying the effects of having fibres with different strength distributions in the composite material. Similar to the study in the previous chapter, this section will be divided by type of hybridization (e.g. carbon-carbon, carbon-glass). The study will be based in the results from Chapter 4, with some additional analysis when necessary. The values for the critical strength (σ_c) and strain (ε_c) were determined considering that the interfacial shear strength was constant and equal to 40 MPa. In this section the gauge length (L) is considered 75 mm and the matrix is considered to have a elastic modulus of 7 GPa and the interfacial shear strength equal to 40 MPa. The fibre properties will be changed according to the hybridized fibres.

5.4.1 Carbon-carbon hybridization

This section will focus on the hybridization of composite materials with different types of carbon fibres. The properties of the carbon fibres are shown in Table 5.7, with the newly defined properties: critical strength (σ_c) and critical strain (ε_c). The failure strain distributions for the carbon fibres are shown Figure 5.8.

Table 5.7: Mechanical properties for carbon fibres.

Material	Reference	σ_0 (MPa)	L_0 (mm)	m	E (GPa)	R (μm)	$\langle\varepsilon\rangle$ @75mm (%)	σ_c (MPa)	ε_c
HTS carbon	Beyerlein 1996 [89]	4493	19	4.8	230	3.5	1.34	8768.34	3.81
AS4 carbon	Curtin 1998 [88]	4275	12.7	10.7	234	3.5	1.48	5778.02	2.47
T300	Curtin 1998 [88]	3170	25	5.1	232	3.5	1.01	6630.25	2.86
T300	R Mili 1996 [87]	3200	30	5.5	232	3.5	1.08	6568.29	2.83
T300-B4C	R Mili 1996 [87]	3150	30	5.4	232	3.5	1.06	6554.82	2.83
700°C	Tanaka 2014 [91]	1400	10	11	55	3.3	2.02	2030.39	3.69
1000°C	Tanaka 2014 [91]	4500	10	4.5	240	2.9	1.09	8384.48	3.49
T800G	Tanaka 2014 [91]	6800	10	4.8	295	2.75	1.39	11530.73	3.91
M30S	Tanaka 2014 [91]	6400	10	4.6	295	2.8	1.28	11143.54	3.78
M40S	Tanaka 2014 [91]	4900	10	5.2	380	2.7	0.81	8491.54	2.23
M50S	Tanaka 2014 [91]	4600	10	9	480	2.65	0.73	6521.74	1.36

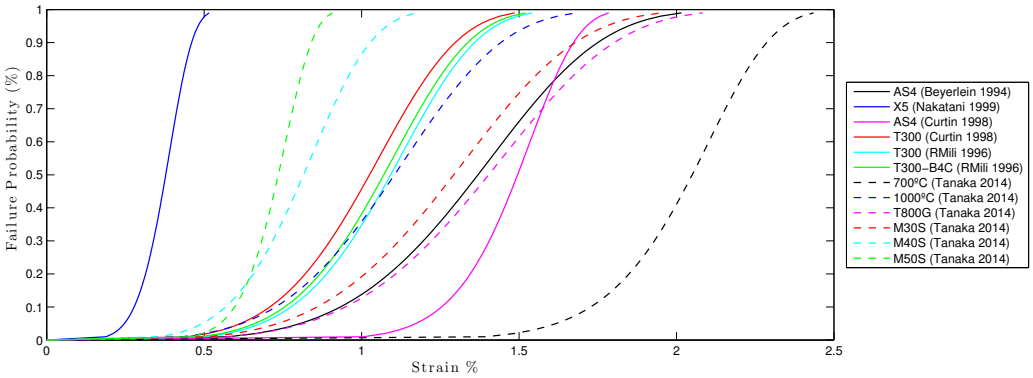

Figure 5.8: Failure strain distributions for different carbon fibres.

AS4-T300 carbon fibre hybridization

In this section it is studied the hybridization of AS4 [88] and T300 [88] carbon fibres. The T300 carbon fibres are considered the low elongation (LE) fibres as their failure strain is lower than that of the AS4 carbon fibres. The resulting stress-strain curves are shown in Figure 5.9 and the main properties are shown in Table 5.8

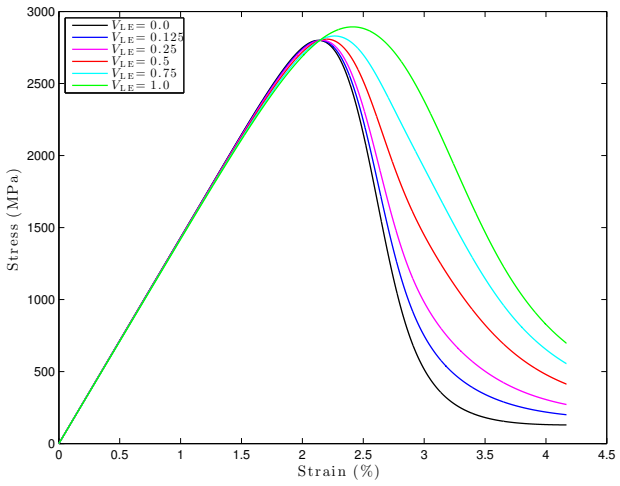

Figure 5.9: Stress-strain diagrams at various hybrid volume fractions for AS4/T300 hybridization.

As it is possible to see in Figure 5.9 the failure strain and strength of the composite composed only of T300 carbon fibres ($V_{LE} = 1$) are higher than those for the AS4 carbon composite ($V_{LE} = 0$), altough the T300 fibres have the LE fibres. This is related to the differences in shape parameters, whose influence was analysed in Section 5.3. The shape parameter of the T300 fibres is equal to 5.1 while that of the AS4 fibres is 10.7, which explains why the T300 carbon fibre composite has a higher failure strength. This behaviour is related to the critical strain for each fibre.

Table 5.8: Stress-strain reference properties for AS4/T300 hybridization.

V_{LE}	Maximum stress (MPa)	Strain at max. stress (%)	ε_d (%)
0	2799.88	2.13	0.18
0.125	2799.55	2.15	0.19
0.25	2800.51	2.16	0.20
0.5	2808.15	2.20	0.23
0.75	2829.91	2.27	0.28
1	2893.32	2.41	0.38

The T300 carbon fibres have a higher critical strain than the AS4 carbon, therefore the T300 carbon fibre composite has a higher failure strain. In terms of pseudo-ductility the results are in accordance to those of the dry tow model, where there was no significant increase in the pseudo-ductile strain (ε_d) due to the hybridization of these two fibre types.

AS4-M40S carbon hybridization

This section studies the hybridization of AS4 and the M40S [91] carbon fibres. The M40S fibres have a lower average failure strain than the AS4 fibres and than the T300 carbon fibres used in the precious hybridization. This leads to a greater difference in failure strains in the hybridized fibres. The difference between the shape parameters between these two fibres is similar to that between the AS4 and the T300 carbon fibres, since the shape parameter for the M40S carbon fibres is equal to 5.1. The tensile stress-strain curves resulting from this hybridization are shown in Figure 5.10.

As it can be seen from analysing Figure 5.10 there is no pseudo-ductile effect in the hybridization with these two types of fibres, which can be confirmed from the results in Table 5.9. These results are not in accordance with those from the dry tow model (Figure 4.13), where some pseudo-ductile behaviour was achieved for a low elongation fibre volume fraction equal to 25%. The differences in theses results may lead to the conclusion that the pseudo-ductile behaviour in composite materials are affected by different parameters than those that affect the behaviour of dry tows.

Analysing the critical strains for both fibre types it is possible to see that they are very similar, 2.47% for the AS4 and 2.23% for the M40S fibres. This causes the non-hybrid composites to have similar failure strains, which causes the tensile

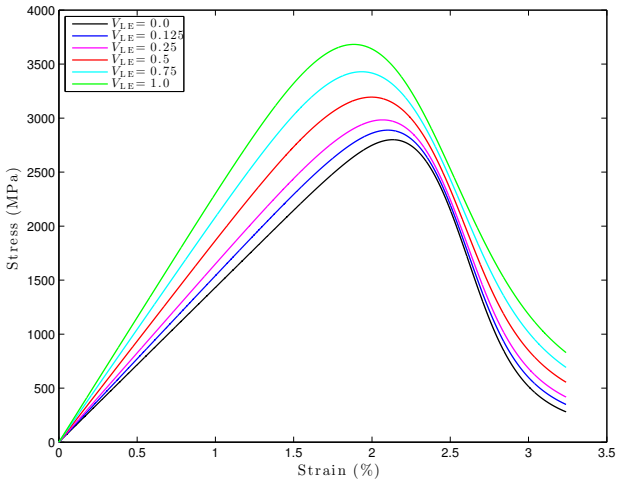

Figure 5.10: Stress-strain diagrams at various hybrid volume fractions for AS4/M40S hybridization.

Table 5.9: Stress-strain reference properties for AS4/M40S hybridization.

V_{LE}	Maximum stress (MPa)	Strain at max. stress (%)	ε_d (%)
0	2799.88	2.13	0.18
0.125	2888.33	2.10	0.23
0.25	2983.37	2.07	0.26
0.5	3194.03	2.00	0.29
0.75	3429.11	1.93	0.29
1	3682.06	1.88	0.29

response of the hybrid composites to not be pseudo-ductile.

AS4-M50S carbon hybridization

This section deals with the hybridization between the AS4 and the M50S [91] carbon fibres. The M50S fibres have a high modulus ($E = 480$ MPa), a low failure strain and a low fibre strength dispersion, with a Weibull shape parameter equal to 9. This shape parameter is the closer to the one for the AS4 carbon fibres. The resulting stress-strain curves for the hybridization of these two types of fibres are shown in Figure 5.11.

For this hybridization there is a tendency for a pseudo-ductile behaviour. For a low elongation fibre volume fraction (V_{LE}) equal to 0.25 the pseudo-ductile strain

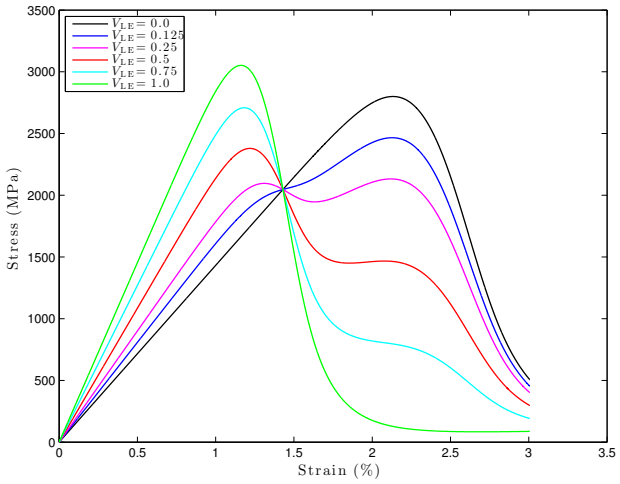

Figure 5.11: Stress-strain diagrams at various hybrid volume fractions for AS4/M50S hybridization.

reaches its maximum value and is equal to 0.94 (see Table 5.10). This values represents a large percentage of the composite total failure strain, that is equal to 2.12%. As in all the cases that shown a pseudo-ductile behaviour, the increase of the pseudo-ductile strain is accompanied by a reduction in the maximum load of the material. Analysing the properties of the hybridized fibres it is possible to conclude that there is a significant difference between their critical strain, which can explain the pseudo-ductile behaviour achieved.

Table 5.10: Stress-strain reference properties for AS4/M50S hybridization.

V_{LE}	Maximum stress (MPa)	Strain at max. stress (%)	ε_d (%)
0	2799.88	2.13	0.18
0.125	2465.91	2.13	0.60
0.25	2132.19	2.12	0.94
0.5	2379.40	1.22	0.12
0.75	2708.83	1.18	0.12
1	3052.04	1.16	0.11

Analysis of the results

From the previous results it is concluded that the behaviour due to hybridization changes drastically from when we consider only a tow of fibres (dry tow) to when we consider the composite material. The introduction of the matrix changes the

behaviour of the material and, therefore, the factors controlling its behaviour.

In the previous chapter (Model for the tensile failure of dry tows), and for a carbon-carbon hybridization, it was seen that there was a pseudo-ductile behaviour for the hybridization between the AS4 and M40S fibres and for the AS4 and M40S fibres, which was explained by the differences in the failure strain distributions. In this section, using the damage model for the composite, it was concluded that there was only pseudo-ductility for the AS4/M50S hybridization.

Analysing the properties of the hybridized fibres, namely the critical strain (ε_c) and the average failure strain ($\langle\varepsilon\rangle$) of the fibres , it is possible to conclude that the main factor controlling the pseudo-ductility is not the difference between the average failure strains, but is the difference between the critical strains, which control the failure strain of the non-hybrid reference composites. This is the case for the AS4 and M50S hybridization, that have critical strains, respectively, 2.47% and 1.36%. Although not present here, it was verified that other combinations of carbon fibres with different critical strains lead to similar results, but this hypotheses will be studied for other types of hybridization in the following sections.

5.4.2 Glass-glass hybridization

This section presents the study of hybridizing composite materials with different types of glass fibres, whose properties are shown in Table 5.11 and failure strain distributions in Figure 5.12. This study will try to support the conclusions withdrawn from the carbon-carbon hybridizations.

Table 5.11: Mechanical properties for Glass fibres.

Material	Reference	σ_0 (MPa)	L_0 (mm)	m	E (GPa)	R (μm)	$\langle\varepsilon\rangle$ @75mm (%)	σ_c (MPa)	ε_c
E-Glass	T.Okabe 2001 [43]	1550	24	6.34	76	6.5	1.59	2883.72	3.79
E-Glass	FEIH 2005 [93]	1649	20	3.09	66.9	7.8	1.44	4526.85	6.77
E-Glass	Pauchard 2002 [94]	2300	10	3.6	70	5	1.69	4975.15	7.11
AR-HP	Foray 2012 [92]	1363	60	9.6	70	7	1.81	2295.99	3.28
AR-HD	Foray 2012 [92]	876	60	4.8	70	7	1.09	2451.92	3.50

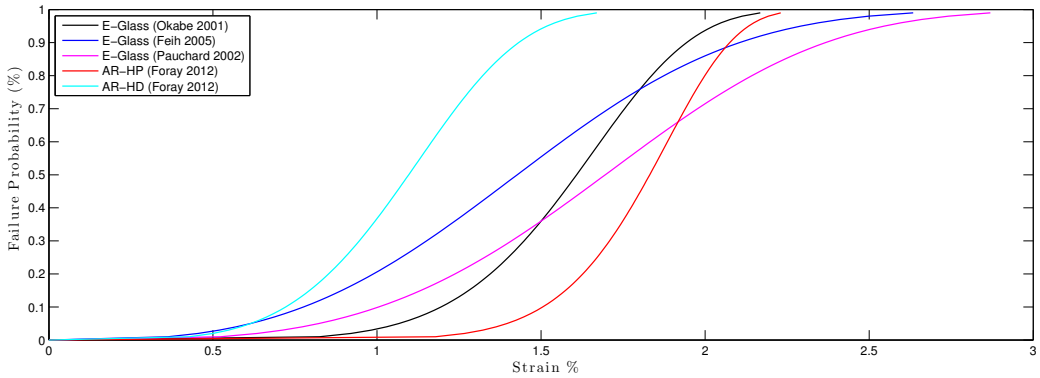

Figure 5.12: Failure strain distributions for several glass fibres.

HD/HP glass hybridization

The hybridization between the HD and HP glass fibres lead to good results in terms of pseudo-ductility in the previous chapter where dry tows were analysed. With the presence of the matrix and using the model implemented here, the results of hybridizing a composite material are shown in Figure 5.13 and Table 5.12.

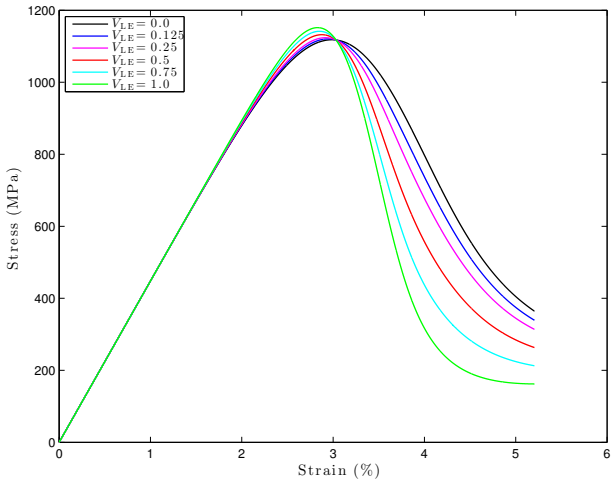

Figure 5.13: Stress-strain diagrams at various hybrid volume fractions for HD/HP glass hybridization.

From the analysis of this results it is possible to conclude that there is no pseudo-ductile response in the hybridization of these two types of fibres, which contradicts the results from the previous chapter. This supports the conclusion that the results of the dry tows cannot be transferred for the composite material. If we analyse the critical strain of both fibre types, we conclude that they are very similar, which may explain why the hybridization leads to this type of response.

Table 5.12: Stress-strain reference properties for HD/HP glass hybridization.

V_{LE}	Maximum stress (MPa)	Strain at max. stress (%)	ε_d (%)
0	1118.02	2.99	0.49
0.125	1120.43	2.95	0.44
0.25	1123.79	2.92	0.41
0.5	1132.10	2.88	0.35
0.75	1141.57	2.85	0.30
1	1151.71	2.83	0.26

HD/E-glass hybridization

As the previous hybridization did not lead to the expected results other hybridization needed to be studied. Following the conclusions from the carbon-carbon hybridization, that fibres with similar critical strain do not have a pseudo-ductile behaviour, the hybridization between the HD glass fibres [92] and the E-glass fibres [93] is presented next. The results from this hybridization are shown in Figure 5.14 and Table 5.13.

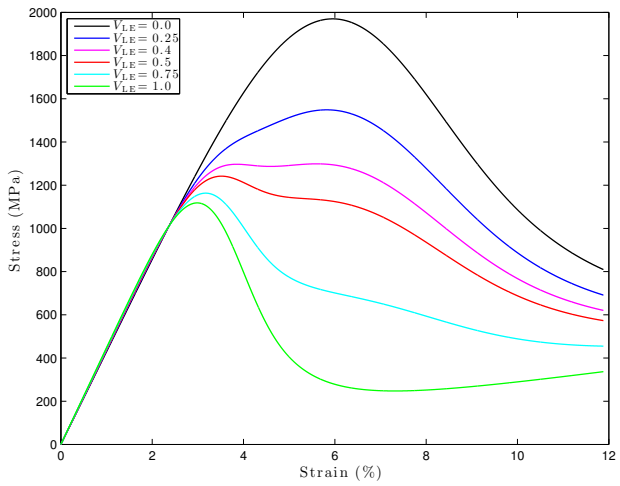

Figure 5.14: Stress-strain diagrams at various hybrid volume fractions for HD/E-glass hybridization.

The present hybridization and for a low elongation volume fraction (V_{LE}) equal to 0.4 the pseudo-ductile strain is maximum and equal to 2.63%. From the analysis of the stress-strain curve in Figure 5.14 we can see that the failure is progressive and that from a strain equal to 3.5% to 6% the failure occurs at a constant stress. Analysing the properties of these two fibres it is possible to see that their critical

strain is quite different, 7.11% for the E-glass and 3.5% for the HD glass fibres. This reinforces the conclusion that the fibres have to have a different critical strain in order to result in a pseudo-ductile behaviour when hybridized.

Table 5.13: Stress-strain reference properties for HD/E-glass hybridization.

V_{LE}	Maximum stress (MPa)	Strain at max. stress (%)	ε_d (%)
0	1969.91	5.95	1.37
0.25	1548.82	5.82	2.26
0.4	1298.82	5.60	2.63
0.5	1241.77	3.52	0.69
0.75	1163.17	3.17	0.55
1	1118.02	2.99	0.49

5.4.3 Kevlar-kevlar hybridization

This section focuses on the study of the hybridization of composite materials with different types of kevlar fibres, whose charecteristics are shown in Table 5.14 and Figure 5.15.

Table 5.14: Mechanical properties for kevlar fibres.

Material	Reference	σ_0 (MPa)	L_0 (mm)	m	E (GPa)	R (μm)	$\langle\varepsilon\rangle$ @75mm (%)	σ_c (MPa)	ε_c
kevlar 29	Naito 2013 [95]	3445.8	25	11.8	85.3	6.895	3.52	4615.08	5.41
kevlar 49	Naito 2013 [95]	4083.3	25	8.2	149.1	5.135	2.26	6215.15	4.17
kevlar 119	Naito 2013 [95]	3101.2	25		11.8 61.4	5.46	4.41	4264.92	6.95
kevlar 129	Naito 2013 [95]	3433	25	10.3	99	5.79	2.97	4855.81	4.90

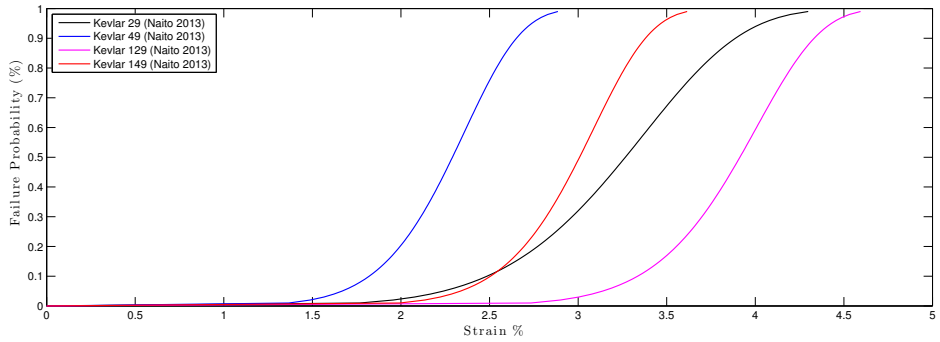

Figure 5.15: Failure strain distributions for several kevlar fibres.

Kevlar 49/119 hybridization

The hybridization between Kevlar 49 and 119 showed great potential in the dry tow model, having a maximum pseudo-ductile strain equal to 1.24% (Figure 4.19). The kevlar 49 are, for this hybridization, considered the LE fibres, as they have an average failure strain equal to 2.26% while the kevlar 119 have an average failure strain equal to 4.41%. The results from the hybridization of these two types of fibres is shown in Figure 5.16 and Table 5.15.

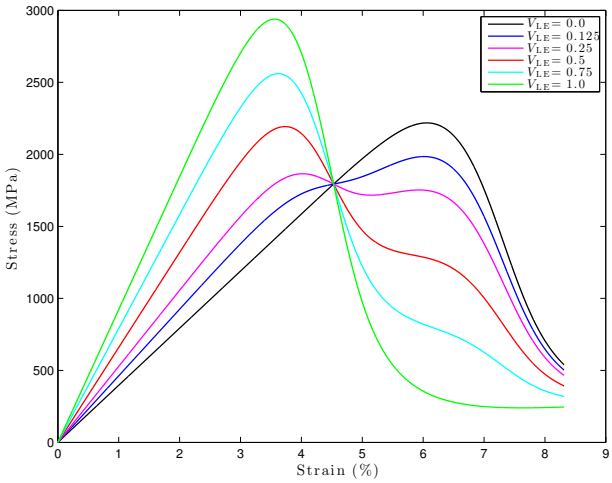

Figure 5.16: Stress-strain diagrams at various hybrid volume fractions for kevlar 49/kevlar 119 hybridization.

Analysing these results it is possible to see that for a LE fibre volume fraction equal to 0.125 the pseudo-ductile strain is maximum and equal to 1.72%. Combining this information to the stress-strain curve from Figure 5.16 gives to the conclusion that this type of hybridization has a pseudo-ductile behaviour. From Table 5.14 it is possible to see that the critical strains for the hybridized fibres are 4.17% and 6.95% for kevlar 49 and kevlar 119, respectively.

Table 5.15: Stress-strain reference properties for kevlar 49/kevlar 119 hybridization.

V_{LE}	Maximum stress (MPa)	Strain at max. stress (%)	ε_d (%)
0	2218.43	6.06	0.46
0.125	1984.58	6.02	1.72
0.25	1865.13	4.02	0.49
0.5	2192.81	3.73	0.41
0.75	2560.16	3.62	0.39
1	2939.01	3.56	0.37

Kevlar 119/129 hybridization

The kevlar 119 and 129 fibres have a closer average failure strain that those for the previous hybridization, as well as a close Weibull shape parameter, respectively 10.3 and 11.8. The stress-strain curves for this hybridization are shown in Figure 5.17.

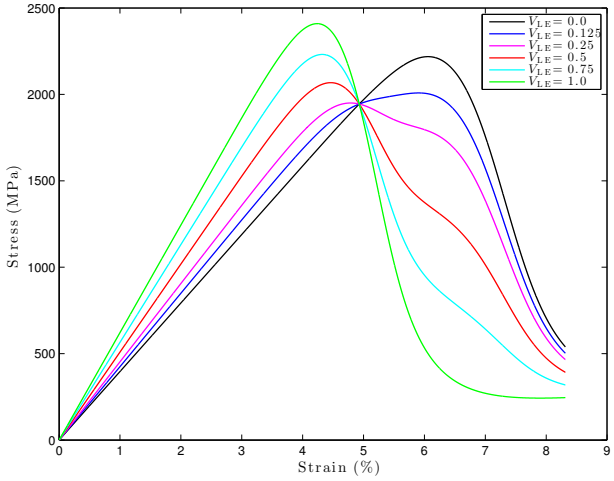

Figure 5.17: Stress-strain diagrams at various hybrid volume fractions for kevlar 119/kevlar 129 hybridization.

Analysing both Table 5.16 and Figure 5.17 it is possible to see that this hybridization leads to a pseudo-ductile behaviour at a LE fibre volume fraction equal to 0.125. Analysing the properties of both hybridized fibres from Table 5.15 it is possible to see that the critical strains of the fibres are equal to 6.95% and 4.9%, for the kevlar 119 and kevlar 149, respectively. This analysis helps supporting the conclusion that it is essential that the fibres have different critical strains in order to achieve a pseudo-ductile behaviour with their hybridization.

Table 5.16: Stress-strain reference properties for kevlar 119/kevlar 129 hybridization.

V_{LE}	Maximum stress (MPa)	Strain at max. stress (%)	ε_d (%)
0	2218.43	6.06	0.46
0.125	2008.39	5.90	1.17
0.25	1950.20	4.79	0.48
0.5	2067.84	4.46	0.40
0.75	2231.20	4.32	0.38
1	2409.35	4.24	0.37

5.4.4 Carbon-glass hybridization

Similarly to Chapter 4, the effects of hybridization with fibres of the same base (carbon, glass and kevlar) were studied. This allowed to achieve some important conclusions about the key parameters to obtain a pseudo-ductile behaviour in hybrid composite materials. This section and the following will address the study of hybridizing composite materials with fibres of different bases, in this case carbon and glass. The properties for the fibres are shown in Table 5.7 and 5.11.

T300 carbon/AR-HP glass hybridization

In the previous chapter (Section 4.3.4) the hybridization of tows with T300 carbon and AR-HP glass fibres was studied and the results demonstrated a pseudo-ductile behaviour. However, as stated in the previous sections, the results from tow hybridization cannot be extrapolated for the composite material as the presence of the matrix affects the material's response. Figure 5.18 presents the stress-strain curves for this hybridization.

Although the failure strain distributions for this two types of fibres are quite different, the fibres have similar critical strains and, therefore, a pseudo-ductile behaviour is not expected for the composite material, which is shown in Figure 5.18. In this figure it is possible to see that the failure strains of the reference composite materials ($V_{LE} = 0$ and $V_{LE} = 1$) are quite similar, in spite of the fibres having quite different average failure strains. This reinforces the conclusion that it is not possible to predict the composite response based, only, in the tow behaviour and that the critical strains of the hybridized fibres control the response of hybrid composite.

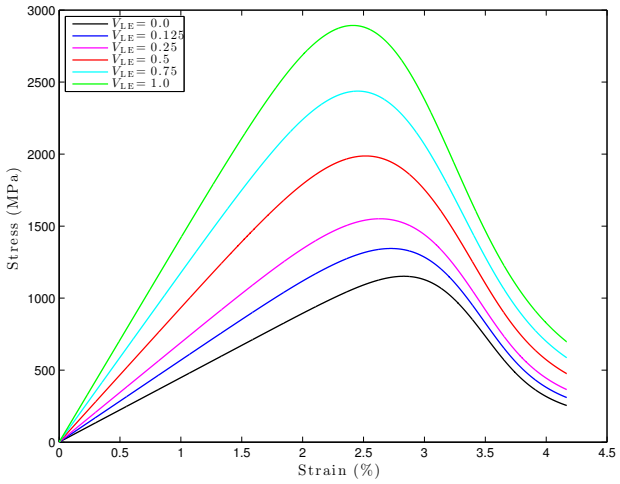

Figure 5.18: Stress-strain diagrams at various hybrid volume fractions for T300 carbon and AR-HP glass hybridization.

M50S carbon/AR-HP glass hybridization

With the previous hybridization it was not possible to achieve the intended pseudo-ductile response. The fibres hybridized in this section are the M50S carbon and the AR-HP glass fibres. This fibres have a higher difference between critical strains, which are equal to 1.36% and 3.28% for the M40S carbon and AR-HP glass fibres, respectively. The results from hybridizing a composite material with these two types of fibres is shown in Figure 5.19 and Table 5.17.

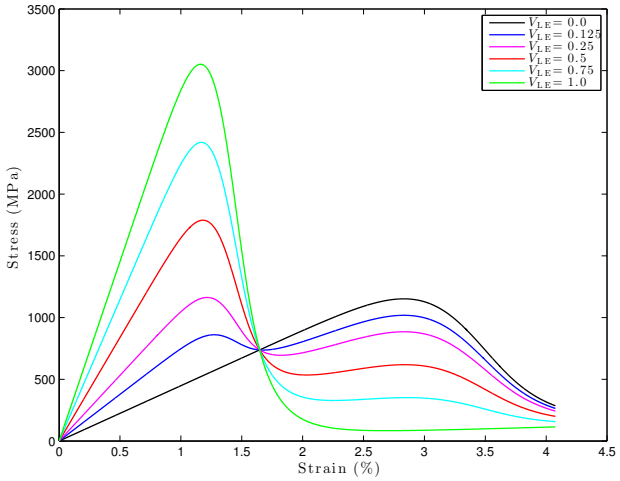

Figure 5.19: Stress-strain diagrams at various hybrid volume fractions for M50S carbon and AR-HP glass hybridization.

The hybridization between these two types of fibres leads to a pseudo-ductile

Table 5.17: Stress-strain reference properties for M50S carbon and AR-HP glass hybridization.

V_{LE}	Maximum stress (MPa)	Strain at max. stress (%)	ε_d (%)
0	1151.71	2.83	0.26
0.125	1018.32	2.83	1.48
0.25	1162.92	1.22	0.12
0.5	1788.55	1.18	0.12
0.75	2419.56	1.17	0.11
1	3052.04	1.16	0.11

behaviour for a volume fraction of carbon fibres (LE fibres) equal to 0.125. Taking as reference the carbon composite material, the addition of glass fibres to this composite does not translate into an improvement the material's behaviour. However, if we consider the addition of carbon fibres to a glass composite, with a volume fraction of carbon fibres equal to 0.125, leads to an increase in the composite stiffness and to a pseudo-ductile behaviour, being that the failure strain of both composites is very similar. However, the hybridization also leads to a small reduction in the composite strength, approximately 12%.

5.4.5 Carbon-kevlar hybridization

In this section it is studied the hybridization of composite materials with carbon and kevlar fibres. This type of hybridization has the most potential to obtain a pseudo-ductile behaviour, as the fibres have the most different average failure strains ($\langle\varepsilon\rangle$) and critical strains ($\varepsilon_c$). The carbon and kevlar fibre properties are shown, respectively, in Table 5.7 and 5.14.

AS4 carbon/kevlar 49 hybridization

The kevlar 49 fibres are the stiffest kevlar fibres, from the data acquired. These fibres also have the lower average failure strain and critical strain of the kevlar fibres. The hybridization of a composite material with AS4 carbon and kevlar 49 results in the stress-strain curves shown in Figure 5.20.

From the analysis of this figure it is possible to see that the behaviour of the composite material with both fibre types is similar to the one of the dry tow, seen in the previous chapter. This response is characteristic of a pseudo-ductile behaviour,

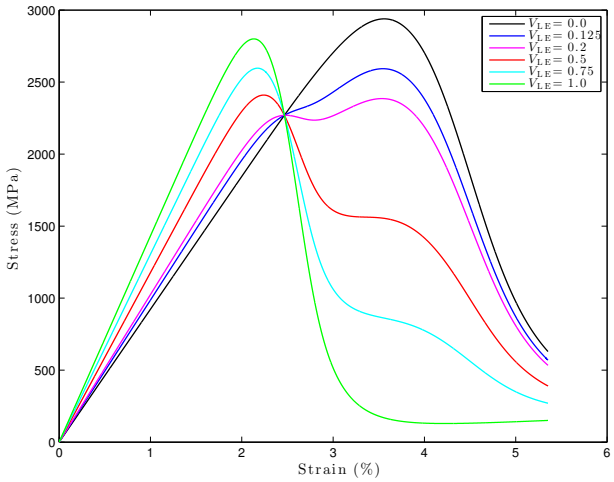

Figure 5.20: Stress-strain diagrams at various hybrid volume fractions for AS4 carbon and kevlar 49 hybridization.

which can be verified from the analysis of the data in Table 5.18. For a LE fibre (carbon fibre) volume fraction equal to 0.2, the pseudo-ductile strain has the maximum value of 1.21%, which is, approximately, 34% of the failure strain of the composite. Analysing the fibre properties that can explain this behaviour, it is possible to see that the critical strains of these types of fibres are different from each other, which explains the differences in behaviours of the non-hybrid composites ($V_{LE} = 0$ and $V_{LE} = 1$). This leads to a pseudo-ductile behaviour when the hybridization is done, mainly for a low LE fibre volume fraction.

Table 5.18: Stress-strain reference properties for AS4 carbon and kevlar 49 hybridization.

V_{LE}	Maximum stress (MPa)	Strain at max. stress (%)	ε_d (%)
0	2939.01	3.56	0.37
0.125	2592.89	3.55	0.92
0.2	2385.42	3.54	1.21
0.5	2409.77	2.24	0.19
0.75	2596.44	2.17	0.18
1	2799.88	2.13	0.18

AS4 carbon/kevlar 129 hybridization

The kevlar 129, in comparison with the kevlar 49 fibres, have a lower stiffness and a higher average failure strain and critical strain, which may lead to a higher pseudo-ductility, as the carbon fibres are the same from the previous hybridization (AS4 carbon). The stress-strain curves for the AS4 carbon and kevlar 129 hybridization are shown in Figure 5.21.

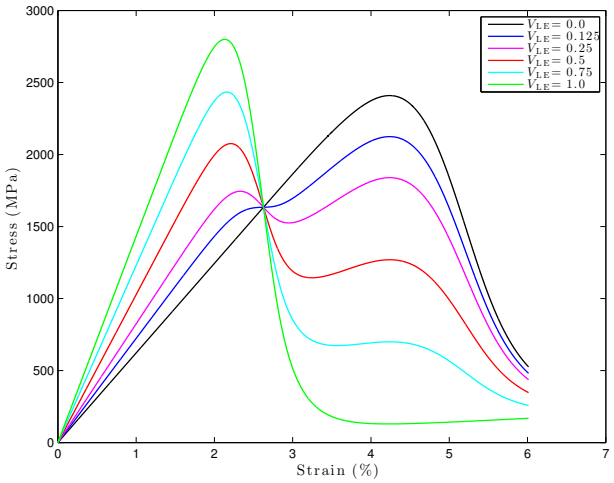

Figure 5.21: Stress-strain diagrams at various hybrid volume fractions for AS4 carbon and kevlar 129 hybridization.

Table 5.19: Stress-strain reference properties for AS4 carbon and kevlar 129 hybridization.

V_{LE}	Maximum stress (MPa)	Strain at max. stress (%)	ε_d (%)
0	2409.35	4.24	0.37
0.125	2124.35	4.24	1.30
0.25	1839.36	4.24	2.01
0.5	2075.83	2.21	0.19
0.75	2433.78	2.16	0.18
1	2799.88	2.13	0.18

As the differences between the average failure strains of the studied fibres is higher than those of the previous hybridization, the non-hybrid composites have failure strains further apart from each other (see Tables 5.18 and 5.21). This differences are transferred to the behaviour of the hybrid composites as, after the failure of the LE fibres, there is a higher drop in the load carrying capability of the material.

Nonetheless, the hybrid composite appears to have a pseudo-ductile behaviour with a higher pseudo-ductile strain.

AS4 carbon/kevlar 119 hybridization

As previously stated, the differences in the critical strains of the hybridized fibres is essential to characterize the response of the hybrid composite material. From the analysed carbon-kevlar hybridizations, the hybridization between AS4 carbon and kevlar 119 fibres is the one where the fibres have the most different critical strains and average failure strains.

Comparing the previous two hybridization, it was concluded that the higher separation of behaviour between the non-hybrid composites lead to a higher load drop in the hybridized composite, but a higher pseudo-ductile strain. The same trend occurs for this hybridization (see Figure 5.22).

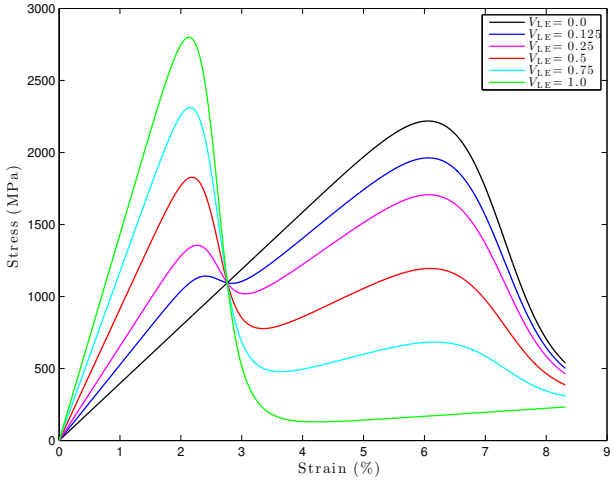

Figure 5.22: Stress-strain diagrams at various hybrid volume fractions for AS4 carbon and kevlar 119 hybridization.

As the non-hybrid composites have a higher difference of failure strains, the hybrid composite behaviour is further away from a pseudo-ductile behaviour and is more similar to a typical hybrid composite (Section 3.2.5). High values of the pseudo-ductile strains are present for this hybridization (Table 5.20), however, this response cannot be characterized as pseudo-ductile.

Table 5.20: Stress-strain reference properties for AS4 carbon and kevlar 119 hybridization.

V_{LE}	Maximum stress (MPa)	Strain at max. stress (%)	ε_d (%)
0	2218.43	6.06	0.46
0.125	1962.37	6.07	2.33
0.25	1706.34	6.07	3.47
0.5	1827.93	2.18	0.19
0.75	2312.18	2.15	0.18
1	2799.88	2.13	0.18

5.5 Conclusion

This chapter focused on the study of the effects of hybridization in the tensile behaviour of composite materials. To achieve this goal, an analytical model was implemented, based on Turon's et al. [5] fragmentation model.

To understand the effects of the hybridization in the tensile behaviour of composite materials it was necessary to understand the effects that the fibre properties have in the response for non-hybrid composites. From this study it was possible to conclude that the failure strength of the composite materials is dominated by the critical strength parameter (σ_c) and that the dispersion of the strength of the fibres have a similar effect in the composite's behaviour as in the tow's behaviour, studied in the previous chapter.

Several hybridizations were performed, with different types of fibres, achieving different behaviours. The main conclusion to be withdrawn from this study is that to achieve a pseudo-ductile behaviour, the failure strains of the reference non-hybrid composites must be different. This means that the critical strains (ε_c) of the hybridized fibres must different. If this happens, the failure of the hybrid composite material is a gradual process and a pseudo-ductile behaviour is achieved. From the hybridizations studied it was possible to conclude that the pseudo-ductile behaviour is usually achieved at low volume fractions of the low elongation fibres.

Chapter 6

Micromechanical models

The previous chapters focused on the study of the effects of hybridization using simple analytical models. These models are useful in understanding some of the main effects of hybridization, however, due to their simpleness, they are not able to take into account all the mechanisms that lead to the longitudinal failure of UD composites. To do so, it is necessary a more complex model that can take into account the more complex mechanisms such as the damage in the matrix, fibres and interface.

To study this complex mechanism it is necessary to develop micromechanical models that are able to take into account the damage mechanisms in the longitudinal failure of composite materials. These models need to be able to correctly represent the behaviour of each of the constituents in the composite. As the fibres and matrix have different characteristics and behaviour two damage models need to be implemented. In order to connect these constituents it is necessary to define the interface between them, which has a large influence the behaviour of the material as the interfacial separation is one important failure mechanism.

The next sections focus on the development and implementation of these models and are proceeded by the results of the micromechanical analysis of hybrid and non-hybrid composites.

6.1 RVE generation

As previously stated in Chapter 2, the fibre arrangement in the material is an important factor in the composite's behaviour, as square and hexagonal fibre arrangements usually lead to unrealistic results. In order to overcome this difficulty it is necessary to generate a Representative Volume Element (RVE) that is represen-

tative of the material, which means having a correct size and being able to represent the microstructure of the composite material.

The algorithm used to generate the random distribution of fibres is based on the algorithm developed by Melro et al. [14], with some changes to allow the RVE to be hybridized, i.e., having multiple types of fibres. The algorithm is composed of three steps, of which only one had major changes, the first step. The flowchart of the algorithm is shown in Figure 6.1. The variable N_i^{max} is the maximum allowed number of iterations of the overall algorithm and N_i is the current number of iterations.

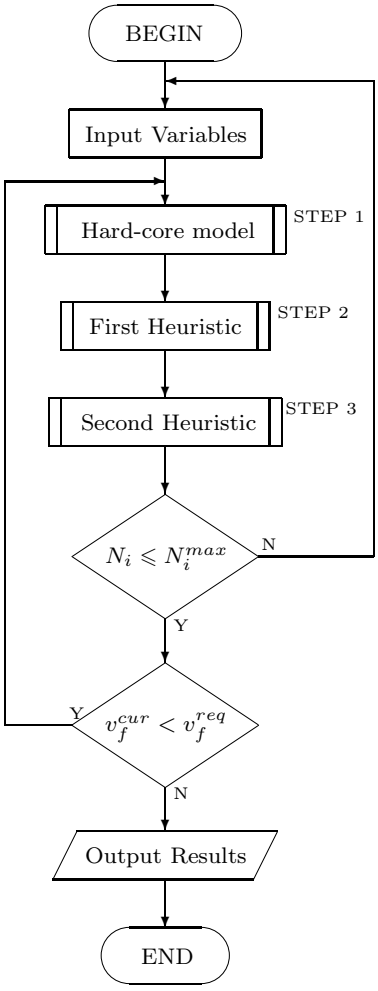

Figure 6.1: Flowchart of RAND_uSTRU_GEN algorithm [14].

The changes that were required to do in the hard-core model (STEP 1) are related with the necessity of guaranteeing that the algorithm is able to generate fibres with different diameters and that it is able to achieve the specified volume fraction of each fibre. The flowchart of the modified hard-core model is shown in Figure 6.2. The variables V_f^{curr} and V_f^{req} define the current and required fibre volume fraction, and with the subscript 1 and 2 represent the volume fractions of each type of fibre

in the hybrid composite. The variable N_g is the current number of iterations in this step and N_g^{max} is the maximum number of iterations before executing the step two of the algorithm.

The changes in this algorithm allowed the generation of a RVE with different fibre volume fractions and hybrid volume fractions, with fibres with different radii. This algorithm also guarantees material symmetry in order to correctly implement the boundary conditions to the RVE. Another important aspect is guaranteeing a minimum distance between fibres in order to inhibit poorly meshed regions in the RVE. As previously stated, an important factor in the composite material's behaviour is the interface between the fibres and the matrix, therefore, it necessary to correctly simulate this interface. This is done by introducing cohesive surfaces in all the interfaces between fibres and matrix.

To correctly simulate the behaviour of UD composite materials under tensile loadings it is necessary to have a RVE with an adequate size to capture the mechanisms of failure of these materials, which leads to the necessity of having a large RVE. The dimensions of the RVE in the direction perpendicular to the fibres directly affect the number of fibres in the RVE. The in-plane dimensions of the RVE need to be such as it is possible to capture the damage mechanisms and cluster formation prior to the failure of the composite. Thefore, the number of fibres must be higher than the expected critical cluster size as this is the main mechanism of failure of UD composites. In terms of the size in the fibre direction, the RVE needs to be long enough to simulate the ineffective length of the fibres. As seen in Section 2.3 is about 15-20 fibre radius. Taking this into account two dimensions of RVEs were studied: $15 \times 15 \times 15$ and $20 \times 20 \times 20$ fibre radius.

As the RVE needs to be representative of the material we are trying to model it is necessary to define correct boundary conditions. The characteristics of a composite material make it necessary to define periodic boundary conditions for the RVE. These boundary conditions define constraints in the displacements and rotations in the faces, edges and vertices that are opposed to each other [98]. As this type of boundary conditions is computationally very expensive, a simplified version of these boundary conditions was used by constrainning the displacements of opposite faces in the RVE, using ABAQUS tie constraints.

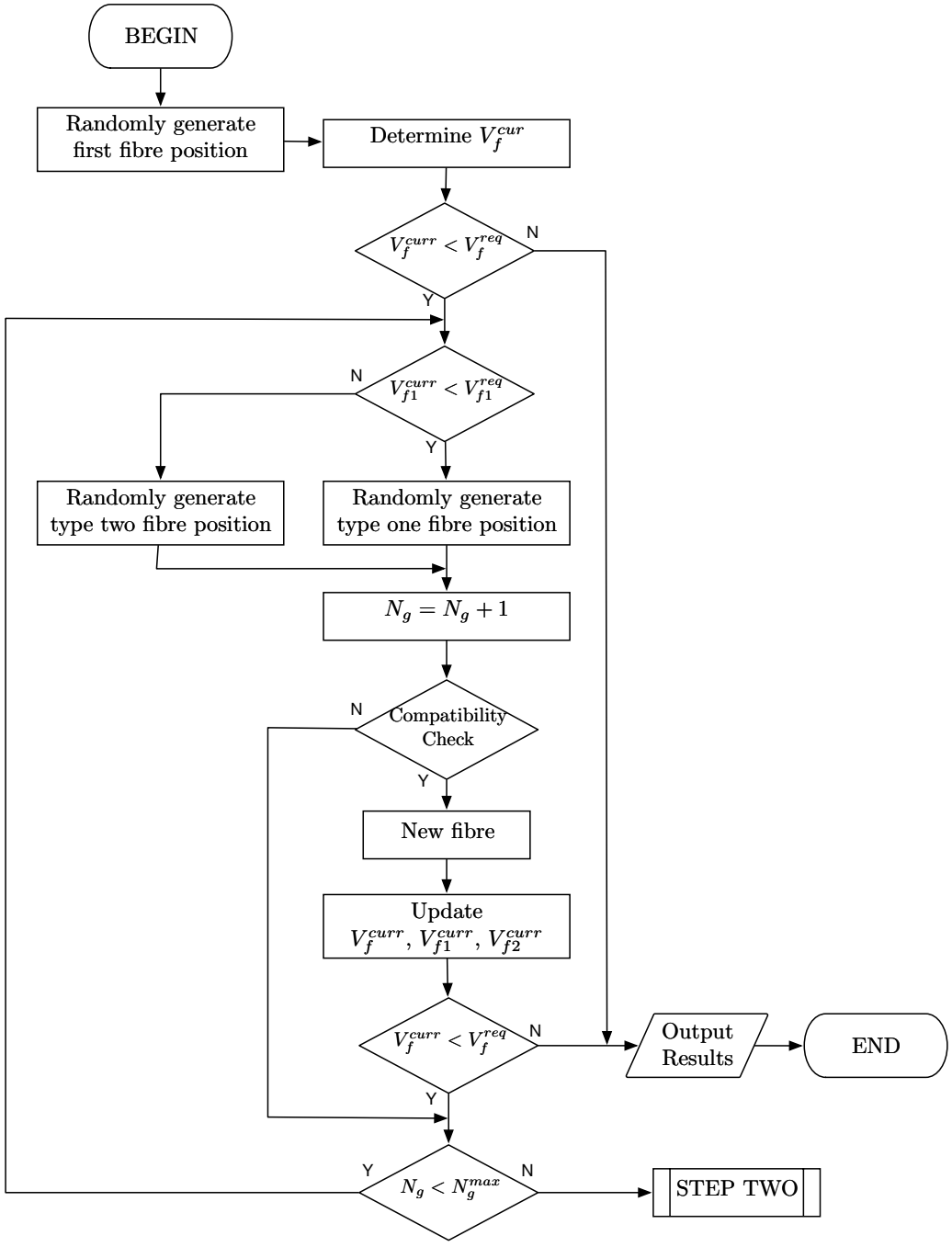

Figure 6.2: Flowchart of the hard-core model for the generation of the microstructure.

6.2 Damage models

To simulate the micromechanical behaviour of composite materials it is necessary to develop material models that are able to represent the behaviour of the constituents in the composite. As the composite materials is constituted by two types of materials, the matrix and the fibres, it is necessary to develop two material models and one additional material model for the interface.

The material model used for the matrix is the one developed by Bai et al. [99], which is a damage model with plasticity based on a modified paraboloid yield criteria, able to capture the thermal and strain-rate dependency in the matrix behaviour. As no modifications were made to this model in order to be implement in this work it will not be presented here.

The material model for the fibres is based on the work of Melro [98] and is presented in the following section.

6.2.1 Damage model for the fibres

The damage model implemented to characterize the behaviour of fibres was based on Melro's work [98] with the modifications needed in order for the fibre strength to be characterized by a Weibull distribution.

It is considered that the fibres possess a transversely isotropic behaviour, however, the damage model considers only one damage variable and is solely activated by the longitudinal stress component.

In order to guarantee a thermodynamically consistent model it is firstly necessary to define the complementary free energy of the material:

$$\begin{aligned}\mathscr{G}_f =& \frac{\sigma_{11}^2}{2E_1\left(1-d_f\right)} + \frac{\sigma_{22}^2+\sigma_{33}^2}{2E_2\left(1-d_f\right)} - \frac{\nu_{12}}{E_1}\left(\sigma_{11}\sigma_{22}+\sigma_{11}\sigma_{33}\right) \\ & - \frac{\nu_{23}}{E_2}\sigma_{22}\sigma_{33} + \frac{\sigma_{12}^2+\sigma_{13}^2}{2G_{12}\left(1-d_f\right)} + \frac{\sigma_{23}^2}{2G_{23}\left(1-d_f\right)} \,,\end{aligned} \tag{6.1}$$

where E_1 and E_2 are the longitudinal and transverse Young's moduli, G_{12} and G_{23} the longitudinal and transverse shear moduli and d_f is the damage variable for the fibres. To ensure that the damage process is irreversible it is necessary to guarantee that the rate of change of the complementary free energy density is greater than the externally applied stress:

$$\dot{\mathscr{G}}_f - \dot{\boldsymbol{\sigma}} : \boldsymbol{\varepsilon} \geq 0 \,, \tag{6.2}$$

which can be written as

$$\left(\frac{\partial \mathscr{G}_f}{\partial \boldsymbol{\sigma}} - \boldsymbol{\varepsilon}\right) : \dot{\boldsymbol{\sigma}} + \frac{\partial \mathscr{G}_f}{\partial d_f}\dot{d}_f \geqslant 0 \ . \tag{6.3}$$

To ensure a positive dissipation of mechanical energy it is necessary that the strain tensor to be equal to the derivative of the complementary free energy density with respect to the stress tensor,

$$\boldsymbol{\varepsilon} = \frac{\partial \mathscr{G}_f}{\partial \boldsymbol{\sigma}} \ . \tag{6.4}$$

The compliance tensor ($\boldsymbol{H_f}$) can be defined as:

$$\boldsymbol{H_f} = \frac{\partial^2 \mathscr{G}_f}{\partial \boldsymbol{\sigma}^2} \ . \tag{6.5}$$

Inverting the compliance tensor results in the stiffness tensor

$$\boldsymbol{C_f} = \frac{1-d_f}{\Delta}\begin{bmatrix} E_1\left(1-\beta^2\right) & E_2\nu_{12}\left(1-d_f\right)\left(1+\beta\right) & E_2\nu_{12}\left(1-d_f\right)\left(1+\beta\right) & 0 & 0 & 0 \\ & E_2\left[1-\gamma\left(1-d_f\right)\right] & E_2\left(1-d_f\right)\left(\nu_{23}+\gamma\right) & 0 & 0 & 0 \\ & & E_2\left[1-\gamma\left(1-d_f\right)\right] & 0 & 0 & 0 \\ & & & G_{12}\Delta & 0 & 0 \\ & & & & G_{12}\Delta & 0 \\ \text{sym.} & & & & & \frac{E_2\Delta}{2(1+\nu_{23})} \end{bmatrix}, \tag{6.6}$$

where

$$\beta = \nu_{23}\left(1-d_f\right) \ , \tag{6.7a}$$

$$\gamma = \nu_{12}\nu_{21}\left(1-f_f\right) \ , \tag{6.7b}$$

$$\Delta = \left(1-\beta\right)\left[1-\beta-2\gamma\left(1-d_f\right)\right] \ . \tag{6.7c}$$

The damage activation function can be defined as:

$$F_f^d = \phi_f^d - r_f \leq 0 \ , \tag{6.8}$$

where ϕ_f^d is the loading function

$$\phi_f^d = \frac{\tilde{\sigma}_{11}}{X_f^t} \ , \tag{6.9}$$

and r_f the internal variable

$$r_f = \max\left\{1, \max_{t\longrightarrow\infty}\left\{\phi_{f,t}^d\right\}\right\} \ . \tag{6.10}$$

The loading function is a function of the fibre tensile strength (X_f^t), which has a stochastic value and will vary from element to element. The loading function is also a function of the effective longitudinal stress $\tilde{\sigma}_{11}$. This is a component of the effective stress tensor given by:

$$\tilde{\boldsymbol{\sigma}} = \boldsymbol{H_f^0}^{-1} : \boldsymbol{\varepsilon} \,, \tag{6.11}$$

where $\boldsymbol{H_f^0}$ is the compliance tensor of the undamaged material, which can be obtained by forcing the damage variable to be null.

To avoid mesh dependency problems and control the energy dissipated in the fracture process, Bažant's crack band model [100] was implemented. The dissipated energy for the fibres is defined as:

$$\Psi_f = \int_0^\infty Y_f \dot{d}_f \, \mathrm{d}t = \int_1^\infty \frac{\partial \mathscr{G}_f}{\partial d_f} \frac{\partial d_f}{\partial r_f} \, \mathrm{d}r_f = \frac{G_{ff}}{l^e} \,, \tag{6.12}$$

where G_{ff} is the fracture toughness the fibres, l^e the characteristic length and Y_f is the thermodynamic force associated with the variable d_f. Using the complementary free energy for the fibres, given by Equation 6.1, it is possible to define Y_f as:

$$Y_f = \frac{\partial \mathscr{G}}{\partial d_f} = \frac{1}{(1-d_f)^2} \left[\frac{\sigma_{11}^2}{2_E 1} + \frac{\sigma_{22}^2 + \sigma_{33}^2}{2E_2} + \frac{\sigma_{12}^2 + \sigma_{13}^2}{2G_{12}} + \frac{\sigma_{23}^2}{2G_{23}} \right] \,, \tag{6.13}$$

that is always positive. The damage evolution law defined for the fibres is given by:

$$d_f = 1 - \frac{e^{A_f\left(1-r_f\right)}}{r_f} \,, \tag{6.14}$$

where A_f is a parameter that must be determined by solving Equation 6.12 as a function of the characteristic length, therefore, this parameter must be computed for each element of the mesh. The derivative of the damage law in order to r_f is given by:

$$\frac{\partial d_f}{\partial r_f} = \frac{e^{A_f\left(1-r_f\right)}}{r_f} \left(A_f + \frac{1}{r_f} \right) . \tag{6.15}$$

In order to solve Equation 6.12 it is necessary to define the relation between the real stress tensor and the effective stress tensor. This is done by imposing the principle of strain equivalence:

$$\left.\begin{array}{l} \boldsymbol{\sigma} = \boldsymbol{C_f} : \boldsymbol{\varepsilon} \\ \tilde{\boldsymbol{\sigma}} = \boldsymbol{C_f^0} : \boldsymbol{\varepsilon} \end{array}\right\} \boldsymbol{\sigma} = \boldsymbol{C_f} : \boldsymbol{C_f^0}^{-1} : \tilde{\boldsymbol{\sigma}} = \boldsymbol{C_f} : \boldsymbol{H_f^0} : \tilde{\boldsymbol{\sigma}} \,, \tag{6.16}$$

where $\boldsymbol{C_f^0}$ is the undamaged stiffness tensor and $\boldsymbol{H_f^0}$ the undamaged compliance tensor.

If the particular case of uniaxial tensile loading is considered, the effective stress tensor ($\tilde{\boldsymbol{\sigma}}$) is given by:

$$\tilde{\boldsymbol{\sigma}} = \begin{bmatrix} \tilde{\sigma}_{11} \\ 0 \\ 0 \\ 0 \\ 0 \\ 0 \end{bmatrix} . \tag{6.17}$$

For this tress state the three normal components of the real stress tensor are:

$$\sigma_{11} = \frac{1-d_f}{\Delta}\left[1-\beta^2-2\gamma\left(1+\beta\right)\right]\tilde{\sigma}_{11} , \tag{6.18a}$$

$$\sigma_{22} = \sigma_{33} = -\frac{1-d_f}{\Delta}\nu_{12}\left(1+\beta\right)d_f\tilde{\sigma}_{11} , \tag{6.18b}$$

the remaining shear components of the tress tensor are equal to zero. Using Equations 6.18 in Equation 6.13 results in:

$$\frac{\partial \mathscr{G}}{\partial d_f}^{UN} = \frac{\left(1+\beta\right)^2}{2E_1\Delta^2}\left[\left(1-\beta-2\gamma\right)^2+2\nu_{12}\nu_{21}d_f^2\right]\tilde{\sigma}_{11}^2 , \tag{6.19}$$

for the uniaxial tensile state. The damage activation function for the uniaxial tensile state is given by:

$$F_f^{dUN} = \frac{\tilde{\sigma}_{11}}{X_f^t} - r_f \leq 0 , \tag{6.20}$$

and for the damage to propagate, this equation needs to be equal to zero. Solving this equation in order to the applied effective stress results in

$$\tilde{\sigma}_{11} = X_f^t r_f . \tag{6.21}$$

Using Equations 6.19, 6.18 and 6.21 in in Equation 6.13 results in:

$$\int_0^\infty \frac{{X_f^t}^2 r_f^2\left(1+\beta\right)^2}{2E_1\Delta}\left[\left(1-\beta-2\gamma\right)^2+2\nu_{12}\nu_{21}d_f^2\right]\frac{\partial d_f}{\partial r_f}\,\mathrm{d}r_f = \frac{G_{ff}}{l^e} , \tag{6.22}$$

which needs to be solved numerically along the damage evolution law (Equation 6.14) to determine the parameter A_f. This variable is forced to be lower than zero in the initial conditions to force the initialization of the algorithm.

The tensile strength assigned to each element with is generated using a process similar to that presented in Chapter 4, resorting to the generation of random numbers. A random number X is generated for each element, using Fortran random

number generator, in the interval 0 to 1. This number represents the failure probability in the Weibull distribution:

$$X = P(\sigma) = 1 - \exp\left(1 - \left(\frac{L}{L_0}\right)\left(\frac{\sigma}{\sigma_0}\right)^m\right) . \tag{6.23}$$

Solving Equation (6.23) for σ, which will be the assigned tensile strength for the fibre (X_f^t) results in:

$$X_f^t = \sigma_0 \left[-\frac{L_0}{L}\ln(1 - X)\right]^{1/m} . \tag{6.24}$$

The fibres used in fibre reinforced composites have a very low energy release rate [91] which means that the maximum element length is very small. If the element length is higher than a critical value (l^e_{max}) there is a snap-back effect, represented by the red line in Figure 6.3.

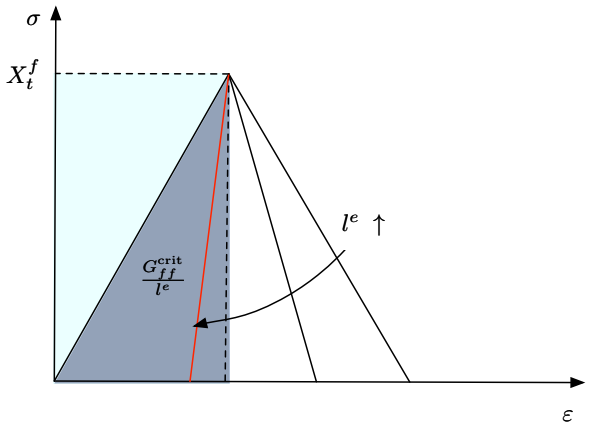

Figure 6.3: Stress-strain diagrams for the fibre damage model for various element lengths.

In order to avoid this issue, without reducing the element's size to values that are too computationally expensive, a strategy was implemented that changes the effective energy release rate of the material to guarantee that there is no occurrence of the snap-back effect. Although this changes the material properties, its effect is reduced as the energy released in fibre failure is very small. To implement this strategy it is necessary to determine the minimum energy release rate (G_{ff}^{crit}) that is required to avoid snap-back in an element of length l^e. This is done by considering the gray triangle in Figure 6.3, which represents minimum energy that needs to be released in the model:

$$\frac{G_{ff}^{\text{crit}}}{l^e} = \frac{1}{2}\frac{X_f^t}{E}X_f^t . \tag{6.25}$$

Solving the previous equation in order to the energy release rate results in:

$$G_{ff}^{\text{crit}} = \frac{1}{2}\frac{{X_f^t}^2}{E} l^e \ . \tag{6.26}$$

For each element the critical energy release rate is determined, as a function of the random tensile strength (X_f^t) and of the characteristic element length (l^e). If the critical energy release rate is higher than the material's energy release rate, then this value is changed to G_{ff}^{crit} in order to avoid snap-back effects. The flowchart of the implemented algorithm for the damage model is shown in Figure 6.4. This damage model was implemented in a VUMAT subroutine of the commercial finite element analysis software ABAQUS.

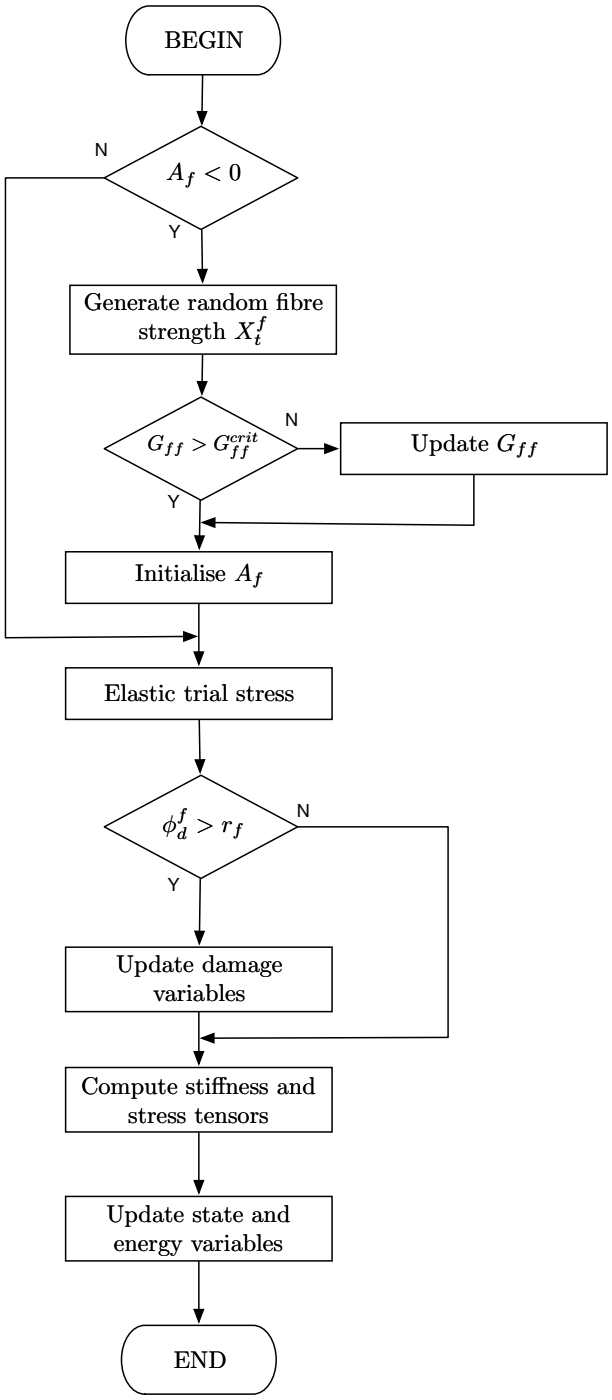

Figure 6.4: Flowchart of the constitutive model for the fibres.

6.3 Analysis of results

This section presents the results from the micromechanical simulations performed for hybrid and non-hybrid composites with different types of fibres.

6.3.1 AS4 carbon composite material

The material presented in this section is a composite based on by AS4 carbon fibres [88, 91, 101] and on an Epoxy 3501-6 matrix [99]. The properties required for the material models are shown in Table 6.1 and 6.2 for the fibres and the matrix, respectively. The energy release rate of the fibres was determined from the fracture toughness by assuming plane stress conditions [91]. Unless otherwise specified these properties will remain constant in all models.

Table 6.1: Fibre properties required for the material models.

E_1 (GPa)	E_2 (GPa)	ν_{12}	G_{12} (GPa)	G_{23} (GPa)	α_{L} $(10^{-6}/°\mathrm{C})$
225	15	0.2	15	7	-0.5
α_{T} $(10^{-6}/°\mathrm{C})$	G_{ff} (N/mm)	σ_0 (MPa)	m	l_0 (mm)	
15	4×10^{-3}	4600	10.7	12.6	

Table 6.2: Matrix properties required for the material models.

E (GPa)	ν	ν_p	σ_{Y_T} (MPa)	σ_{Y_C} (MPa)
4.6	0.34	0.3	44.4	112.7
σ_{Y_S} (MPa)	α_C^m	α_T^m	α_S^m	G_m (N/mm)
30.3	0.0042	0.0	0.0	0.09

The properties for the cohesive surfaces in the interfaces between the fibres and the matrix are present in Table 6.3.

Two types of random number generators were used to obtain the random distribution for the strength of the fibres. In Figure 6.5 it is shown two distributions of the fibre strength of all fibre elements for the AS4 carbon fibres, obtained using both algorithms. The gauge length was considered to be the longidutinal size of the RVE, which for the RVE of the size $15 \times 15\times$ fibre radius is 52.5 μm. The same methodology was followed for the RVEs with other sizes and materials.

Table 6.3: Properties for the cohesive surfaces in the fibre-matrix interfaces.

Interface maximum strengths	
τ_1 (MPa)	70
τ_2 (MPa)	70
τ_3 (MPa)	50
Maximum displacement	
δ_τ (mm)	0.001
Friction	
μ_τ	0.52

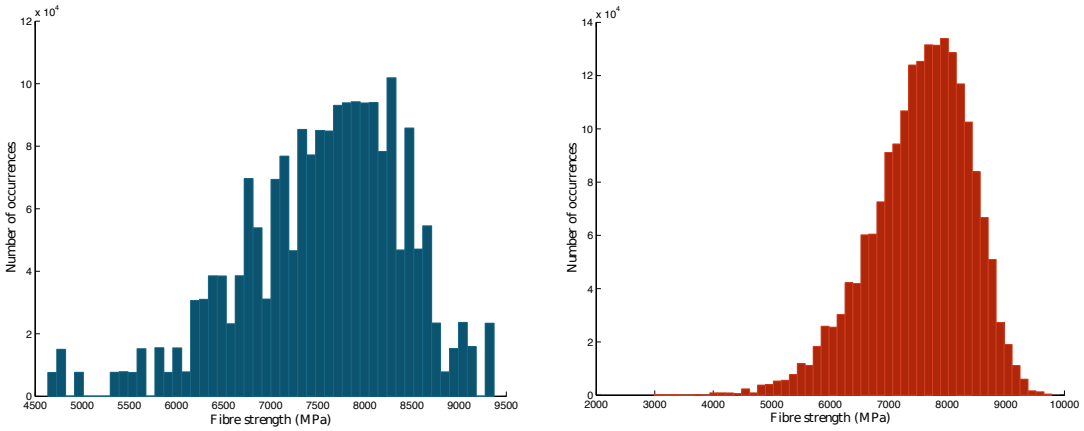

Figure 6.5: Distributions of tensile strength of all the elements present in the model, for two different random generators.

Although having the same input properties it is possible to see that both algorithms generate quite different distributions. In Figure 6.6 it is possible to see the stress-strain curves for the composite materials with the each fibre strength distribution. The colors of the curves are in accordance to those of the histograms. The RVE used for this simulation had a size of $15 \times 15 \times 15$ fibre radius. It is possible to see that, as the fibre strength distribution in orange is wider, having elements with very low and very high, the failure of the composite occurs more gradually. This can be attributed to the lower resistance fibres break at low strains, but the high resistance ones only break at higher strains.

Analysing the data from the stress-strain curves it is possible to see that the tensile strength of the composite material differs when comparing both generators. For the generator that produced the curve in red the maximum stress is 2153 MPa. This value needs to be compared to the tensile strength of a composite material based on AS4 carbon fibres on an Epoxy 3501-6 matrix. The reference value for the tensile

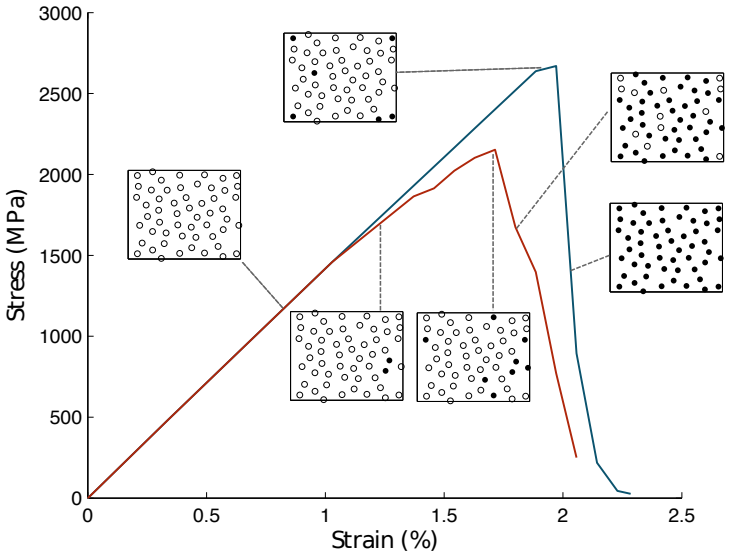

Figure 6.6: Stress-strain curves for the AS4 carbon and epoxy matrix for a RVE of dimensions $15 \times 15 \times 15$ fibre radius.

strength of a composite material with a fibre volume fraction of 0.62, from the Hexcel product data sheet [102], is 310 ksi which is equal to 2137 Mpa. Soden et al [101], for an AS4 carbon on Epoxy 3501-6 matrix composite with a fibre volume fraction equal to 0.6, provides the reference value for the tensile strength of 1950 MPa. These reference values are very similar to the ones from the micromechanical model, being the generator in red that gives the more accurate results. This leads to the conclusion that the generator in red generates a more accurate distribution for the strength of the fibres.

As the size of the RVE can be an important factor and influences the results obtained, a RVE with a size equal to $20 \times 20 \times 20$ fibre radius was generated, thus having a dimension of 70 μm. The results obtained with that RVE for the AS4 carbon composite, with the same fibre and matrix properties as the previous simulations is shown in Figure 6.7. In this figure, the dashed lines represent the results using the $15 \times 15 \times 15$ sized RVE while the solid lines represent the bigger $20 \times 20 \times 20$. The results were done using both random number generation algorithms and the microstructures for the $20 \times 20 \times 20$ RVE are also shown.

Comparing the results it is possible to see that increasing the size of the RVE beyond $15 \times 15 \times 15$ fibre radius does not significantly change the results obtained, however it has a large effect in the computational time. This leads to the conclusion that the RVE with this size is representative of the material and mechanisms of failure of UD composites.

In Figure 6.6 alongside the stress-strain curves it is also possible to see the evo-

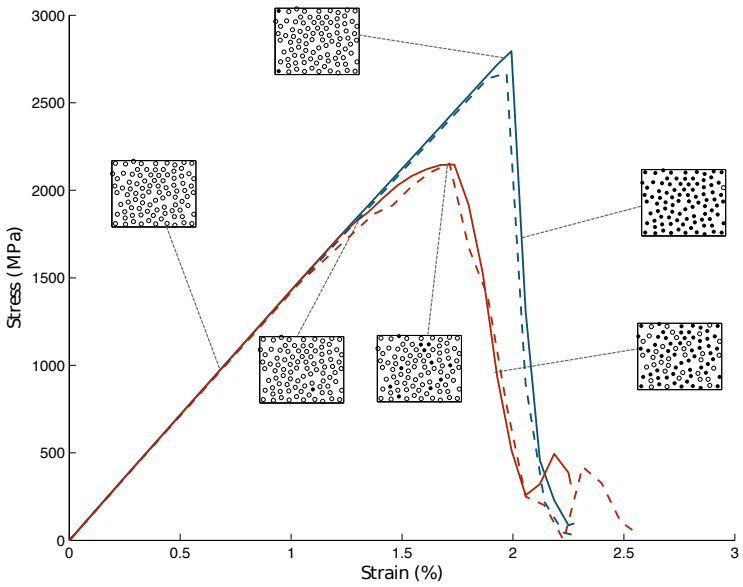

Figure 6.7: Stress-strain curves for the AS4 carbon and epoxy matrix: solid line - RVE $20 \times 20 \times 20$; dashed line - RVE $15 \times 15 \times 15$.

lution of the microstructure of the composite material. The circles represent the fibres and when in full the respective fibre is broken. It is possible to see that the behaviours are quite different and that the failure strain and resistance of the composite materials is different. For the curve in blue there only a few fibres are broken shortly before the composite fails, where in the red the fibres start to fail at lower strains, approximately at 1%. Nonetheless, the majority of the fibres fail at approximately the same stress level, leading to the catastrophic failure of the composite.

One important fact that these models were able to capture was the fibre failure that exists prior to the failure of the composite material. Fact that is responsible for some non-linear behaviour prior to the failure of the composite and that has been experimentally demonstrated with acoustic emission.

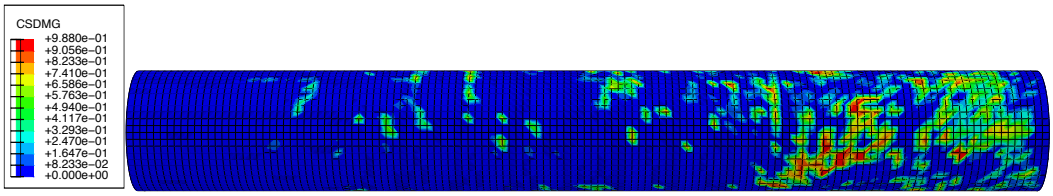

Figure 6.8: Damage in the interface of a broken fibre.

As one of the objectives of these simulations is to study the failure mechanisms it is necessary to understand the sequence of damage in the components of the composite material. In both simulations it is possible to see that the matrix is

damaged prior to the failure of the fibres, having some small transverse cracks. This effect is more pronounced in the curve in blue as the first fibre failure occurs at higher strains. However, after a fibre fails it is possible to see that a crack rapidly propagates in the matrix. This crack is also associated with decohesions in the fibre-matrix interface (Figure 6.8). The progression of the fibre and matrix damage variables (d_f and d_m) in the full RVE is shown in Figure 6.9 , from the initial stages off damage, prior to fibre failure (Figure 6.9a), to the catastrophic failure of the composite with multiple fibre breaks (Figure 6.9c). After a fibre fails the fibres nearby have a localized increase in stress. The fibres failure seem not to be affected by the location of the first break, as the next fibres to fail are not close to the first and the fracture plane is not that corresponding to the first fibre break.

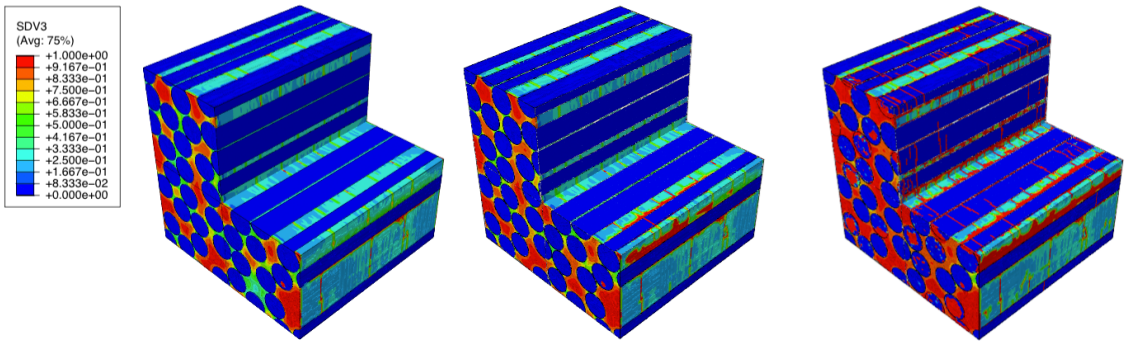

(a) (b) (c)

Figure 6.9: Damage progression in the RVE: (a) damage prior to fibre failure; (b) damage after first fibre failure; and (c) damage after failure of the composite material.

As the fibre failure is a dynamic phenomena, it is possible to see that after a fibre breaks it is loaded in compression (Figure 6.10b), acting as a spring, however this is a transitory effect and after this dynamic effect stabilizes the fibre is loaded in the expected stress profile. As the fibre is fractured it is not able to carry stress near the fracture but is still able to do so away from the original failure plane. The stress carrying capabilities of the fibre are increase away from the failure plane, until it fully regains its capacity. This observations show that the model developed is also able to capture the ineffective length previously reported. This length is approximately 0.03 mm which is equivalent to 8.5 fibre radius which is similar to the results from Swolfs et al. [11, 16].

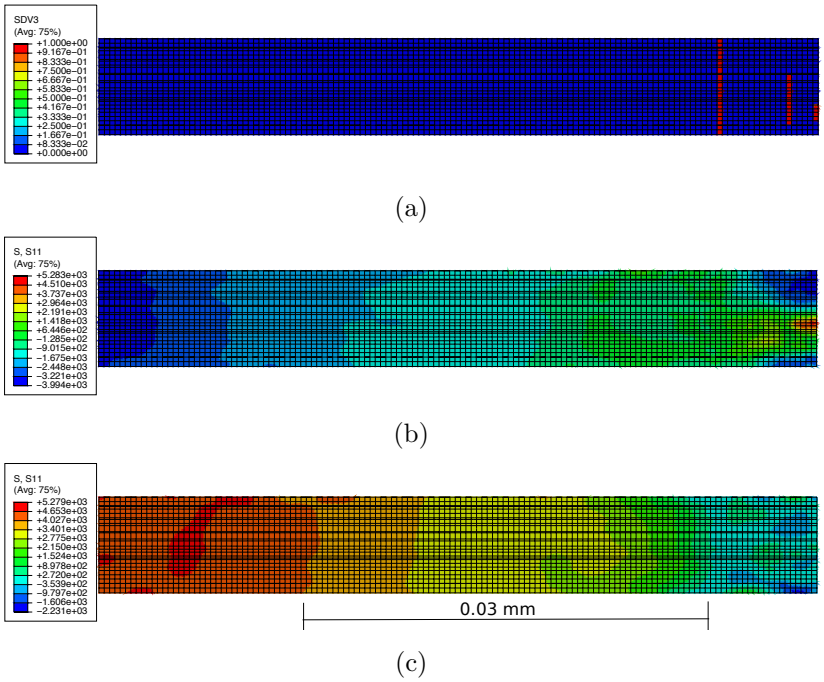

Figure 6.10: Broken fibre: (a) Location of the fibre break; (b) Stress field at fibre failure and (c) Stress field after dynamic effect.

6.3.2 M50S carbon composite

This section presents the results from the micromechanical simulations of the M50S [91] carbon fibre in epoxy 3501-6 matrix. Due to lack of information regarding the properties of these carbon fibres, the properties were considered to be the same as those of the AS4 carbon. However, the longitudinal Young's moddlus (E_1) was changed to 480 MPa, as well as the Weibull strength distribution parameters: $\sigma_0 =$ 4600 MPa, $m = 9$ and $l_0 = 10$ mm. With these properties the fibre strengths generated by both algorithms result in the distributions shown in Figure 6.11 and the resulting stress-strain curves and the diagrams of fibre failure are shown in Figure 6.12.

As the M50S fibres have a lower mean failure strain than the AS4 carbon, the failure strain of the composite material is also reduced. This lower failure strain means that there is no damage in the matrix prior to fibre failure, however, after a fibre fails it is possible to see that a cracks propagates in the matrix (Figure 6.13a). The fibre break also cause stress concentrations in its neighbouring fibres (Figure 6.13b). It is possible to see that this stress concentrations act in a very small area surrounding the broken fibre which, by comparing both fibres it is possible to see that is similar to the area of the crack in the matrix. This can be seen immediately after the fibre failure however , with increasing the applied strain and with the fracture of others fibres, the matrix cracks and the stress state near the broken fibres become

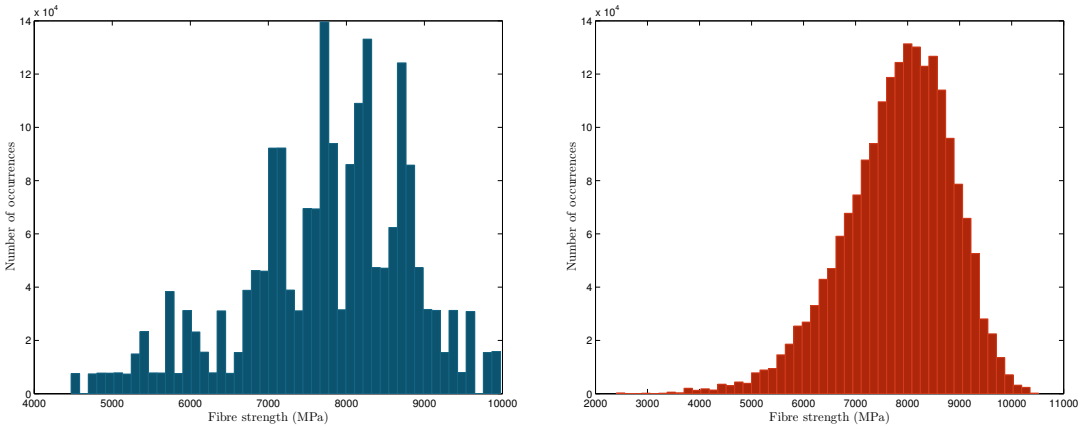

Figure 6.11: Distributions of tensile strength of all the elements present in the model for the M50S fibres using both random generators.

more complex.

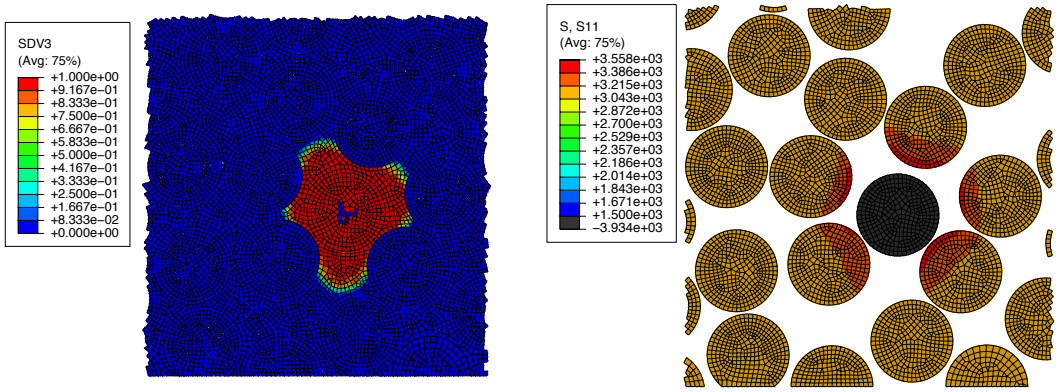

(a) (b)

Figure 6.13: Matrix crack developed after a fibre breaks (a) and stress concentrations in the neighbouring fibres of a broken one (b).

The overall failure mechanisms are similar in both studied composites. The failure of the subsequent fibres is a semi-random process that occurs throughout the hole RVE in multiple planes, being dominated by fibre deffects, e.i., regions of the fibres with lower tensile strength.

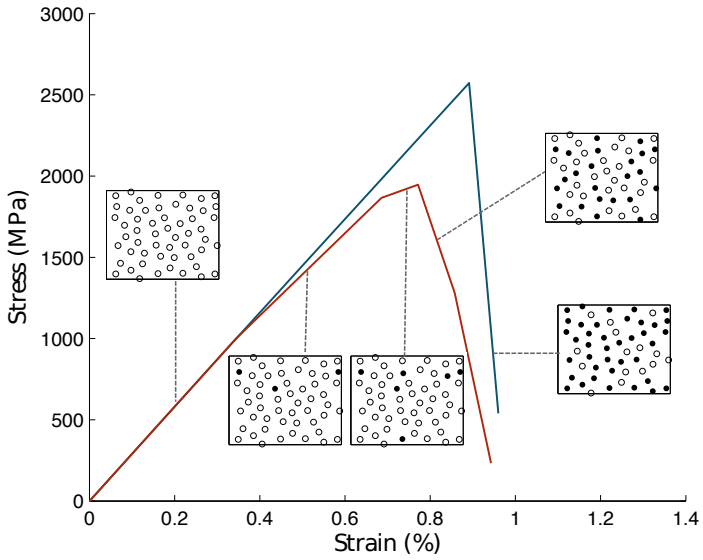

Figure 6.12: Stress-strain curves for the M50S carbon and epoxy matrix.

6.3.3 M30S carbon composite

The composite presented in this section has the same epoxy matrix as the previous but the fibres are the M30S carbon fibres [91]. These fibres have a higher strength dispersion due to having a lower Weibull modulus ($m = 4.6$). The Weibull scale parameter (σ_0) is equal to 6400 MPa at the reference length (l_0) of 10 mm. This leads to a wider strength distribution, shown in Figure 6.14 and the stress-strain curves for both distributions are shown in Figure 6.12.

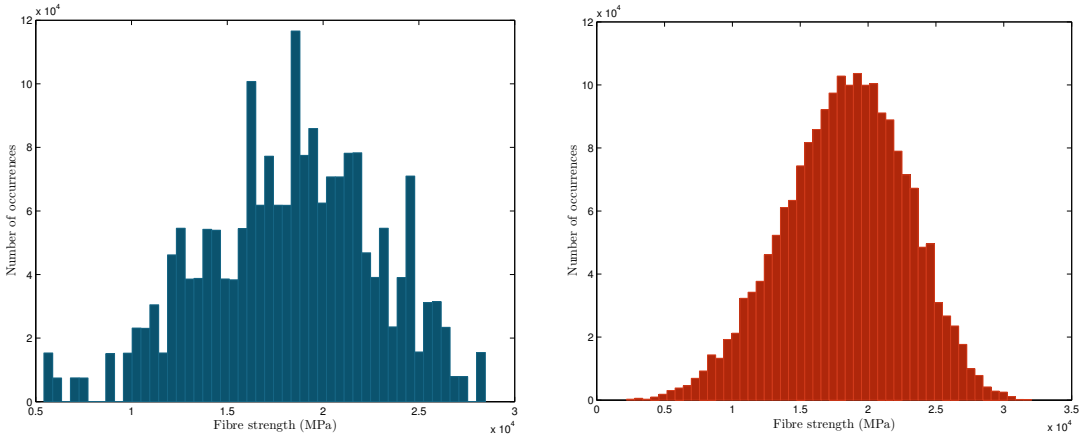

Figure 6.14: Distributions of tensile strength of all the elements present in the model for the M30S fibres using both random generators.

From these results it is possible to see that, as there is a higher dispersion of the strength of the fibres, the failure is more gradual, with fibres breaking at considerably

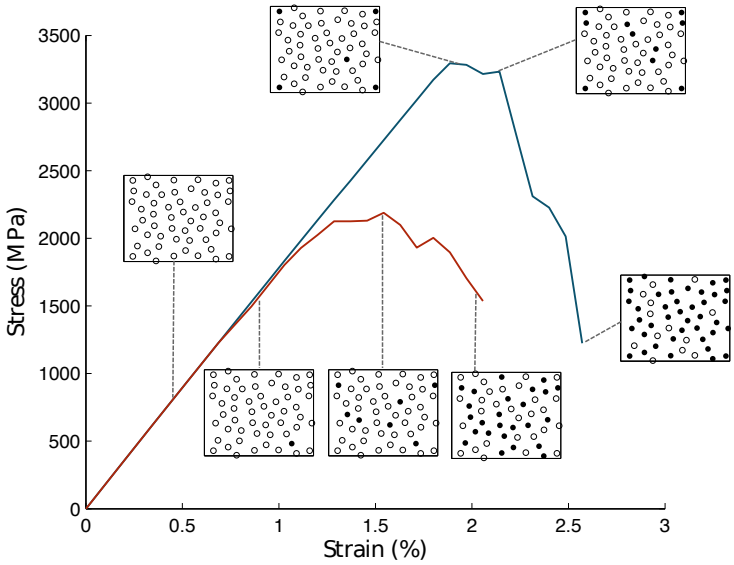

Figure 6.15: Stress-strain curves for the M30S carbon and epoxy matrix.

different strains. The failure of a small percentage of the fibres leads to the non-linearity that is possible to see in the curve in red. However, if enough fibres fail the load carrying capabilities of the material are reduced and the composite fails. As the strength associated with each element has a higher variability there are zones of the fibres with lower resistance and zones with very high resistance. As the fibres have a tendency to break in the zones with lower resistance, they do not tend to fail in the same plane but develop breaks in multiple planes. A similar sequence of mechanisms that lead to the failure of the composite material is present in this type of material. The high failure strain of the fibres leads to the development of small cracks in the matrix prior to fibre failure, however, it is the failure of a fibre that damages the matrix the most, leading to large cracks surrounding the broken fibre, as shown in Figure 6.16.

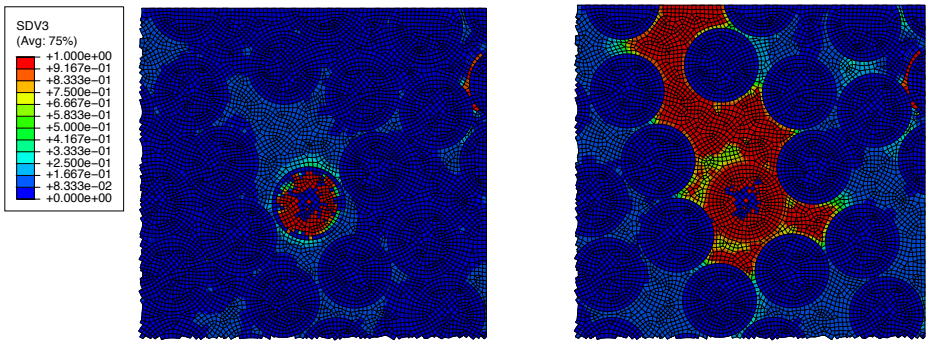

(a) (b)

Figure 6.16: Crack development in the matrix: (a) Fibre failure and (b) development of a crack in the matrix surrounding the broken fibre.

6.3.4 Hybrid AS4-M50S carbon composite

The previous sections were dedicated to the analysis of the behaviour of non-hybrid composites with different fibre types. The information reported enabled the identification of the failure mechanisms and served as a preliminary validation of the models. The present section is dedicated to the effects of mixing two types of fibres in one hybrid composite material. The fibres being hybridized in this section are the AS4 and the M50S carbon fibres, which have already been presented. The choice of this hybridization is due to the fact that it was the one that shown more potential in Chapter 5 to achieve a pseudo-ductile behaviour. The pseudo-ductility was attributed to the fact that the fibres have different failure and critical strains, which lead to non-hybrid composites with different failure strains. This difference is also present in the micromechanical models previously analysed (Figure 6.6 and 6.12), where the AS4 carbon composite has a failure strain between 1.5 and 2% while the M50S carbon composite has a failure strain between 0.8 and 1%.

In order to study the effects of hybridization it is necessary to obtain RVEs with multiple fibres and having different volume fractions of each fibre, as this is an important parameter in hybrid composites, which was done using the RVE generator previously presented. The dimension of the for this study is $15 \times 15 \times 15$ fibre radius, leading to a cubic RVE with 52.5 μm, as the fibre radii of both fibres are equal and equal to 3.5 μm.

The resulting stress-strain curves for the tensile loading of the AS4-M50S hybrid composites is shown in Figure 6.17. For this hybridization the low elongation fibres (LE) are the M50S fibres as they have a lower failure strain. This results were obtained with the random number generator that was represented in blue in the non-hybrid composites.

In Figure 6.17 it is possible to analyse the effects of hybridization in composite materials in relation to the non-hybrid composites. It is possible to see that as the content of M50S fibres (LE fibres) increases so does the initial Young's modulus of the composite material as the M50S fibre have a higher Young's modulus. It is also possible to see that the introduction of two fibre types with different failure strains reduces the resistance of the composite material, as the LE fibres will break before the HE fibres reach the maximum load carrying capacity. As there is a large difference between the failure strains of the AS4 fibres and the M50S it is verified that the M50S fibres usually fail before the any of the AS4 carbon fibres. The failure of these hybrid composites occurs in two different stages. Firstly the LE fibres break, without damaging the HE fibres, which results in the load drop shown in the stress-strain curves. Secondly, with the increase of the applied strain, the HE fibres fail and so does the composite material. The fibre failure sequence for all hybrid composites is shown in the microstructures present in Figures 6.18 to 6.21.

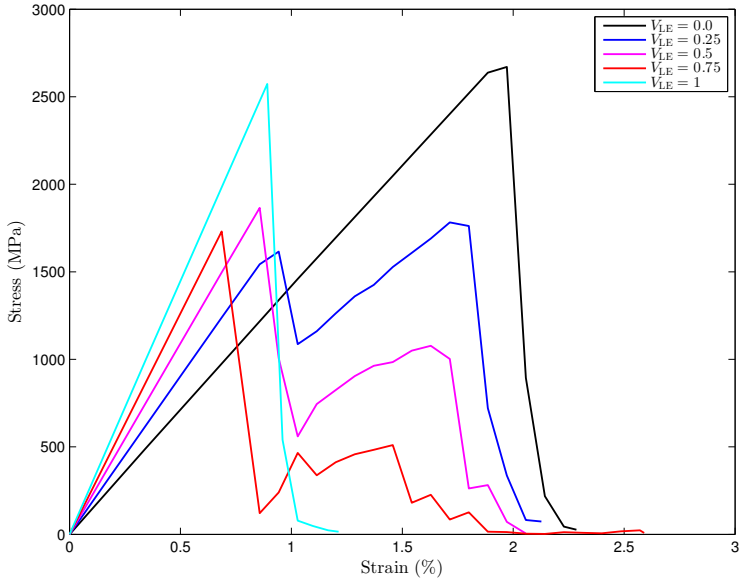

Figure 6.17: Stress-strain curves for the hybridization between the AS4 and M50S carbon fibres.

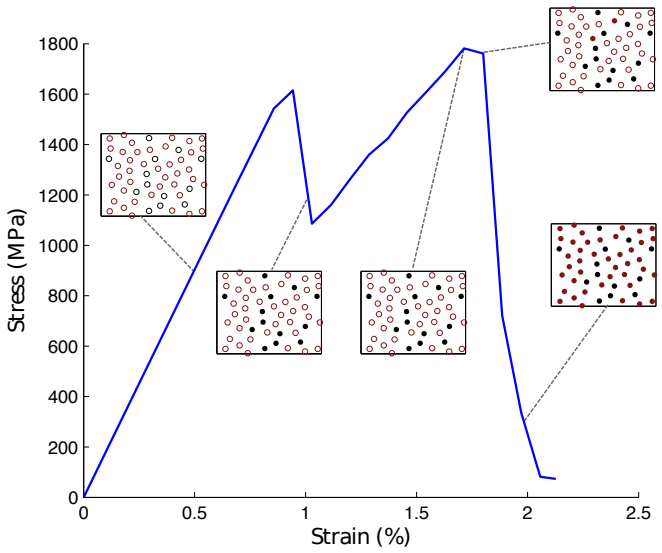

Figure 6.18: Stress-strain curves for the hybrid composite with a volume fraction equal to 0.75 of AS4 carbon fibres and 0.25 of M50S (LE) carbon fibres.

In Figure 6.18, after the first load drop, due to the failure of the M50S fibres, it is possible to see that there is no failure of new fibres until the applied strain reaches approximately 1.8% and the AS4 fibres break. However it is possible to see that there are some non-linearities in this stage. This non-linearities are due to the fact that the broken M50S carbon fibres are still able to carry stress and, therefore, may still break in locations away from the first break. This means that, in this

stage, the LE fibres are still be damageable and can break in multiple planes, as shown in Figure 6.19. In this composite material, as the content of HE fibres is high enough, the maximum stress in the stress-strain curves occurs after the LE fibres have failed, therefore the HE fibres are responsible for the strength of the composite material.

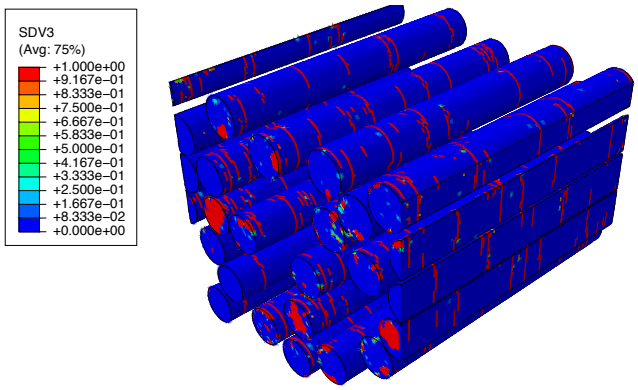

Figure 6.19: Multiple fractures of the M50S (LE) carbon fibres for a composite with a $V_{\mathrm{LE}} = 0.5$.

For the composite material with an equal volume fraction of each fibre type (Figure 6.20) the failure sequence is similar but, as the content of M50S fibres is increased, the maximum stress after the failure of the M50S fibres is reduced, and the load drop after the failure of these fibres is increased. Nonetheless, the composite presents a higher stiffness and a higher resistance, but a lower failure strain.

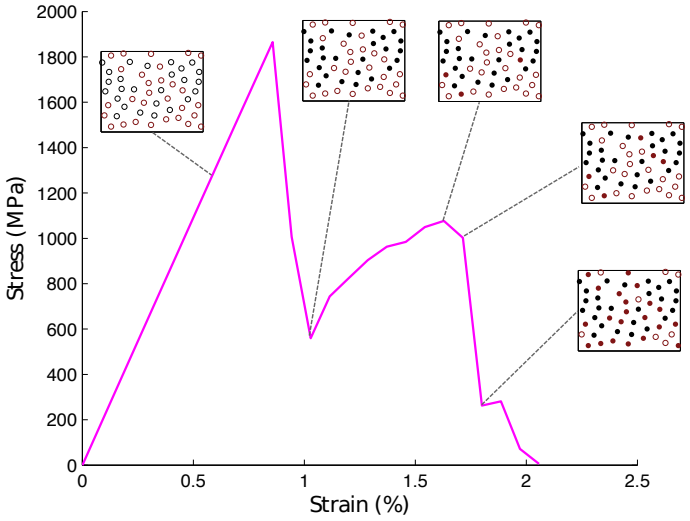

Figure 6.20: Stress-strain curves for the hybrid composite with a volume fraction equal to 0.5 of AS4 carbon fibres and 0.5 of M50S carbon fibres.

The composite material whose results are shown in Figure 6.21 has a volume content of M50S fibres equal to 0.75 of the overall fibre content. In comparison with the other hybrid composites this material has the higher stiffness, but has the lowest failure strain, which is lower than that of the non-hybrid M50S composite. As the content of HE fibres is reduced, after the LE fibres have failed the composite presents only a residual load carrying capability, being only able to support stress of, approximately, 500 MPa. AS the content of LE fibres is higher in this composite, after the failure of these fibres the material is much more damaged and more and more severe cracks have developed in the matrix.

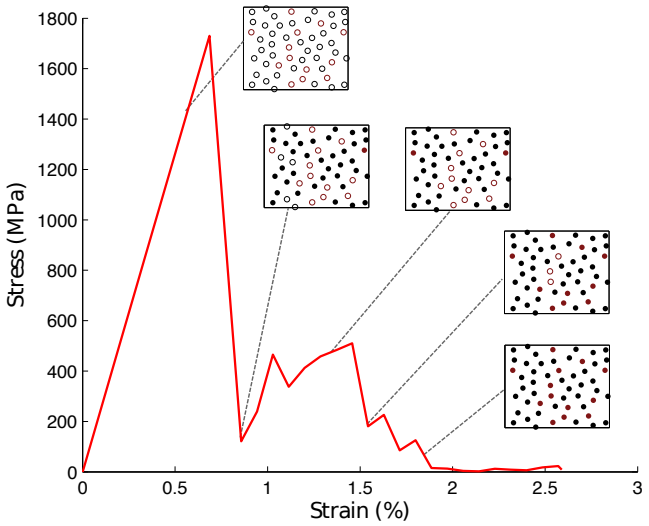

Figure 6.21: Stress-strain curves for the hybrid composite with a volume fraction equal to 0.25 of AS4 carbon fibres and 0.75 of M50S (LE) carbon fibres.

The stress field in the composite material after the LE fibres have failed is quite complex as the failure of these fibres occurs in multiple planes and each fibre can break in multiple locations, leading to decohesions in the interfaces and complex cracking in the matrix. In Figure 6.22 it is possible to see the sequence of failure of a high elongation fibre in the hybrid composite with a volume fraction of each fibre type equal to 0.5, of the total fibre content.

Analysing Figure 6.22 it is possible to see all the process of failure of a fibre. In Figure 6.22a it is shown the fibre strength for each element and it is possible to see that it is not uniform, having zones of high strength and zones of very low strength that represent a defect in the fibre, for instance the region marked in red. Comparing Figure 6.22b and Figure 6.22c it is possible to see that the fracture of the fibre did not occur in the zone where the stress is maximum. However, comparing with Figure 6.22a it is possible to see that the fracture occurred in a zone where the fibre has elements with very low tensile strength. This information, associated with the fact that the fracture of the fibres rarely occurs in the same plane, allows to

conclude that the main factor contributing for the failure of the fibres is the presence of defects, represented in the model by regions of low tensile strength. This effect is more pronounced than the stress concentrations due to the fibre failure and can help to explain the fact that the fibres fail in multiples planes. From the analysis Figure 6.22d it is possible to see that after the failure of the fibre, there is a length where the stresses in the fibre are reduced, the ineffective length.

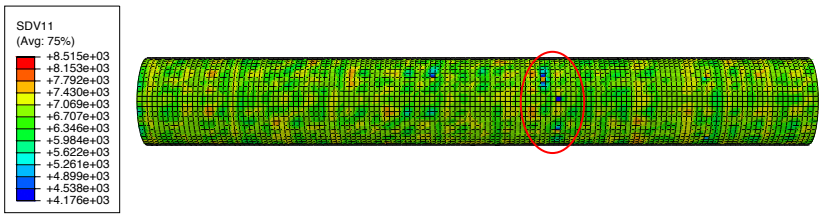

(a) Distribution of fibre strength.

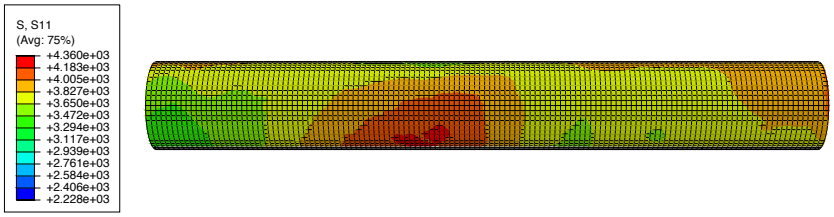

(b) Stress field in the intact fibre.

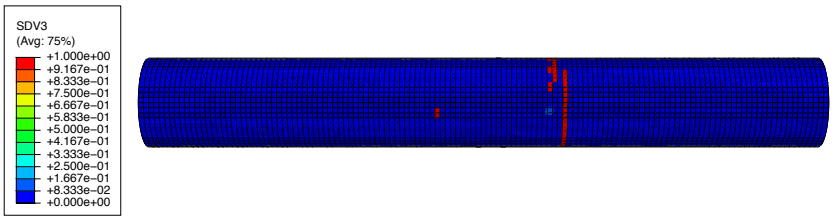

(c) Location of the fracture.

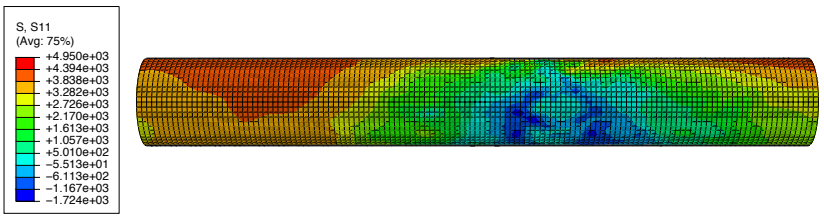

(d) Stress field after the fracture of the fibre.

Figure 6.22: Fracture process of an high elongation fibre (AS4 carbon) for a hybrid composite.

6.4 Conclusion

This chapter was dedicated to the micromechanical modelling of the tensile failure of unidirectional hybrid an non-hybrid composite. The models and the RVE

generation, as well as the main driving motivations for each chosen parameter are presented.

Several analysis were preformed to understand, firstly the mechanisms of failure in UD non-hybrid composites and secondly the effects of hybridization in these mechanisms and in the tensile behaviour of the composite.

The analysis of the non-hybrid composites allowed the analysis of the failure mechanism in the composites. It was shown that the fibre failure is phenomena dominated by flaws in the fibres and that the fibre failure rarely occurs in the same plane, usually failing in multiple plains according to the locations of these weaker regions. The failure of the first fibre can be preceded by matrix cracking if the failure strain of the matrix is lower than that of the fibres. Nonetheless, the fracture of the fibres leads to the development of cracks in the matrix and decohesion between the fibre-matrix interface. The failure of the fibres and the matrix cracks lead to stress concentrations in the intact fibres that surround a broken one. This intact fibres act as barriers to the propagation of the cracks in the matrix.

After its failure, a fibre is loaded in compression, acting as a spring, however this is a transient effect and after it stabilises it is possible to see that the fibre is loaded in a similar profile as the one from the shear-lag model. In the fracture plane the stress in the fibre is null, however as we move away from the fracture plane the fibre regains its load carrying capabilities until it is fully able to carry stress. This makes it possible for the same fibre to break in multiple locations.

The hybridization, by introducing to types of fibres in a single composite, drastically changes its tensile behaviour. For the studied AS4-M50S hybridization it is possible to see that the hybrid fibre volume content has a large effect in the composite's tensile behaviour. For a low LE fibre volume content the load drop after the failure of these fibres is reduced and the maximum stress is achieved after this point, fact that does not occur for at higher LE fibre volume contents.

As the hybridized fibres have very different failure strains the LE and HE fibres fail in two very distinct moments. In-between the failure of both fibre types it is possible to see that the LE, even already broken, keep breaking in multiple locations, leading to a non-linear behaviour and increasing the extent of matrix cracking.

Although it was predicted in Chapter 5 that the AS4-M50S hybridization would lead to a pseudo-ductile behaviour, the micromechanical simulations showed otherwise as both fibre types failed at very distinct moments. This allows to conclude that the failure of these composite is more complex and that the fragmentation model is not able to accurately predict the failure of these composites.

Chapter 7

Conclusions and future work

This chapter is intended to summarize the main conclusions of the thesis, reporting the main developments and results achieved. The future work to be done to improve the knowledge in the field of hybrid composites and micromechanical modelling is also proposed.

7.1 Conclusions

The information presented in Chapter 2 leads to the conclusion that the failure of UD non-hybrid composites results from the unstable propagation of a cluster of broken fibres after it has reached a critical size. This cluster is created by the progressive failure of multiple fibres and several clusters are formed within the composite prior to the failure.

In a modelling perspective it was seen that there are several models available, which come from different backgrounds and whose results and accuracy vary. However, several key points are common in the majority of the models. It is well accepted that composite materials are affected by size effects and that scaling methods are needed to extrapolate the results from coupon testing to the modelling of large structures. Another important factor to consider when modelling the tensile failure of UD composites, a fibre dominated process, is that the properties of the fibres are not deterministic and, therefore, accurate statistical distributions are needed to characterise these properties, mainly the tensile strength, which is a property dominated by surface and volumetric flaws. There are several statistical distributions to characterize this property, however, the majority of the authors agree that the Weibull distribution is an accurate distribution to describe it.

Having understood the mechanics of non-hybrid composites it was necessary to

study how this knowledge could be transferred to hybrid composites. A brief analysis on the effects of hybridization on different mechanical properties of composite materials was presented and it was possible to conclude that hybridization could have positive or negative effects, depending on the property of interest. This positive or negative effect was entitled hybrid effect and is a measure of the improvement of a specific property due to hybridization. It was shown that hybridization could lead to interesting effects being the most relevant the pseudo-ductile behaviour, possible to achieve with an accurate design of the material and control of the failure mechanisms in these composites. Similarly to the Chapter 2 the models for the tensile failure of hybrid composites, from simple analytical models to more complex numerical models based on Monte Carlo simulations, were presented. However it was concluded that the existing models still lacked in ability to accurately represent all the failure mechanisms present in these composites. Nonetheless, it was possible to gather information about the main factors that affect the tensile failure of hybrid composites.

As the tensile failure of composite materials is a fibre dominated process a model for the tensile failure of tows of fibres was developed. This is a simplified model based on the statistics for fibre strength that considers a tow of fibres to be constituted by a number of parallel fibres that do not interact with each other, i.e., the model does not consider the presence of the matrix. Although being a simple model it is very useful to understand the effects of key parameters such as the Weibull statistical parameters in the tensile failure of the fibres. Furthermore, it was possible to study the hybridization of tows using real fibre strength distributions and understand the effects in the tensile behaviour of the tows. It was concluded that, to achieve a tow with a higher ductility, the hybridized fibres needed to have strength distributions that allow the failure of the high elongation fibres to start immediately after the low elongation fibres have failed. When this happens the failure of the tow is gradual process and it is possible to achieve a tow with higher ductility without having a load drop in-between the failure of the high and low elongation fibres, typical of hybrid composites.

In order to connect the results from the tow model to the reality of the failure of composite materials it was necessary to include in a model the matrix material. This introduction drastically changes the behaviour of the material as the fibres no longer act independently but are connected by the matrix. The model developed for hybrid composites is based on the fragmentation of a single fibre. This model allowed to do a parametric study of hybrid composites, now with the effects of the matrix material, using real fibre strength distributions and understand the effects of hybridization on the tensile behaviour of composites. Although this is a simplified model it was possible to understand that the effects of hybridization in the composite's behaviour differ from those of the dry tows. It was concluded that the main controlling factor

of the hybrid composite's behaviour was the relation between the critical strains of the fibres. The critical strain is a property that relates the fibre and matrix properties and is directly related to the tensile strain of the composite material. To achieve a pseudo-ductile behaviour it is necessary that the fibres have different critical strains and that the reference non-hybrid composites have different failure strains. Nonetheless, it was possible to achieve a pseudo-ductile behaviour with this model for several hybridizations, including hybridizations with different materials, e.g., carbon and kevlar fibres.

The models for the failure of dry tows and the fragmentation models developed, although useful, are simplified models and are not able to take into account all the factors contributing to the tensile failure of composite materials. The model for dry tow only takes into account the statistical characterization of the fibres and disregards many other parameters such as the effects of the matrix and the interaction between fibres. Some of these problems were solved with the fragmentation model implemented in Chapter 5 with the inclusion of the matrix. Even so, this model still does not consider some important mechanisms such as the dynamics effects in the failure of the composites and the stress concentrations introduced due to the failure of the fibres.

To accurately simulate the tensile behaviour of composite materials and be able to analyse the mechanisms and sequence of failure it is necessary to use direct numerical simulations using micromechanical models. To correctly capture the mechanisms of failure it is necessary that each of the constituents of the composite to be model correctly. This includes not only the fibres but also the matrix and the interfaces between these two constituents. A model for the fibre material that is able to capture the the statistical variability of the strength of the fibres was implemented. This was done by generating, for each element, a random number between 0 and 1 and resorting to the Weibull probability density function, assigning a strength for that element. The material model used for the matrix is a damage model, developed by Bai et al. [99], that is able to capture the thermo-visco-plastic behaviour of this material. The interfaces between the matrix and the fibres were modelled using cohesive surfaces in order to correctly simulate the separation that occurs when a fibre breaks.

Several representative volume elements (RVEs) were generated using a modified version of Melro's [98] random fibre generator that is able to generate RVEs with multiple types of fibres with different radii. To be representative the size of the RVE must be so as to capture the mechanisms of failure of the composites. This makes it necessary to have a RVE with large dimensions, as it is necessary that, in the longitudinal direction, the model is able to capture the full extent of the fibre's ineffective length and in the transverse direction it is necessary to guarantee that the RVE has a sufficient number of fibres to simulate the critical cluster.

Different composite materials were studied, including hybrid and non-hybrid ones. The non-hybrid allowed to understand the sequence of failure mechanisms that lead to the failure of composites. It was concluded that the failure of the fibres is a flaw dominated process, as the fibres usually fail in the regions of lower strength. Prior to the failure of the first fibre it was, in some cases, noted some damage and cracks in the matrix, however the larger cracks are developed after the failure of a fibre in the plane of the fracture. This fractures can spread through large areas of the RVE, however the intact fibres act as crack arresters. The failure of a fibre did not usually lead to the failure of the neighbouring fibres and did not lead to their fracture in the same plane as the original fracture. Instead it was verified that the fibres failed in seemingly random locations, being that this locations were usually regions of lower strength, which means regions with more severe defects.

As already stated the fibre fracture is a dynamic phenomena. Some authors had verified that there was a dynamic effect that cause a wave of stress to propagate along the longitudinal direction of a fibre. This effect was captured in the model as, after the fracture, a fibre was loaded in compression for a small period of time. After the dynamic effect stabilizes, the fibre is loaded in a similar profile as the one predicted by the shear-lag model. In the fracture plane the fibre is not able to carry stress however, moving from the fracture plane in the longitudinal direction, the fibre regains its load carrying capability until it is fully recovered. This allows the fibres to fail multiple times in multiple locations.

From the results of the hybrid composites it was possible to conclude that the failure mechanisms are very similar to the ones in non-hybrid composites, however, as there are two types of fibres with different failure strains, the fibres do not fail all at similar strains. The fibres with lower failure strain are the first to fail, but the composite does not fully lose its load carrying capacity as there are still intact fibres, the high elongation fibres. Increasing the applied strain, and prior to the failure of the high elongation fibres, it was possible to see that the stresses in the low elongation fibres caused them to fracture multiple times and increasing the applied strain sufficiently leads to the failure of the HE fibres and therefore of the composite material.

The model developed is able to capture the main failure mechanisms of polymer composites and the results obtained for the tensile strength closely relate with experimental data.

7.2 Future work

This thesis presented a development on the modelling of the tensile failure of hybrid and non-hybrid polymer composites, however, there are still developments to be made, either in terms of the micromechanical modelling or in terms of experimental validation.

The material models developed are able to correctly predict the behaviour of the constituents of a composite material, however, it was verified that the generation of the random tensile strength strongly affected the results. In order to improve the reliability of the model it is necessary to develop a strategy for the generation of the random strength that accurately represents the strength distributions in the fibres. The Weibull distribution has been shown to characterise this property well enough, however, other distribution can be implemented using a similar strategy and their results and accuracy should be compared.

The interface between the fibres and the matrix greatly affects the performance and behaviour of composite materials. This interface was represented using cohesive surfaces in the micromechnaical models, however, it is necessary to gather more information in relation to the properties of the interfaces to guarantee a correct modelling of this constituent.

The distributions for fibre strength are usually obtained from single fibre fragmentation tests and these tests are able to provide good information, not only in relation to the fibre strength but also in relation to the interface properties. The development of a micromechanical model to represent this tests can be a good way to validate and tune some specific properties of the material models.

The hybridization of composite materials is a subject of increasing interest, however, there is still a lack of experimental data regarding this subject. Therefore, further experimental studies may be conducted, not only to better characterize these materials, but also to understand the failure mechanisms and the controlling factors in the failure of these composites. This, along side the micromechanical models, will allow a full understanding of the tensile failure of hybrid composites.

Bibliography

[1] M. Wisnom, "Size effects in the testing of fibre-composite materials," *Composites Science and Technology*, vol. 59, no. 13, pp. 1937–1957, 1999.

[2] Y. Swolfs, *Hybridisation of Self-reinforced Composites: Modelling and Verifying a Novel Hybrid Concept*. PhD thesis, KU Leuven, 2015.

[3] A. Scott, I. Sinclair, S. Spearing, A. Thionnet, and A. Bunsell, "Damage accumulation in a carbon/epoxy composite: Comparison between a multiscale model and computed tomography experimental results," *Composites Part A: Applied Science and Manufacturing*, vol. 43, no. 9, pp. 1514 – 1522, 2012.

[4] S. Pimenta, "Fibre failure modelling," in *Numerical Modelling of Failure in Advanced Composite Materials* (P. P. Camanho and S. R. Hallet, eds.), ch. 25, Woodhead Publishing, 2015.

[5] A. Turon, J. Costa, P. Maimí, D. Trias, and J. Mayugo, "A progressive damage model for unidirectional fibre-reinforced composites based on fibre fragmentation. part i: Formulation," *Composites Science and Technology*, vol. 65, no. 13, pp. 2039 – 2048, 2005.

[6] S. Pimenta and S. T. Pinho, "Hierarchical scaling law for the strength of composite fibre bundles," *Journal of the Mechanics and Physics of Solids*, vol. 61, no. 6, pp. 1337 – 1356, 2013.

[7] Y. Swolfs, L. Gorbatikh, and I. Verpoest, "Fibre hybridisation in polymer composites: A review," *Composites Part A: Applied Science and Manufacturing*, vol. 67, no. 0, pp. 181 – 200, 2014.

[8] C. Dong, J. Duong, and I. Davies, "Flexural properties of s-2 glass and tr30s carbon fiber-reinforced epoxy hybrid composites," *Polymer Composites*, vol. 33, no. 5, pp. 773–781, 2012. cited By (since 1996)2.

[9] Z. Wu, X. Wang, K. Iwashita, T. Sasaki, and Y. Hamaguchi, "Tensile fatigue behaviour of {FRP} and hybrid {FRP} sheets," *Composites Part B: Engineering*, vol. 41, no. 5, pp. 396 – 402, 2010.

[10] M. Jalalvand, G. Czél, and M. R. Wisnom, "Numerical modelling of the damage modes in {UD} thin carbon/glass hybrid laminates," *Composites Science and Technology*, vol. 94, no. 0, pp. 39 – 47, 2014.

[11] Y. Swolfs, L. Gorbatikh, and I. Verpoest, "Stress concentrations in hybrid unidirectional fibre-reinforced composites with random fibre packings," *Composites Science and Technology*, vol. 85, no. 0, pp. 10 – 16, 2013.

[12] S. Pimenta and P. Robinson, "Modelling the tensile response of unidirectional hybrid composites," *European Conference on Composite Materials, ECCM*, 2014.

[13] Y. Swolfs, R. M. McMeeking, I. Verpoest, and L. Gorbatikh, "The effect of fibre dispersion on initial failure strain and cluster development in unidirectional carbon/glass hybrid composites," *Composites Part A: Applied Science and Manufacturing*, vol. 69, no. 0, pp. 279 – 287, 2015.

[14] A. Melro, P. Camanho, and S. Pinho, "Generation of random distribution of fibres in long-fibre reinforced composites," *Composites Science and Technology*, vol. 68, no. 9, pp. 2092 – 2102, 2008.

[15] A. Argon, "Statistical aspects of fracture," in *Composite Materials: Fatigue and Fracture* (L. Broutman, ed.), vol. 5, ch. 4, pp. 153–190, New York: Academic Press, 1974.

[16] Y. Swolfs, L. Gorbatikh, V. Romanov, S. Orlova, S. Lomov, and I. Verpoest, "Stress concentrations in an impregnated fibre bundle with random fibre packing," *Composites Science and Technology*, vol. 74, no. 0, pp. 113 – 120, 2013.

[17] W. Weibull, "A statistical distribution function of wide applicability," *Journal of Applied Mechanics - Transactions of the ASME.*, vol. 58, no. 7, pp. 1001–1010, 1951.

[18] V. Calard and J. Lamon, "Failure of fiber bundles," *Composites Science and Technology*, vol. 64, no. 5, pp. 701 – 710, 2004.

[19] M. R'Mili, N. Godin, and J. Lamon, "Flaw strength distributions and statistical parameters for ceramic fibers: The normal distribution," *Phys. Rev. E*, vol. 85, p. 051106, May 2012.

[20] W. A. Curtin, "Tensile strength of fiber-reinforced composites: Iii. beyond the traditional weibull model for fiber strengths," *Journal of Composite Materials*, vol. 34, no. 15, pp. 1301–1332, 2000.

[21] J. Watanabe, F. Tanaka, H. Okuda, and T. Okabe, "Tensile strength distribution of carbon fibers at short gauge lengths," *Advanced Composite Materials*, vol. 23, no. 5-6, pp. 535–550, 2014.

[22] H. Peterlik and D. Loidl, "Bimodal strength distributions and flaw populations of ceramics and fibres," *Engineering Fracture Mechanics*, vol. 68, no. 3, pp. 253 – 261, 2001.

[23] W. J. Padgett, S. D. Durham, and A. M. Mason, "Weibull analysis of the strength of carbon fibers using linear and power law models for the length effect," *Journal of Composite Materials*, vol. 29, no. 14, pp. 1873–1884, 1995.

[24] S. Hallett, B. Green, W. Jiang, and M. Wisnom, "An experimental and numerical investigation into the damage mechanisms in notched composites," *Composites Part A: Applied Science and Manufacturing*, vol. 40, no. 5, pp. 613–624, 2009.

[25] W. Curtin, "Dimensionality and size effects on the strength of fiber-reinforced composites," *Composites Science and Technology*, vol. 60, no. 4, pp. 543 – 551, 2000.

[26] C. M. Landis and R. M. McMeeking, "Stress concentrations in composites with interface sliding, matrix stiffness and uneven fiber spacing using shear lag theory," *International Journal of Solids and Structures*, vol. 36, no. 28, pp. 4333 – 4361, 1999.

[27] B. W. Rosen, "Tensile failure of fibrous composites," *AIAA Journal*, vol. 2, pp. 1985–1991, 2015/02/24 1964.

[28] A. A. Gusev, P. J. Hine, and I. M. Ward, "Fiber packing and elastic properties of a transversely random unidirectional glass/epoxy composite," *Composites Science and Technology*, vol. 60, no. 4, pp. 535 – 541, 2000.

[29] M. Ibnabdeljalil and W. Curtin, "Strength and reliability of fiber-reinforced composites: Localized load-sharing and associated size effects," *International Journal of Solids and Structures*, vol. 34, no. 21, pp. 2649 – 2668, 1997.

[30] D. R.-B. Aroush, E. Maire, C. Gauthier, S. Youssef, P. Cloetens, and H. Wagner, "A study of fracture of unidirectional composites using in situ high-resolution synchrotron x-ray microtomography," *Composites Science and Technology*, vol. 66, no. 10, pp. 1348 – 1353, 2006.

[31] Q.-D. Zeng, Z.-L. Wang, and L. Ling, "A study of the influence of interfacial damage on stress concentrations in unidirectional composites," *Composites Science and Technology*, vol. 57, no. 1, pp. 129 – 135, 1997.

[32] P. van den Heuvel, T. Peijs, and R. Young, "Failure phenomena in two-dimensional multi-fibre microcomposites. part 4: a raman spectroscopic study on the influence of the matrix yield stress on stress concentrations," *Composites Part A: Applied Science and Manufacturing*, vol. 31, no. 2, pp. 165 – 171, 2000.

[33] Y. Swolfs, R. M. McMeeking, I. Verpoest, and L. Gorbatikh, "Matrix cracks around fibre breaks and their effect on stress redistribution and failure development in unidirectional composites," *Composites Science and Technology*, vol. 108, no. 0, pp. 16 – 22, 2015.

[34] T. Hobbiebrunken, B. Fiedler, M. Hojo, and M. Tanaka, "Experimental determination of the true epoxy resin strength using micro-scaled specimens," *Composites Part A: Applied Science and Manufacturing*, vol. 38, no. 3, pp. 814 – 818, 2007.

[35] A. de Morais, "Prediction of the longitudinal tensile strength of polymer matrix composites," *Composites Science and Technology*, vol. 66, no. 15, pp. 2990 – 2996, 2006.

[36] L. M. Jr. and P. Brøndsted, "Micromechanical modeling of damage and fracture of unidirectional fiber reinforced composites: A review," *Computational Materials Science*, vol. 44, no. 4, pp. 1351 – 1359, 2009.

[37] H. E. Daniels, "The statistical theory of the strength of bundles of threads. i," *Proceedings of the Royal Society of London A: Mathematical, Physical and Engineering Sciences*, vol. 183, no. 995, pp. 405–435, 1945.

[38] W. A. Curtin, "Theory of mechanical properties of ceramic-matrix composites," *Journal of the American Ceramic Society*, vol. 74, no. 11, pp. 2837–2845, 1991.

[39] J. M. Hedgepeth, "Stress concentrations in filamentary structures," tech. rep., NASA Langley Research Center; Hampton, VA United States, May 1961.

[40] J. M. Hedgepeth and P. Van Dyke, "Local stress concentrations in imperfect filamentary composite materials," *Journal of Composite Materials*, vol. 1, no. 3, pp. 294–309, 1967.

[41] D. G. Harlow and S. L. Phoenix, "The chain-of-bundles probability model for the strength of fibrous materials i: analysis and conjectures," *Journal of composite materials*, vol. 12, no. 2, pp. 195–214, 1978.

[42] D. G. Harlow and S. L. Phoenix, "The chain-of-bundles probability model for the strength of fibrous materials ii: a numerical study of convergence," *Journal of composite materials*, vol. 12, no. 3, pp. 314–334, 1978.

[43] T. Okabe, N. Takeda, Y. Kamoshida, M. Shimizu, and W. Curtin, "A 3d shear-lag model considering micro-damage and statistical strength prediction of unidirectional fiber-reinforced composites," *Composites Science and Technology*, vol. 61, no. 12, pp. 1773 – 1787, 2001.

[44] T. Okabe, H. Sekine, K. Ishii, M. Nishikawa, and N. Takeda, "Numerical method for failure simulation of unidirectional fiber-reinforced composites with spring element model," *Composites Science and Technology*, vol. 65, no. 6, pp. 921 – 933, 2005.

[45] W. Curtin and N. Takeda, "Tensile strength of fiber-reinforced composites: I. model and effects of local fiber geometry," *Journal of composite materials*, vol. 32, no. 22, pp. 2042–2059, 1998.

[46] I. J. Beyerlein and S. Phoenix, "Stress concentrations around multiple fiber breaks in an elastic matrix with local yielding or debonding using quadratic influence superposition," *Journal of the Mechanics and Physics of Solids*, vol. 44, no. 12, pp. 1997 – 2039, 1996.

[47] C. M. Landis, I. J. Beyerlein, and R. M. McMeeking, "Micromechanical simulation of the failure of fiber reinforced composites," *Journal of the Mechanics and Physics of Solids*, vol. 48, no. 3, pp. 621 – 648, 2000.

[48] S. Blassiau, A. Thionnet, and A. Bunsell, "Three-dimensional analysis of load transfer micro-mechanisms in fibre/matrix composites," *Composites Science and Technology*, vol. 69, no. 1, pp. 33 – 39, 2009. Mechanical Response of Fibre Reinforced Composites.

[49] A. Thionnet, H. Chou, and A. Bunsell, "Fibre break processes in unidirectional composites," *Composites Part A: Applied Science and Manufacturing*, vol. 65, no. 0, pp. 148 – 160, 2014.

[50] A. Matzenmiller, J. Lubliner, and R. Taylor, "A constitutive model for anisotropic damage in fiber-composites," *Mechanics of Materials*, vol. 20, no. 2, pp. 125 – 152, 1995.

[51] A. K. Kaw, *Mechanics of Composite Materials*. Tayler and Francis, 2nd ed., 2006.

[52] T. Hayashi, "On the improvement of mechanical properties of composites by hybrid compositon.," *Proc 8th int reinforced plastics conference*, pp. 149–52, 1972.

[53] G. Kretsis, "A review of the tensile, compressive, flexural and shear properties of hybrid fibre-reinforced plastics," *Composites*, vol. 18, no. 1, pp. 13 – 23, 1987.

[54] G. Marom, S. Fischer, F. Tuler, and H. Wagner, "Hybrid effects in composites: conditions for positive or negative effects versus rule-of-mixtures behaviour," *Journal of Materials Science*, vol. 13, no. 7, pp. 1419–1426, 1978.

[55] Z. S. Wu, C. Q. Yang, Y. H. Tobe, L. P. Ye, and T. Harada, "Electrical and mechanical characterization of hybrid cfrp sheets," *Journal of Composite Materials*, vol. 40, no. 3, pp. 227–244, 2006.

[56] M. Phillips, "Composition parameters for hybrid composite materials," *Composites*, vol. 12, no. 2, pp. 113 – 116, 1981.

[57] P. Manders and M. Bader, "The strength of hybrid glass/carbon fibre composites," *Journal of Materials Science*, vol. 16, no. 8, pp. 2246–2256, 1981.

[58] C. Zweben, "Tensile strength of hybrid composites," *Journal of Materials Science*, vol. 12, no. 7, pp. 1325–1337, 1977.

[59] M. Wisnom, B. Khan, and S. Hallett, "Size effects in unnotched tensile strength of unidirectional and quasi-isotropic carbon/epoxy composites," *Composite Structures*, vol. 84, pp. 21–28, June 2008.

[60] Y. Xia and C. Ruiz, "Analysis of damage in stress wave loaded unidirectional composites," *Computers and Structures*, vol. 38, no. 3, pp. 251 – 258, 1991.

[61] J. Xing, X.-R. Liu, and T.-W. Chou, "Dynamic stress concentration factors in unidirectional composites," *Journal of Composite Materials*, vol. 19, no. 3, pp. 269–275, 1985.

[62] J. Xing, G. C. Hsiao, and T.-W. Chou, "A dynamic explanation of the hybrid effect," *Journal of Composite Materials*, vol. 15, no. 5, pp. 443–461, 1981.

[63] I. Taketa, *Analysis of Failure Mechanisms and Hybrid Effects in Carbon Fibre Reinforced Thermoplastic Composites*. PhD thesis, KU Leuven, Leuven, 2011.

[64] C. Wonderly, J. Grenestedt, G. Fernlund, and E. Cĕpus, "Comparison of mechanical properties of glass fiber/vinyl ester and carbon fiber/vinyl ester composites," *Composites Part B: Engineering*, vol. 36, no. 5, pp. 417 – 426, 2005.

[65] C. Dong and I. J. Davies, "Optimal design for the flexural behaviour of glass and carbon fibre reinforced polymer hybrid composites," *Materials and Design*, vol. 37, no. 0, pp. 450 – 457, 2012.

[66] J. W. Giancaspro, C. G. Papakonstantinou, and P. Balaguru, "Flexural response of inorganic hybrid composites with e-glass and carbon fibers," *Journal of Engineering Materials and Technology*, vol. 132, no. 2, p. 021005, 2010.

[67] M. Sayer, N. B. Bektaş, and O. Sayman, "An experimental investigation on the impact behavior of hybrid composite plates," *Composite Structures*, vol. 92, no. 5, pp. 1256 – 1262, 2010.

[68] B. Jang, L. Chen, C. Wang, H. Lin, and R. Zee, "Impact resistance and energy absorption mechanisms in hybrid composites," *Composites Science and Technology*, vol. 34, no. 4, pp. 305 – 335, 1989.

[69] N. Naik, R. Ramasimha, H. Arya, S. Prabhu, and N. ShamaRao, "Impact response and damage tolerance characteristics of glass–carbon/epoxy hybrid composite plates," *Composites Part B: Engineering*, vol. 32, no. 7, pp. 565 – 574, 2001.

[70] F. Sarasini, J. Tirillò, M. Valente, T. Valente, S. Cioffi, S. Iannace, and L. Sorrentino, "Effect of basalt fiber hybridization on the impact behavior under low impact velocity of glass/basalt woven fabric/epoxy resin composites," *Composites Part A: Applied Science and Manufacturing*, vol. 47, no. 0, pp. 109 – 123, 2013.

[71] I. De Rosa, F. Marra, G. Pulci, C. Santulli, F. Sarasini, J. Tirillò, and M. Valente, "Post-impact mechanical characterisation of e-glass/basalt woven fabric interply hybrid laminates," *Express Polym Lett*, vol. 5, no. 5, pp. 449–459, 2011.

[72] R. Park and J. Jang, "Effect of laminate geometry on impact performance of aramid fiber/polyethylene fiber hybrid composites," *Journal of Applied Polymer Science*, vol. 75, no. 7, pp. 952–959, 2000.

[73] A. Peijs and J. de Kok, "Hybrid composites based on polyethylene and carbon fibres. part 6: Tensile and fatigue behaviour," *Composites*, vol. 24, no. 1, pp. 19 – 32, 1993.

[74] K. D. Jones and A. T. DiBenedetto, "Fiber fracture in hybrid composite systems," *Composites Science and Technology*, vol. 51, no. 1, pp. 53 – 62, 1994.

[75] G. Czél and M. Wisnom, "Demonstration of pseudo-ductility in high performance glass/epoxy composites by hybridisation with thin-ply carbon prepreg," *Composites Part A: Applied Science and Manufacturing*, vol. 52, no. 0, pp. 23 – 30, 2013.

[76] Y. Liang, C. Sun, and F. Ansari, "Acoustic emission characterization of damage in hybrid fiber-reinforced polymer rods," *Journal of Composites for Construction*, vol. 8, no. 1, pp. 70–78, 2004.

[77] G. Czél, S. Pimenta, M. R. Wisnom, and P. Robinson, "Demonstration of pseudo-ductility in unidirectional discontinuous carbon fibre/epoxy prepreg composites," *Composites Science and Technology*, vol. 106, no. 0, pp. 110 – 119, 2015.

[78] G. Czél, M. Jalalvand, and M. R. Wisnom, "Demonstration of pseudo-ductility in unidirectional hybrid composites made of discontinuous carbon/epoxy and continuous glass/epoxy plies," *Composites Part A: Applied Science and Manufacturing*, vol. 72, no. 0, pp. 75 – 84, 2015.

[79] Y. Swolfs, Y. Meerten, P. Hine, I. Ward, I. Verpoest, and L. Gorbatikh, "Introducing ductility in hybrid carbon fibre/self-reinforced composites through control of the damage mechanisms," *Composite Structures*, vol. 131, no. 0, pp. 259 – 265, 2015.

[80] H. Yu, M. L. Longana, M. Jalalvand, M. R. Wisnom, and K. D. Potter, "Pseudo-ductility in intermingled carbon/glass hybrid composites with highly aligned discontinuous fibres," *Composites Part A: Applied Science and Manufacturing*, vol. 73, no. 0, pp. 35 – 44, 2015.

[81] D. G. Harlow, "Statistical properties of hybrid composites. i. recursion analysis," *Proceedings of the Royal Society of London A: Mathematical, Physical and Engineering Sciences*, vol. 389, no. 1796, pp. 67–100, 1983.

[82] H. Fukunaga, T.-W. Chou, and H. Fukuda, "Probabilistic strength analyses of interlaminated hybrid composites," *Composites Science and Technology*, vol. 35, no. 4, pp. 331 – 345, 1989.

[83] H. Fukuda, "An advanced theory of the strength of hybrid composites," *Journal of Materials Science*, vol. 19, no. 3, pp. 974–982, 1984.

[84] L. M. Jr. and G. Dai, "Hybrid carbon/glass fiber composites: Micromechanical analysis of structure–damage resistance relationships," *Computational Materials Science*, vol. 81, no. 0, pp. 630 – 640, 2014.

[85] P. W. Manders, *The strength of mixed fibre composites*. PhD thesis, University of Surrey, UK, 1979.

[86] P. Ren, Z. Zhang, L. Xie, F. Ren, Y. Jin, Y. Di, and C. Fang, "Hybrid effect on mechanical properties of m40-t300 carbon fiber reinforced bisphenol a dicyanate ester composites," *Polymer Composites*, vol. 31, no. 12, pp. 2129–2137, 2010.

[87] M. R'Mili, T. Bouchaour, and P. Merle, "Estimation of weibull parameters from loose-bundle tests," *Composites Science and Technology*, vol. 56, no. 7, pp. 831 – 834, 1996. 9th French National Colloquium on Composite Materials.

[88] W. A. Curtin and N. Takeda, "Tensile strength of fiber-reinforced composites: Ii. application to polymer matrix composites," *Journal of Composite Materials*, vol. 32, no. 22, pp. 2060–2081, 1998.

[89] I. J. Beyerlein and S. Phoenix, "Statistics for the strength and size effects of microcomposites with four carbon fibers in epoxy resin," *Composites Science and Technology*, vol. 56, no. 1, pp. 75 – 92, 1996.

[90] M. Nakatani, M. Shioya, and J. Yamashita, "Axial compressive fracture of carbon fibers," *Carbon*, vol. 37, no. 4, pp. 601 – 608, 1999.

[91] F. Tanaka, T. Okabe, H. Okuda, I. A. Kinloch, and R. J. Young, "Factors controlling the strength of carbon fibres in tension," *Composites Part A: Applied Science and Manufacturing*, vol. 57, no. 0, pp. 88 – 94, 2014.

[92] G. Foray, A. Descamps-Mandine, M. R'Mili, and J. Lamon, "Statistical flaw strength distributions for glass fibres: Correlation between bundle test and afm-derived flaw size density functions," *Acta Materialia*, vol. 60, no. 9, pp. 3711 – 3718, 2012.

[93] S. Feih, A. Thraner, and H. Lilholt, "Tensile strength and fracture surface characterisation of sized and unsized glass fibers," *Journal of Materials Science*, vol. 40, no. 7, pp. 1615–1623, 2005.

[94] V. Pauchard, A. Chateauminois, F. Grosjean, and P. Odru, "In situ analysis of delayed fibre failure within water-aged gfrp under static fatigue conditions," *International Journal of Fatigue*, vol. 24, no. 2–4, pp. 447 – 454, 2002.

[95] K. Naito, "Tensile properties and weibull modulus of some high-performance polymeric fibers," *Journal of Applied Polymer Science*, vol. 128, no. 2, pp. 1185–1192, 2013.

[96] W. Curtin, "Stochastic damage evolution and failure in fiber-reinforced composites," in *Advances in Applied Mechanics* (E. van der Giessen and T. Y. Wu, eds.), vol. 36 of *Advances in Applied Mechanics*, pp. 163 – 253, Elsevier, 1998.

[97] X. Martínez, *Micro-mechanical simulation of composite materials using the serial/parallel mixing theory.* PhD thesis, Ph. D. thesis, Departament de Resistència de Materials i Estructures a l'Enginyeria (RMEE)—UPC. Director: Sergio Oller, 2008.

[98] A. R. Melro, *Analytical and numerical modelling of damage and fracture of advanced composites.* PhD thesis, Faculdade de Engenharia da Universidade do Porto, 2011.

[99] X. Bai, M. A. Bessa, A. R. Melro, P. P. Camanho, L. Guo, and W. K. Liu, "High-fidelity micromechanical modeling of the thermo-visco-plastic behavior of carbon fiber polymer matrix composites," *to be published*, 2015.

[100] Z. Bažant and B. Oh, "Crack band theory for fracture of concrete," *Matériaux et Construction*, vol. 16, no. 3, pp. 155–177, 1983.

[101] P. Soden, M. Hinton, and A. Kaddour, "Lamina properties, lay-up configurations and loading conditions for a range of fibre-reinforced composite laminates," *Composites Science and Technology*, vol. 58, no. 7, pp. 1011 – 1022, 1998.

[102] Hexcel-Composites, "3501-6 epoxy matrix - product data."